


1-1-2016

Development Of Carbon Based Neural Interface For Neural Stimulation/recording And Neurotransmitter Detection

Wenwen Yi
Wayne State University,

Follow this and additional works at: https://digitalcommons.wayne.edu/oa_dissertations

 Part of the [Biomedical Engineering and Bioengineering Commons](#), and the [Electrical and Computer Engineering Commons](#)

Recommended Citation

Yi, Wenwen, "Development Of Carbon Based Neural Interface For Neural Stimulation/recording And Neurotransmitter Detection" (2016). *Wayne State University Dissertations*. 1498.
https://digitalcommons.wayne.edu/oa_dissertations/1498

This Open Access Dissertation is brought to you for free and open access by DigitalCommons@WayneState. It has been accepted for inclusion in Wayne State University Dissertations by an authorized administrator of DigitalCommons@WayneState.

**DEVELOPMENT OF CARBON BASED NEURAL INTERFACE FOR
NEURAL STIMULATION/RECORDING AND
NEUROTRANSMITTER DETECTION**

by

WENWEN YI

DISSERTATION

Submitted to the Graduate School

of Wayne State University,

Detroit, Michigan

in partial fulfillment of the requirements

for the degree of

DOCTOR OF PHILOSOPHY

2016

MAJOR: ELECTRICAL ENGINEERING

Approved By:

Advisor

Date

© COPYRIGHT BY

WENWEN YI

2016

All Rights Reserved

DEDICATION

To my family.

ACKNOWLEDGEMENTS

I would first like to thank my advisor, Professor Mark Cheng. I am truly grateful that he gave me this great opportunity to work on this very interesting topic. Professor Cheng gave me plenty of room to grow freely, while he was always there to provide instructive advice. From him, I learned how to work with different people, how to coordinate different projects, and how to handle stressful situations. I am deeply impressed by Professor Cheng's creativity and broad range of knowledge. I will continue to benefit from all I learned after my graduation.

I would like to thank Professor John Cavanaugh and his group: Chaoyang Chen, Zhaoying Feng, and Chengpeng Zhou, for their guidance and support in the rat experiments for my thesis work. In particular, the discussion with Professor John Cavanaugh and Professor Chaoyang Chen about the electrophysiological experiments has been really inspiring and helpful.

I would also like to thank Professor Yong Xu and his group: Eric Kim, Hongen Tu, and Yating Hu. They were always willing to share knowledge, experience and some resources for microfabrication. I also thank Professor Greg Auner for serving on my thesis committee and for providing critical and constructive feedback to this work.

I appreciate Professor Parry Hashemi and her student: Yuanyuan yang, for helping me in the fast scan cyclic voltammetry testing in their lab. I especially thank Professor Hashemi for her continuous support even after she had moved on with her career.

During the past few years, I spent many long days and nights in the nano fabrication (nFab) core facility at Wayne State University. I would like to thank the staff in NFab: Bill Funk and Dan Duris. They were always friendly, responsive and ready to help.

It has been a pleasant experience working in Professor Cheng's lab. I do enjoy the friendship with every group member: Xuebin Tan, Jinho Yang, Peng Zeng, Ali Shahini, Qingsong Cui, Jianjun Xia, Qianghua Wang, Ehsan Majidi, Nirul Masurkar, Chad Huard, Jimmy Ching-Ming Chen, Jing Yang. I thank all my fellow labmates for their help and valuable advices in my research.

I also gratefully acknowledge the financial support from the Department of Electrical Engineering, Wayne State University and the National Science Foundation.

Finally, and most importantly, I thank my parents for all the trust and support they gave me. Special thanks go to my husband, Bo and son, Qiao, for giving me endless love and support.

TABLE OF CONTENTS

DEDICATION	ii
ACKNOWLEDGEMENTS	iii
LIST OF TABLES.....	ix
LIST OF FIGURES	x
CHAPTER 1 INTRODUCTION	1
1.1 Neural interface	1
1.2 Neural stimulation and recording.....	2
1.2.1 Transduction of electrical signals in neurons	2
1.2.2 Types of stimulation/recording electrodes	3
1.2.3 Requirements for electrode materials.....	7
1.2.4 Electroactive nanomaterials for neural interface	8
1.3 Neurochemical detection.....	12
1.3.1 Neurotransmitters.....	12
1.3.2 Techniques for sensing neurotransmission.....	14
1.3.3 Electrodes for neurotransmitter detection.....	17
CHAPTER 2 INTEGRATION OF FLEXIBLE PARYLENE SUBSTRATE WITH FREELY STANDING CARBON NANOTUBES AS NEURAL INTERFACE	20
2.1 Background and motivation	20
2.1.1 Carbon nanotube MEA for neuronal recording and stimulation	20
2.1.2 Flexible CNT MEA for recording and stimulation	22
2.1.3 Challenges and motivations.....	24
2.2 Experimental	25

2.2.1 Fabrication of flexible CNT MEA.....	25
2.2.2 Appearance of the flexible device	26
2.2.3 Characterization of CNTs	28
2.2.4 Electrochemical characterization of the flexible CNT MEA	28
2.2.5 Electrophysiological experiments.....	28
2.3 Results and Discussion.....	29
2.3.1 Characterization of the flexible device and CNTs.....	29
2.3.2 Electrochemical characterization of CNTs electrode.....	31
2.3.3 Neural stimulation and recording by flexible CNTs electrode	35
2.4 Conclusions	40
CHAPTER 3 CARBON NANOFIBER MICROELECTRODE ARRAYS FABRICATED BY PLASMA ASSISTED PYROLYSIS FOR FAST SCAN CYCLIC VOLTAMMETRY ANALYSIS	43
3.1 Background and motivation	43
3.1.1 Carbon based microelectrodes for electrochemical detection.....	43
3.1.2 Fast scan cyclic voltammetry	44
3.1.3 Challenges and motivations.....	45
3.2 Experimental	47
3.2.1 Chemicals.....	47
3.2.2 Electrode fabrication	47
3.2.3 Electrode characterizations.....	50
3.2.4 Instrumentation and data acquisition.....	50
3.2.5 Flow Injection Analysis	50
3.3 Results and Discussion.....	51

3.3.1 Electrode design and fabrication.....	51
3.3.2 Characterization of PPF MEAs.....	54
3.3.3 FSCV Characterizations.....	60
3.4 Conclusions	66
CHAPTER 4 FLEXIBLE CNT BASED CUFF ELECTRODE FOR PERIPHERAL STIMULATION	67
4.1 Background and motivation	67
4.1.1 Functional electrical stimulations and applications in peripheral nervous system	67
4.1.2 Cuff electrodes for peripheral nerve stimulation	69
4.1.3 Motivations	71
4.2 Experimental	73
4.2.1 Fabrication of flexible CNT based cuff electrode	73
4.2.2 Characterization of flexible CNT based cuff electrode	74
4.2.3 Electrophysiological experiments.....	74
4.3 Results and discussion.....	76
4.3.1 Characterization of device	76
4.3.2 Comparison of the CNTs and Pt based flexible cuff electrode for neural stimulation	83
4.3.3 Effect of electrode positions.....	84
4.3.4 Effect of stimulation frequency.....	86
4.3.5 Summary of rat experiments and root cause analysis	87
CHAPTER 5 CONCLUSIONS AND FUTURE WORKS	90
5.1 Conclusions	90
5.2 Future works.....	92

BIBLIORGRAPHY	94
ABSTRACT	112
AUTOBIOGRAPHICAL STATEMENT.....	114

LIST OF TABLES

Table 3.1 Parameters for dual oxygen plasma treatment in the device fabrication	47
Table 3.2 Comparison of ID/IG and O/C ratio of electrodes under different treatments	56
Table 4.1 Analysis of experimental failure	87

LIST OF FIGURES

Figure 1.1 (a) Neural signal transduction model in neurons. (b) Model of voltage potential at the membrane of a neuron. (c) Cathodic electrical stimulation model [4].....	2
Figure 1.2 (a) Microwires [1] (b) Utah array [5] (c) Michigan probe [8] (d) flexible MEAs [9].....	5
Figure 1.3 (a) Carbon fiber microelectrode [2] (b) Carbon fiber microdisc [6] (c) Carbon fiber microelectrode arrays [7].....	18
Figure 2.1 Fabrication process flow.....	27
Figure 2.2 (a) optical image of the flexible devices, (b) white light image of the electrode area, (c) SEM image of the as grown CNTs, (d) SEM image of the flexible CNT electrode before neural stimulation and recording, (e) higher magnification SEM of (d), (f) Raman spectra of the CNT electrode.....	31
Figure 2.3 CV of the CNT electrode and Pt electrode, the inset is the CV for Pt electrode at different scale.....	32
Figure 2.4 (a) magnitude of impedance spectra, (b) phase of impedance spectra (red is the Pt electrodes, black if the CNT electrodes).....	33
Figure 2.5 Impedance spectra of flexible devices before, after 20 times and 50 times bending.....	34
Figure 2.6 (a) schematic of experimental set-up for physiological testing (b) neural stimulation at sciatic nerve with flexible CNT electrode (c) neural recording at spinal cord with flexible CNT electrode.....	36
Figure 2.7 (a) neural recording with the flexible CNT electrodes (b) neural recording with the Pt electrodes.....	37
Figure 2.8 (a) neural stimulation with the flexible CNT electrodes (b) neural stimulation with the Pt electrodes.....	38
Figure 2.9 SEM image of flexible CNT electrodes after neural recording and stimulation.....	40
Figure 3.1 Schematic of FSCV working theory [3].....	45
Figure 3.2 Process flow for the fabrication and treatment of carbon nanofiber MEAs. A description of each step can be found in Section 3.2.2.....	49

Figure 3.3 Optical (a-b)images of carbon nanofiber MEAs, (c) and (d) SEM images showing the microstructure of the pyrolyzed photoresist without and with primary oxygen plasma treatment respectively.....	51
Figure 3.4 AFM images with associated line plots collected at electrodes CMEA 100 (a), CMEA 103 (b), CMEA 200 (c), and CMEA 203 (d). The primary oxygen plasma treatment does contribute to increase the surface roughness, while secondary oxygen plasma treatment does not.....	55
Figure 3.5 Raman spectra of photoresist derived carbon electrode with different treatments.....	57
Figure 3.6 XPS comparison of photoresist derived carbon electrode with different treatments.....	59
Figure 3.7 (a) a FIA response of electrode CMEA 202 to injection of 1 μ M DA. (a) shows a CV taken at the vertical white dashed line from the color plot in (b). (c) shows a plot of response current vs time, which was determined by taking i vs t from the horizontal white dashed line in the color plot (b).....	60
Figure 3.8 Effect of pre and post treatment on the sensitivity. The pre-treated samples show greater response current than non-pre-treated ones. 20s post-pyrolysis treatment saturates the surfaces with oxygen containing functional group.....	63
Figure 3.9 Detection limit (sensitivity) of the optimized electrodes. The plot shows voltammetric peak current as a function of dopamine concentration. The error bars are the standard deviation ($n=12$). Inset: linear range of dopamine on MEAs. All measurements were done at 400 v/s, 10Hz in TRIS buffer, pH 7.4.....	64
Figure 3.10 Effect of oxygen plasma pre-treatment on device stability. Figure (a) and (b) show the peak oxidation current of successive DA injection onto pre-treated and unpretreated MEAs respectively with FIA (positive potential limit +1.3V, negative potential limit -0.4V, scan rate 400 V/s). Horizontal lines indicate SD limits.....	65
Figure 4.1 Schematic of the flexible CNTs cuff electrode (a); improved uniformity of electric field generated by CNT electrodes (b).....	72
Figure 4.2 Experiment setup for siatic nerve stimulation.....	74
Figure 4.3 Cuff electrode design plots: (a) the size of the whole device, (b) the size of electrodes.....	75
Figure 4.4 (a) photos of the fabricated device, (b) the implanted device, (c) the CNTs on Si before the coating of parylene (d) CNT electrodes on flexible substrate.....	77

Figure 4.5 The measured force magnitude and the corresponded EMG magnitude for each pair of electrodes. The inset is the representative peak for each plot.....82

Figure 4.6 The calculated area under curve of EMG peaks at the stimulation voltage 10 V for Pt/Pt electrode pair and CNT/Pt electrode pair.....83

Figure 4.7 Duration (a) and AUC (b) of EMG peaks generated by 10V stimulation via electrode pairs positioned with different distances.....85

Figure 4.8 Threshold voltage of 10V stimulation via electrode pairs positioned at different distances.....86

Figure 4.9 (a) EMG magnitude at different stimulation frequency. (b) The percentage of force generated at 1Hz and 10Hz related to the normalized force at 100Hz.....87

CHAPTER 1 INTRODUCTION

1.1 Neural interface

In the nervous system, electrical signals are generated by neurons and conducted through a complex network. Since 1950s, the development of devices to interface the nervous system has attracted a lot of interest. Such devices connect neurons via electrical, chemical, magnetic, mechanical or optical activation of neurons. Electrical recording and stimulation are applied in neuroscience research to understand the physiological processes at the cellular level, and in the treatment systems for neurological disorders such as Parkinson's disease [10], epilepsy [11], and Tourette syndrome [12]. With rapid advances in the past three decades, their application is also extended to neural prosthetics to help restore functions in the nervous system, such as retinal implants, cochlear implants, and for urinary bladder function restoration, and limb control in paralyzed individuals [13, 14]. In all these applications, the most essential part in the neural interface, where implantable microelectrode arrays work as a bridge between nerve cells and outside equipment for transferring charge. Besides of stimulating and recording, neural electrodes are also designed to detect neurochemical and electrophysiological signals to understand the role of the specific chemical in brain function. This type of electrodes is also known as sensing electrodes. The detected neurochemicals include dopamine, norepinephrine, serotonin, ascorbate, uric acid, adenosine, and acetylcholine.

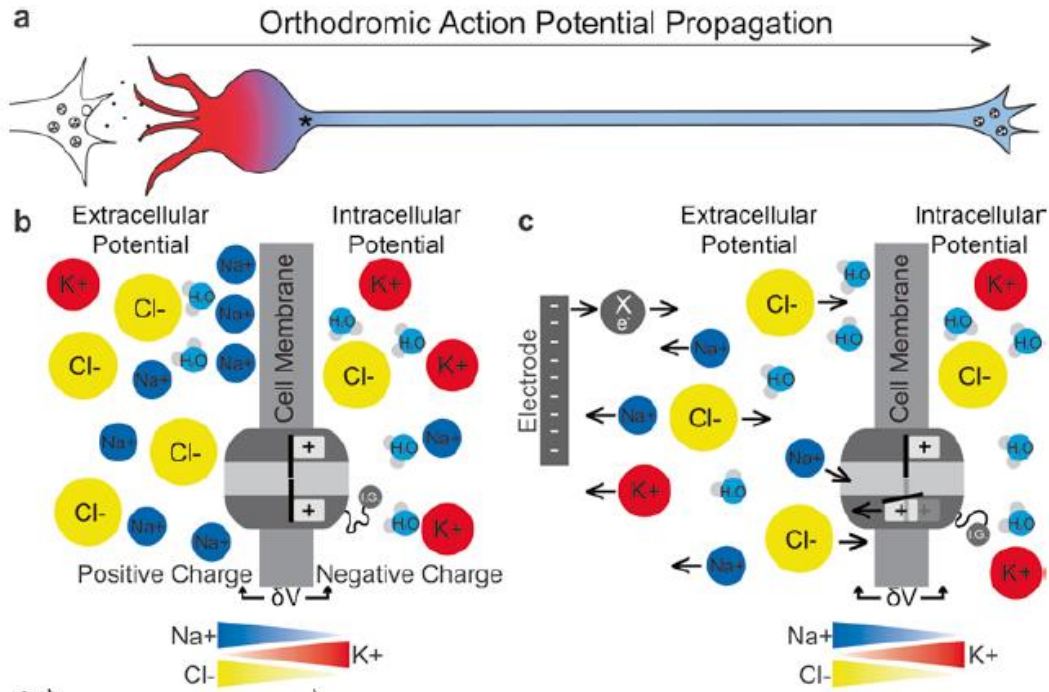


Figure 1.1 (a) Neural signal transduction model in neurons. (b) Model of voltage potential at the membrane of a neuron. (c) Cathodic electrical stimulation model [4].

1.2 Neural stimulation and recording

1.2.1 Transduction of electrical signals in neurons

The signal transductions in neurons are modeled in Figure 1.1 [15]. The resting membrane potential of neurons maintain in the order of -60 to -95 mV through active pumping of positively charged sodium ions out of the cell. Neurons are typically activated by the receptors that open ion channels in the membrane in response to specific triggers, such as neurotransmitters [16]. After ion channels are open, sodium ions flow into the cell, the intracellular potential becomes less negative relative to the extracellular space and approaches zero. The cell is depolarized. When ions keep flowing into the cell,

nearby voltage-gated sodium channels open [17], allowing further influx of sodium that consequently depolarizes other adjacent channels [4]. The action potential propagates by activating and opening a sufficient number of voltage-gated sodium channels. Action potentials normally travel in one direction from the soma to the axon terminal. Under orthodromic signal conduction, neurotransmitters released from the axon terminal bind to receptors on the target neuron, which are generally on the dendrites (Fig. 1.1(a)). Once the neurotransmitters bind to the target receptors, ion channels open and contribute to the depolarization of the membrane [18].

Electrical stimulation generates action potential by introducing an artificially generated electrical impulse. Charge is delivered to neurons with a cathodic (negative) current pulse. In general, a stimulation electrode is placed near the cells being targeted. A larger *counter* electrode is placed at a distant site to complete the circuit. During a cathodic (negative) stimulation pulse, a negatively charged microenvironment is created in the extracellular space around neurons near the electrode. This leads to the depolarization of the cellular membrane, opening of the voltage-gated ion channels, and further depolarization of the cell (Fig. 1.1(b, c)).

1.2.2 Types of stimulation/recording electrodes

Microwires

The first generation of neural interface was sharpened metal wires, such as stainless steel, tungsten (W), platinum (Pt), iridium (Ir), or gold (Au). [1]. Microwires are coated with a non-cytotoxic insulator material, except for the tips. Figure 1.2 (a) shows a typical microwire arrays fabricated by Plexon. The non-insulated tips were used to record the highly localized extracellular potentials from the neurons close to the tips and also to inject

the localized stimulation current to excite neurons [1]. Their narrow structures make it possible for the microwires to be placed very close to single neurons in vivo, causing minimal damage in tissue. They give long-lasting individual neurons recording, sometimes more than one year. Nicolas et al. recorded 247 individual cortical neurons from 384 out of 704 chronically implanted microwires in monkey's brain up to 18 months after implantation [19]. One particular advantage of microwires is that they can be applied to access deep brain structures. By using the arrays of microwires, simultaneous recording at the level of neuronal populations is possible. However, the metal wires are easily bent during the implementation, so that the accurate location of the electrode tips relative to each other is not controllable. There are also some issues related to the materials in use. For example, stainless steel is fragile near the tips; tungsten has higher stiffness and rugged structure to provide very stable recordings; however, tungsten is very noisy at low frequencies. In fact, metal electrodes generally have less SNR because of higher impedance for the frequency range of spike signals. As a result, porous and conductive coatings are being applied. Platinum electrodes plated with platinum black provide stable recordings, high SNR, and create a porous low-impedance structure, although it is mechanically fragile. Recently, CNTs and conductive polymers have been used to coat the tips of the metal wire electrodes. In 2008, a research group coated the tips of conventional tungsten and stainless steel wire electrodes with a combination of CNTs and polymer for the first time. After the deposition of CNTs on indiumtin oxide MEAs, the impedance decreased from 940 k Ω to 38 k Ω at a frequency of 1 kHz, and showed ~40-fold increase in charge transfer before and after coating [20].

Micro-machined electrodes

The second generation of neural electrodes is micro-electromechanical system (MEMS) electrodes, which can be fabricated into complicated structures using microfabrication

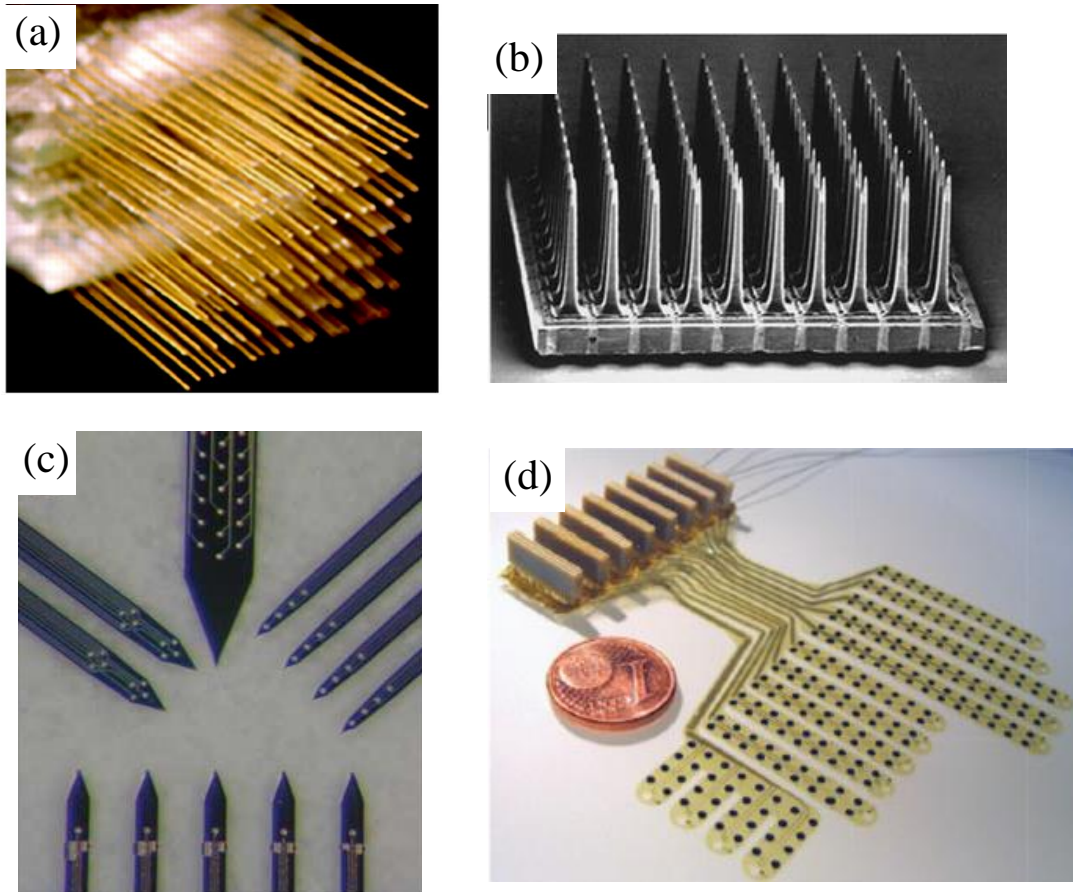


Figure 1.2 (a) Microwires [1] (b) Utah array [5] (c) Michigan probe [8] (d) flexible MEAs [9].

techniques. Microfabrication techniques provided enabled small size and accurate dimensional control that have been demonstrated by integrated circuit (IC). Recently, the techniques have been used to fabricate microelectrode arrays (MEAs) for simultaneously recording from or stimulating from a number of neurons. Different micromachining techniques are used in Bio-MEMS applications such as micro needles and implantable microelectrodes. Compare to the microwire tips that may move apart during implantation, the spatial relation between electrodes in microfabricated arrays is determined during the microfabrication process and remains fixed.

There are two major types of silicon microelectrode array: the Michigan probe and the Utah array. Michigan probe [8], made at Michigan University during 1970s, is a single-shank electrode having several recording sites on the shank surface. Figure 2(a) shows a basic structure of a micro-machined microelectrode probe for recording or stimulation in the central nervous system. The recording sites are typically made of iridium, gold, conductive polymers such as polypyrrole (PPy) or poly (3, or 4- ethylenedioxythiophene) (PEDOT), and recently CNTs. One of the advantages of these microelectrodes is a high density of sensors with predetermined locations with high spatial resolution. Furthermore, multiple sites can be formed over the shank of the electrode, thus enabling simultaneous recording of neuronal activities in the various layers of the cortex.

Another type of silicon-based microelectrodes is Utah arrays [5]. These electrodes consist of conductive, sharpened silicon needles electrically isolated from each other. The typical length of the Utah array is 1.5 mm. The tips of the needles are coated with platinum or iridium oxide (IrOx). The rest is insulated with biocompatible polymers such as polyimide or parylene-C. The architecture of these electrodes enables single-unit recording with high spatial resolution, as well as exciting the neurons by electrical stimulation. Such microelectrode array can also be safely inserted into the brain. The Utah microelectrode arrays have been extensively used in research for the last 20 years. Figure 2(b) shows the architecture of Utah arrays. Needles of different height (thus 3D) in Utah arrays also have been demonstrated.

Most MEAs are based on rigid substrates and cause neural damage and inflammation at the implant site for intracortical implantation. Flexible arrays are developed to improve the mechanical mismatch between the stiff planar silicon electrodes and the soft three-

dimensional tissues of the brain. Different polymers such as polyimide and parylene have been used as structural substrates. Parylene-based MEAs demonstrate extremely flexibility, highly conformal coverage of the muscle surface and a stable electrical contact, resulting in an improved signal-to-noise-ratio (SNR) [9]. The flexible surface of electrodes cause less tissue damage; however, surface electrodes have low sensitivity and selectivity. In addition, it is difficult to insert the flexible electrodes precisely into the nervous tissue.

1.2.3 Requirements for electrode materials

In the neural networks, ionic currents are carried via chemical species in electrolytic media (cerebrospinal fluid) to support the bioelectric potentials for the neuron communications. The communication involves the exchange of energy that is present in the form of ionic carriers and in the form of electronic carriers (electrons and holes). This is completed by means of capacitive coupling (without net charge transfer) and or by charge transfer reactions (Faradic reactions). Two most commonly used models to describe the electrochemical behavior are capacitive mechanisms (charging and discharging of the electrode double layer, no electron transfer) and Faradaic mechanisms (chemical oxidation or reduction, reversible or irreversible).

Up to now, different materials such as platinum, alloys of platinum and indium, iridium, iridium oxide, titanium nitride, conductive polymers and carbon derivatives such as graphene, carbon nanotubes, etc. have been used for the electrode arrays. It is important to consider the following properties when selecting an electrode material.

- Good biocompatibility.
- Smaller geometry size to improve selectivity.
- Safe charge injection capability with small power consumption.

- Reversible reaction during charge injection to avoid the formation of toxic product at electrode-tissue interface.
- Low polarization and impedance at the phase boundary for efficient injection of charge.
- Long term mechanical stability and corrosion resistance for chronic stimulation applications.
- Visible to MRI, X-ray and other noninvasive diagnostic techniques.

1.2.4 Electroactive nanomaterials for neural interface

The development of new materials is important in the design of seamless neural interfaces with a high degree of sensitivity. It is essential to maintain a high degree of electrode sensitivity, especially when measuring single unit action potentials with signals on the order of microvolts. Long-term stability is another motivation for the design of novel materials. Electroactive nanomaterials such as metal nanoparticles [21, 22], carbon nanotubes [20, 23], silicon nanowires [24, 25], graphene [26, 27], and conducting polymer nanostructures [28, 29] has the potential to achieve stable and sensitive chronic neural interfaces by significantly increasing the SNR. By reducing the dimensions to several orders of magnitude smaller than the dimension of the cell, the neural probe may penetrate into the neurons and have chance to accurately measure intracellular action potentials. It has also been suggested that these nanomaterials may integrate into the cell membrane and create electrical shortcuts. Therefore, the responsiveness of the neurons may be improved by forming tight contacts with the cell membranes which might favor electrical shortcuts between the proximal and distal compartments of the neuron.

Metal nanoparticles [21, 22]

Gold and platinum are the most commonly used metals for neural electrodes. They are known to be more inert under biological environments compared to other metals. For a given micrometer-sized electrode, to reduce the interfacial impedances, the surface area must be increased. Electrochemical deposition of Pt or Au is one of the measures to achieve the goal. Depositing platinum results in a highly porous electrode surface with a dendritic structure (platinum black). When a current density of $100 \text{ nA}/\mu\text{m}^2$ was applied, the sensitivity has increased by a factor of 1000. The electrode impedance was reduced from $1.4 \text{ M}\Omega$ to $10 \text{ k}\Omega$ for a $10 \mu\text{m}$ -diameter microelectrode using this method. Although it is not suitable for long-term use or implantation because of mechanical properties, platinum black has served as a standard material that enhances the sensitivity of neural sensors for extracellular recordings. Careful engineering of electrodeposition conditions can produce a stable and robust nanoporous platinum structure, with an impedance of $2.4 \text{ k}\Omega$ and a charge injection limit of $3 \text{ mC}/\text{cm}^2$ for a $45\text{-}\mu\text{m}$ -diameter microelectrode.

To enhance the electrode sensitivity by increasing the surface area, gold nanostructures have also been fabricated on microelectrodes. Nano-sized thin gold pieces (“nanoflakes”) were formed on micro-sized gold electrodes by electrodeposition, resulting in an impedance of $11 \text{ k}\Omega$ for a $50 \mu\text{m}$ -diameter microelectrode. Gold nanopillar electrodes were also fabricated using template-based methods. To directly measure action potentials (in-cell recording), three-dimensional (3D) protruding microelectrodes were introduced by the Spira group at the Hebrew University of Jerusalem. They used the electroplating process to fabricate arrays of rounded protruding gold microelectrodes (“gold spines”) that could be engulfed by neurons. The surface of these 3D gold electrodes was coated with polypeptides that bind to the cell membrane receptor proteins. In this way, a tight sealing

between the cell membrane and electrode surface was formed. They were able to record neural signals on the order of a few mV. They can also detect sub-threshold membrane activity that is generally not measurable by extracellular recording techniques.

Carbon nanotubes [20, 23]

The unique structure and properties of carbon nanotubes (CNTs) have been shown to modify electrical interfaces effectively. First, CNTs can dramatically decrease the electrode impedance and increase the charge injection limit. The interface impedance values can be reduced to 1 ~ 10 k Ω , and the charge injection limit can reach 3 mC/cm². Second, CNTs produce a stronger mechanical bond with cells, which was found to be another reason for the larger neural signals were recorded from CNT electrodes. Neurons spontaneously migrated and adhered to pristine CNT surfaces within two weeks have been reported, showing higher affinity to chemical vapor deposited CNTs than silicon nitride surfaces. This high physical affinity to the electrode surface accounts for the large signals on the order of a few hundred microvolts, or 10 times larger than conventional microelectrodes. Third, the penetration of the cell membrane by CNT fibers could enhance electrophysiological properties of neurons cultured on CNTs. This nanoscale interfacing could significantly alter the intrinsic cell properties by electrically short-circuiting neuronal compartments.

Silicon nanowires [24, 25]

Silicon nanowires have been implemented in field effect transistor (FET)-type active sensors for *in vitro* neural interface platforms. Silicon nanowire field-effect transistors (NW-FETs) arrays with active sensing areas ranging from 0.01 ~ 0.06 μm have been reported. The work shows the possibility of simultaneous recordings from the axon and

dendrites of a single neuron with NW-FET arrays. A NW-FET array (device sensitivity 31.1 nS/mV) on a flexible transparent substrate has been used to record neural signals ranging from 0.3–3 mV from neural circuits in brain slices. These works showed that the NW-FET is a promising sensor that can provide sufficient sensitivity with unprecedented spatial selectivity ($\sim 0.06 \mu\text{m}^2$). Silicon nanowires have also been used as nanoelectrodes for the neural interface. Park et al. developed a vertical silicon nanowire array with individual nanowires 150 nm thick and 3 μm high. A group of several wires can cover a single neuron, and an array of grouped nanowires was used to interrogate a small neural circuit. A high signal-to-noise ratio was achieved on the order of 100 with the measured signal amplitude on the order of a few mV.

Graphene [26, 27]

The limitations of silicon and metals include their poor stability in biological environments, relatively high electrical noise, and rigid mechanical properties which damage the surrounding tissue. Researchers have attempted to find other potential materials. As one of the candidates, graphene have attracted many attentions due to its unique properties, including its electrical conductivity and mechanical stability. Graphene is a two-dimensional single-layer sheet of sp^2 -hybrid carbon atoms in a hexagonal arrangement. Graphene has shown exceptional properties at room temperature, including high elastic modulus (ca. 1.0 TPa), remarkable thermal conductivity ($3000 \text{ W m}^{-1} \text{ K}^{-1}$), high electron mobility ($200\,000 \text{ cm}^2 \text{ V}^{-1} \text{ s}^{-1}$), excellent electrical conductivity (1 S m^{-1}), and low resistivity (ca. $10^{-6} \Omega$). Especially, the ability of easy functionalization and good biocompatibility make graphene suitable for biomedical applications. Moreover, graphene has a large specific surface area ($2630 \text{ m}^2 \text{ g}^{-1}$) and good chemical stability.

Thanks to all these distinctive properties, graphene is attractive as an attractive alternative to silicon for neural applications.

Conductive polymers [28, 29]

Conductive polymers are newly emerged type of neural interface materials for recording and stimulation. The conductivity of conductive polymers such as polypyrrole (PPy) and poly(3,4-ethylenedioxythiophene) (PEDOT) can be controlled by an electrochemical polymerization process. With the control, it is possible to lower the interfacial impedance for neural sensors. Typically, impedance of conductive polymer electrodes was ranged from 10 to 100 k Ω for 1250 μm^2 electrode. The electrical polymerization process was also found be beneficial for entrapping biological materials such as nerve growth factors or peptides on electrode surfaces. Recently, PPy or PEDOT nanotubes were also fabricated. Microelectrodes with these nanotubes had lower impedances and higher charge injection limits than those with thin-film PPy or PEDOT. In addition, longer neurites on nanotubes was also observed.

1.3 Neurochemical detection

1.3.1 Neurotransmitters

In the mammalian brain, information propagates throughout an intricate system of neuronal networks by electrical and chemical transmission. Electrical signals, also named as action potentials, are generated by ion movement (mainly Na⁺, K⁺, Cl⁻) across the neuronal cell membrane [18]. Action potentials are received in the dendritic regions of the cell, summated at the cell body. Subsequently the signal propagates via a series of voltage gated ion channels located along axonal regions, which ultimately excites or inhibits other neurons within the network. The point of communication between two neurons is known

as a synapse. At a synapse, chemical messengers (called neurotransmitters) are secreted by the presynaptic cell through a process known as exocytosis. Exocytosis is initiated as the action potential reaches the terminal region of the presynaptic terminal, voltage gated calcium channels open causing an influx of calcium into the presynaptic cell [30]. This influx of calcium signals the fusion of intercellular neurotransmitter-packed vesicles to the cell membrane, which subsequently release their content into the extracellular space between the two neurons, called the synaptic cleft.

Neurotransmitters in the biogenic amine class are consisted of catecholamines (dopamine, norepinephrine, and epinephrine), serotonin, and histamine. This “small molecule” class of neurotransmitters serves mainly to modulate neural function rather than to provide excitatory or inhibitory input. Studying this particular class of neurotransmitters collects important information in treating physiological defects that lead to developmental and cognitive disorders, as well as neurodegenerative disease states. For example, serotonin and norepinephrine have influences on mood and anxiety disorders [31], regulation of sleep-wake cycles [32], Alzheimer’s Disease [33]. Dopamine has effects in Parkinson’s Disease [34], schizophrenia [35], drug addiction and reward pathways [36].

Unfortunately, more than one biogenic amine works on each of these diseases. Additionally, biogenic amines have shown influence to each other [37]. This interaction also has clinical relevance in the treatment of a lot of diseases, e.g., schizophrenia. This integrative effect of a variety of biogenic amine terminals has also been implied in drugs of abuse, such as cocaine. Therefore, a truly integrative detection technique is required that is able to function in real-time *in vivo*, in order to appropriately study the fast, integrative and multifaceted nature of small molecule neurotransmission.

1.3.2 Techniques for sensing neurotransmission

Although many imaging and analytical techniques existed, they are not suitable for studying neurotransmitter concentration fluctuations. Neurotransmission in the brain is an extremely localized event in which neurotransmitters are released in to the extracellular space in small “microenvironments”; occurring on the millisecond to second time scale. The sampling resolution alone would exclude many available detection techniques. However, the techniques of microdialysis and electrochemistry meet the requirements and suitable for detection in such microenvironments.

Microdialysis

Microdialysis is a sampling technique that has been widely used in neuroscience. It collects extracellular fluid through a microdialysis probe (typically 150-250 μm in diameter) via the perfusion of fluid through a dialysis membrane. The dialysate can then be analyzed, either online or offline, with a variety of analytical techniques. The chromatographic and spectroscopic techniques have already been maturely developed for distinguishing neurotransmitters from possible interferents (e.g. ascorbate, urate, and acidic metabolites of monoamines) as well as from each other. However, the significant drawback of microdialysis is the poor temporal resolution at which it operates. It is generally on the time scale of minutes [38].

Electrochemistry

The significant benefit of electrochemical techniques is the fast data collection which is unattainable by microdialysis, although the sensitivity and selectivity of electrochemical sensors are still relatively low. To use the electrochemical technique, the analyte of interest must be electrochemically active. Fortunately, many molecules present within the brain are

electrochemically active. The electrochemically detectable small molecules include biogenic amines (described earlier) and hydrogen peroxide. Other physiological processes such as fluctuations in soluble gasses (e.g. nitric oxide, oxygen) and pH (via electrochemical interaction with surface groups on carbon electrodes) can also be monitored with electrochemical methods [39].

In contrast to microdialysis, electrochemical sensors are *in situ* detection methods, inherently possessing greater temporal resolution. The carbon fiber ultramicroelectrode (CFM) is the most widely used sensor for electrochemical neurobiological studies. These ultramicroelectrodes (sub 25 μm) enable even faster detection speeds because of small ohmic drops in resistive solutions, small electrochemical diffusion distances, and small double-layer capacitances [40]. The small size of the carbon fiber microelectrode also facilitates the detection of neurotransmitters in small brain areas with minimal tissue damage.

The small sensor size and fast temporal resolution make electrochemical detection an optimal choice for *in vivo* neurotransmitter monitoring. The most widely used electrochemical strategies for studying neurotransmitter fluctuations include: a potentiostatic method called constant potential amperometry, and a potentiodynamic technique called fast scan cyclic voltammetry (FSCV). The sensing mechanisms of both techniques involve the application of a voltage to an electrode which is sufficient enough to oxidize or reduce the molecule of interest at the surface of the electrode. Dopamine, for example, can be oxidized to dopamine-*o*-quinone in a two electron process. Typically these redox reactions induce a current flow in the pico to milli ampere range, depending on the type of sensor, detection strategy, and concentration of analyte.

FSCV at CFMs has been used for years to detect and identify neurotransmitters both *in vivo* and *in vitro* in real-time [41]. Redox reactions are initiated at the working electrode by the application of a triangular potential “waveform” with respect to a non-polarizable reference electrode (typically Ag/AgCl). By responding to the potential, analytes are oxidized on the forward scan and subsequently reduced on the reverse scan. Waveform is altered for different types of sensor, as well as to achieve maximum sensitivity and/or selectivity for target analytes. For example, the most effective waveform for the detection of dopamine is scanning from a resting potential of -0.4 V to 1.3 V and back to -0.4 V at a scan rate of 400 V/s. Large nonfaradaic “charging currents” was induced by such fast scan rates, due to the fast application of a voltage to the capacitive electrical double layer that exists between the solution-electrode interface. Fortunately, this capacitive current is relatively stable. After data acquisition, this background current can be digitally subtracted to yield only the faradaic constituent (current from analyte redox reactions) in the form of a cyclic voltammogram (CV).

Constant potential amperometry (or simply “amperometry”) utilizes a static D.C. voltage to generate current from analyte oxidation (~0.7 V for dopamine). The temporal resolution of FSCV is determined by the rate of successive scans (typically 10-60 Hz). In the contrast, constant potential amperometry can operate on the microsecond timescale, thus able to monitor even more rapid events, for example, the individual vesicular release events from single cells at a carbon fiber microelectrode [6]. While this technique does offer exquisite time resolution, it compromises selectivity and sensitivity. The positive holding potential limits preconcentration of all analyte which limits the sensitivity. The static potential also precludes analyte identification, which also makes it unpractical in a

multi-analyte environment like the intact brain, where many electroactive species interfere with each other (i.e. ascorbate, urate, neurotransmitter metabolites, etc.) in high concentrations.

1.3.3 Electrodes for neurotransmitter detection

Single carbon fiber electrode

The carbon fiber ultramicroelectrode is the most widely used sensor for electrochemical neurobiological studies since 1980's (Figure 1.3(a)). The fabrication of CFM generally involves the aspiration of a single carbon fiber into a small glass capillary. The capillary is then subsequently pulled around the carbon fiber to form a water-tight seal [2]. The final dimensions of the CFM are then determined by cutting the fiber under a microscope (typically 100 μm in length) to form a cylindrical electrode. The electrode can also be polished on a micropolisher to create a very small sensor that is suitable for use in single cell studies [6] (Figure 1.3(b)).

The use of carbon electrodes in electrochemical techniques enabled the direct observation of neurotransmitter fluctuations within *in vivo* and *in vitro* [41]. This coupling laid important foundation for an entire field of study within the neurosciences. On the other hand, the ability of carbon fiber microelectrodes to probe microenvironments could also be a limitation: the information is only gained about one small environment within a highly integrative system.

Multiple carbon fiber arrays

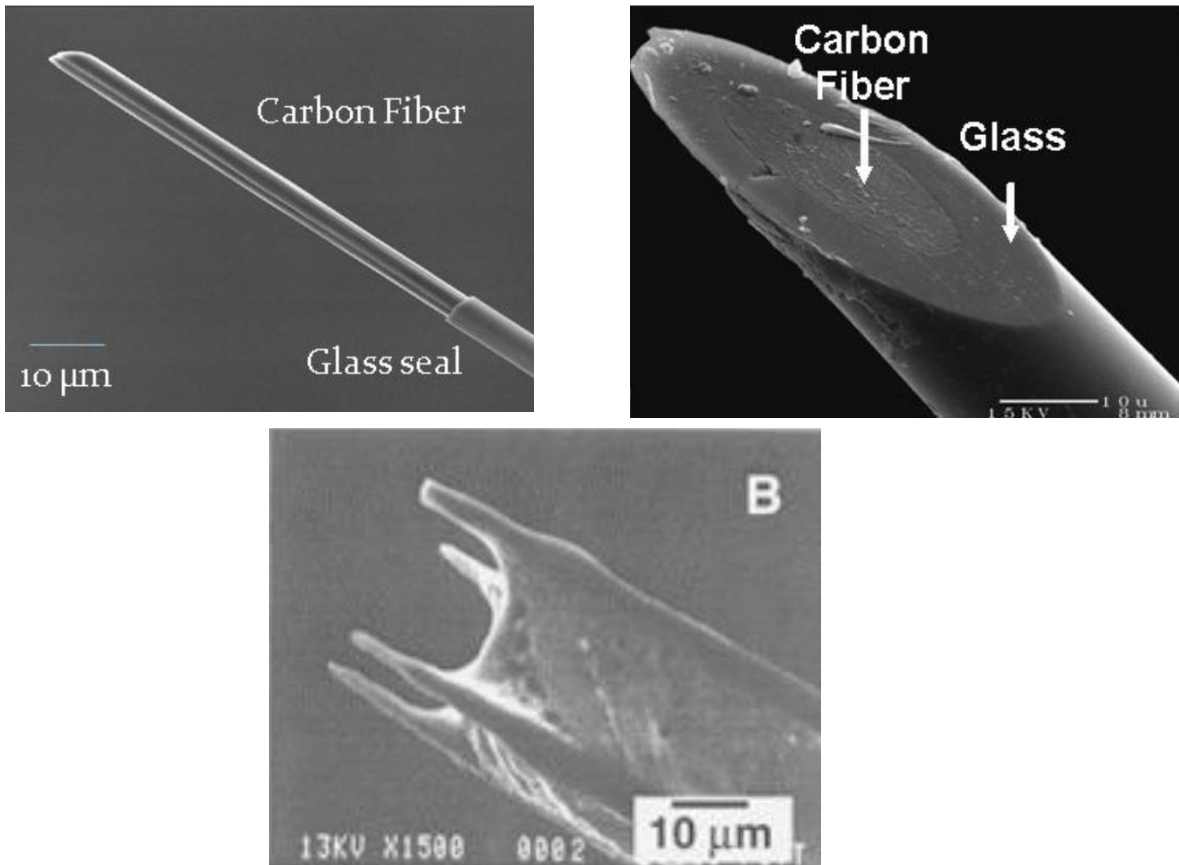


Figure 1.3 (a) Carbon fiber microelectrode [2] (b) Carbon fiber microdisc [6] (c) Carbon fiber microelectrode arrays [7].

As a matter of fact, in the studies such as catecholamine release and reuptake, neurological diseases and disorders, drug addiction and their respective treatments, microelectrode arrays (MEAs) are in need to monitor neurochemical fluctuations at spatially different locations. For years, researchers have attempted to fabricate spatially separated sensors with the ability to simultaneously monitor multiple neurochemical events. However, the conventional fabrication strategies have constraints. Such fabrication generally placed carbon fiber electrodes in multi-barreled glass capillaries, and subsequently pulling and polishing carbon fiber electrodes into multidisc electrodes (Figure 1.6(c)) [7]. The microelectrodes fabricated in this way are individually addressable,

yet not able to monitor spatially separate neurochemical events. The diffusion distance for a typical FSCV experiment done at 10 Hz, for example, is estimated to be approximately 11 μm in each direction [42]. Interestingly, the diffusion of dopamine from a synapse was also shown to be around 10 μm [43]. The arrays obtained in traditional way are not apart far enough, therefore only being able to monitor a single neurochemical event. A truly efficacious microelectrode arrays should monitor neurochemical fluctuations at spatially different locations for more applications in the neurosciences.

Microfabricated microelectrode arrays

An FSCV coupled MEA would be a valuable research tool that enables integrative electrochemical detection of neurotransmitters *in vivo*. Such a probe should be sensitive and selective towards electrochemically active molecules, with adequate fast time-response. The microfabrication of such probes would have significant advantages over other traditional fabrication methods, in the aspects of a higher degree of reproducibility, batch fabrication, and the ability to spatially separate the electrode sites at predetermined geometrical arrangements.

CHAPTER 2 INTEGRATION OF FLEXIBLE PARYLENE SUBSTRATE WITH FREELY STANDING CARBON NANOTUBES AS NEURAL INTERFACE

2.1 Background and motivation

2.1.1 Carbon nanotube MEA for neuronal recording and stimulation

The design and fabrication of CNT MEAs is the mainstream of the use of CNT in neuro-applications recently [44]. Such MEAs are generally composed of islands of high density CNTs. Both MWCNTs and SWCNTs structures have been used. CNTs were either deposited as a coating on top of metal electrodes [20, 45, 46] or directly grown from a catalyst patterned substrate [44, 47, 48].

Many works have been done by coating CNTs on metal MEAs. CNT coating has been shown effective for improving recording and stimulation. Keefer and co-workers [20] have coated indium-tin oxide MEAs with MWCNT/gold. Pristine CNT coatings were also used for coating. The fabricated MEAs were used to record and stimulate mice cortical cultures. SWCNTs were also directly deposited onto standard platinum MEAs by Gabriel et al. via drop coating and drying. The CNT coating enhanced electrical properties, decreased impedance and increased capacitance. The electrodes successfully performed extracellular recordings from ganglion cells of isolated rabbit retinas [45]. Micro-contact printing technique is another measure for coating CNTs. Fuchsberger and co-workers [46] used this technique to deposit MWCNT layers onto TiN microelectrode arrays by using PDMS stamps. The coated MEA have shown the capability for the electrochemical detection of dopamine and electrophysiological measurements of rat hippocampal neuronal cultures. MWCNT coated microelectrodes were found to have recording properties superior to those of commercial TiN microelectrodes. Drop coating and micro-contact printing methods are

quite simple to implement CNT coating. However, the synthesized film may have weak adhesion to the surface compared with covalent or electrochemical techniques, therefore limiting their wide applications.

CNT MEAs are also fabricated by direct growth of CNTs on substrates. Superior electrical properties of CNT microelectrodes were reported. Gabay and co-workers fabricated the CNT MEAs by growing high density MWCNT islands on a silicon dioxide substrate [44]. The intrinsic texture of the CNT electrodes offers a very large surface area, and consequently contributes to high electrode specific capacitance (non-Faradaic behavior was validated) and low frequency dependence of the electrode impedance. By using these electrodes, spontaneous activity of rat cultured neurons was recorded. Shein et al. [49] also directly synthesize CNT on microelectrodes and demonstrated direct electrical interfacing on rat cultured neuron. Each electrode recorded the activity from a cluster of several neurons; this activity was characterized by bursting events (see Figure 5). Later on, the same group reported the studies of the electrical activity of neuronal networks [50] and the neural interface with mice retina [51]. The results revealed gradual improvement of SNR of CNT electrode over time in the tissue-electrode coupling.

All the works above produced only randomly distributed CNTs as electrodes or coatings. Wang and co-workers presented microelectrodes composed of vertically aligned MWCNT pillars on a quartz substrate [47]. The nanotubes were functionalized with PEG to create a hydrophilic surface. The obtained hydrophilic CNT microelectrodes demonstrate a high charge injection limit without Faradic reactions. *In vitro* electrical stimulation of embryonic rat hippocampal neurons was monitored by observing intracellular calcium level change using a calcium indicator. Yu et al. [48] also fabricated

VACNF MEA and used it for potential electrophysiological applications. Extracellular stimulation and recording of both spontaneous and evoked activity in organotypic hippocampal slices was completed. Works also have been done to systematically compare PPy-coated VACNF MEA with tungsten wire electrodes, planar platinum MEA, and an as-grown VACNF MEA for the recording of evoked signals from acute hippocampal slices [52]. Recently Su and co-workers synthesized CNTs on a cone-shaped silicon tip by catalytic thermal CVD. The CNT surface was treated by oxygen plasma to convert the CNT surface from hydrophobic to hydrophilic, in order to improve CNT wettability and electrical properties. The oxygen plasma-treated three dimensional CNT probes revealed lower impedance and higher capacitance compared with the bare silicon tip. The oxygen treated CNT probes were also employed to record signals of a crayfish nerve cord [53]. These researches reveal a number of important advantages of CNT MEAs over silicon probes used in current neuroscience research and clinical applications. Silicon probes typically consist of a silicon support, silicon nitride, and silicon dioxide insulation layer. A major shortcoming of these devices is the metallic materials in use which exhibit Faradaic characteristics (compared with the capacitive CNT electrodes). In addition, the metals have shown no affinity to neuronal cells compared with the preferred neuronal adhesion to the rough CNT surfaces.

2.1.2 Flexible CNT MEA for recording and stimulation

The existing neural electrodes mostly employ silicon as substrate that is rigid and stiff, not conformal to the organs with curvilinear surface. This mismatch would induce tissue damage that is most undesirable for acute and chronic neural recording. As a result, developing soft and flexible electrode substrates has become actively pursued research area.

To date, many flexible electrodes are metals deposited on polyimide, parylene, or PDMS. Recently, the combination of flexible substrates and CNTs electrodes for neuronal applications has gained attention.

Recently a novel all-CNT flexible electrode suited for recording and stimulation of neuronal tissue has been developed. High density MWCNT films were transferred onto a flexible PDMS film to realize the flexible devices [54]. The direct growth of the CNTs on SiO₂ resulted in poor adhesion. The poor adhesion between the CNT film and the substrate make it easy of the transfer of the CNTs to the PDMS substrate. The technology is simple and the resulting stimulating electrodes showed extraordinary electrochemical properties. The capacitance was revealed to be 2 mF/cm² which is similar to that of TiN and pristine MWCNTs electrodes fabricated on a rigid silicon substrate. (2 and 10 mF/cm², respectively). Recording and stimulation tests with chick retina validate the device suitability for high-efficacy neuronal stimulation applications.

Lin and co-workers [55] implemented a flexible CNT-based electrode array for neuronal recording. The CNT electrode array was grown and patterned on a silicon substrate, then transferred onto a flexible Parylene-C film. The process included four-steps: CNT growth, polymer binding, flexible film transfer, and partial isolation. The resulting vertically aligned CNTs were partially embedded into the polymer film. Recording the electrophysiological response of a crayfish nerve cord was performed with three electrode set-up. The SNR of the flexible CNT electrode was 257.

Flexible CNT electrodes were also obtained by direct growth of CNTs on flexible polyimide substrates by catalyst-assisted CVD [56]. The growth was completed under low temperatures (<400°C). The synthesized MWCNTs resulted in decreased impedance and

increased capacitance. UV-ozone exposure was used to improve the interfacial properties between the CNT electrodes and the electrolyte by increasing the surface wettability (changing it from super hydrophobic to hydrophilic). UV-ozone treatment has shown to yield a 50-fold impedance reduction. Interestingly, flexible CNT electrodes were found to exhibit resistive characteristics, in contrast to other reports that suggested that capacitive conduction dominates. Examination of neuronal cell cultures indicated good biocompatibility. Furthermore, recordings of evoked action potential from lateral giant neurons in the abdominal ganglia of crayfish were performed. SNR was about 150, comparatively good as that of a suction pipette and better than gold electrodes (SNR of 122 and 36, respectively). Following this work, a flexible CNT MEA integrated with a chip containing 16 recording amplifiers was presented [57]. CNTs were also grown directly on a polyimide flexible substrate. The CNT microelectrode had shown electrode impedance ten times lower and capacitance six times higher than a gold microelectrode of the same size, as well as better charge injection capacity compared. Tests with cultured neurons validated the biocompatibility of the device. *In vitro* spontaneous spikes were recorded from a caudal photoreceptor from the tail of the crayfish neuron with SNR of 6.2. The *in vivo* electrocorticography (ECoG) of a rat motor cortex was also recorded by the flexible CNT MEAs.

2.1.3 Challenges and motivations

The existing fabrication methods for flexible CNT electrodes fall into two categories [19, 24, 54, 56-64]: transferring and direct growth of CNTs on polymers at low temperature ($\leq 400^{\circ}\text{C}$). Adhesion between CNTs and substrate is a big issue that hinders the development of transferring techniques. In addition, transferring processes always involve

pressing and release that can only produce mesh CNTs. Yet, CNT mesh is approximately 2D surface and not as effective as 3D structure when interfacing with neural networks [65, 66]. Recently, Lin et al. [55] developed a polymer binding method to transfer vertically aligned CNTs. This method is simple but has less control over the height of CNTs. Direct growth of CNTs on polymers can also generate 3D neural interface. But the growth of CNTs at low temperature results in inferior graphitization thus deteriorated properties of CNTs. It is also hard to control the density and height of CNTs under the low temperature limitation. Hence, it will be a significant breakthrough for neural interface technology if we can integrate vertically aligned CNTs with flexible substrate without compromising their properties. Here we develop a new technique that combines a chemical vapor deposition (CVD) of parylene and xenon difluoride (XeF_2) etching in order to integrate hybrid CNT electrodes on a ultrathin ($<10\mu\text{m}$) polymer substrate without the need for a transfer process or lowering the growth temperature. The CNT microelectrode arrays on a flexible polymer substrate have also been tested in-vivo.

2.2 Experimental

2.2.1 Fabrication of flexible CNT MEA

Flexible CNT MEAs were fabricated using the process flow as demonstrated in Figure 2.1. The process steps are described as follows. (a) After standard cleaning, 300nm low stress silicon-rich nitride was grown on a silicon substrate using a low pressure chemical vapor deposition (LPCVD). Ti/Pt (20nm/200nm) was evaporated and then patterned by lift-off to serve as electrodes, contact pads, and interconnects. Arrays of holes were defined on Pt to serve as etching windows for the final release step. The typical diameter of the etching holes is 10 μm with spacing of 50 μm . (b) In a second lift-off step, TiN (100nm) was

selectively patterned on the electrode areas, followed by RF sputtering of a 2nm thick Fe layer. The wafers were then loaded to the thermal CVD chamber for the CNT growth. The growth took place in a gas atmosphere of C_2H_4/NH_3 at 80 torr for 30 min. (c) To protect the synthesized CNT arrays from the following process steps, a layer of photoresist was spun to coat the CNTs. (d) Afterwards, a 3um thick parylene C layer was deposited by CVD. (e) Then oxygen plasma etching was applied to open the etching holes. XeF₂ isotropic gas phase silicon etchant is applied to undercut the bulk silicon in the handle wafer for device release. This technology is simple and CMOS compatible. No transfer printing process is involved. (f) Subsequently, a second parylene layer (10um) was deposited to encapsulate the device and seal the etching window as well. Finally, electrodes and contact pads were opened by oxygen plasma before the release of the flexible device from the substrate.

2.2.2 Appearance of the flexible device

The overall view of the device was captured by Bruker White Light Interferometer. It is a powerful 3D optical microscopy technique in characterizing large surface with 3D features.

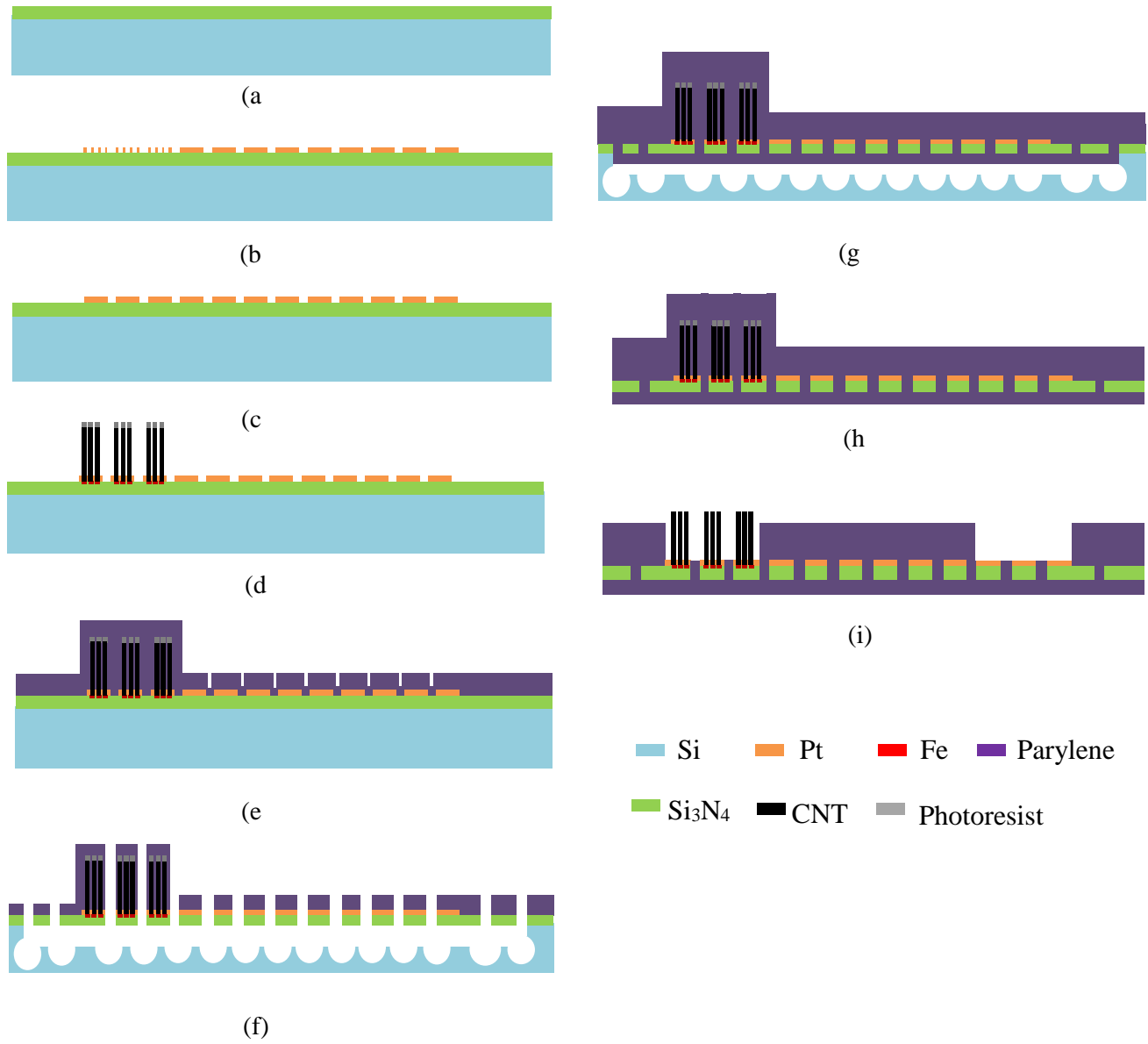


Figure 2.1 Fabrication process flow

2.2.3 Characterization of CNTs

The morphologies of the synthesized CNTs were analyzed by Scanning Electron Microscopy (SEM). The images were obtained using a JSM-6510LV SEM at 15KV accelerating voltage. The degree of graphitization for CNTs was measured using the E-Z Raman spectroscopy system at 532 nm excitation.

2.2.4 Electrochemical characterization of the flexible CNT MEA

Electrochemical measurements were performed in Phosphate-buffered saline (PBS, pH7.4) solution. Experiments were done in a glass beaker using a three-electrode system inside a Faraday cage. The flexible CNTs/Graphene electrode served as working electrode, and a Pt wire acts as counter electrode. A commercial Ag/AgCl was used as reference. All the electrodes were connected to the impedance analyzer (HP4284) to apply with an alternating current (AC) of 50mV at swept-frequency of 20 Hz to 100 kHz. The same configuration was used for cyclic voltammograms (CV). The measurement instrument was Gamry PC4 Potentiostat. The potential window was ranged from -0.3V to 0.9V. All the measurements were taken after an initial electrochemical cleaning step where the electrode potential was cycled at 2V/s until a stable and reproducible response was observed.

2.2.5 Electrophysiological experiments

The capability of the flexible CNT MEA to stimulate and record neural activity in vivo was examined. All procedures were approved by the Wayne State University Animal Investigation Committee. The experiments were performed on adult male Sprague-Dawley rats weighing 350-400g. They were sedated and anesthetized by an intramuscular injection of ketamine hydrochloride (43 m/kg), xylazine (7 mg/kg), and butorphanol (0.1 mg/kg). Supplemental doses were used as needed to maintain anesthesia throughout the

experiment. After operation, the L5 lumbar spinal nerve and left sciatic nerve were exposed. After cutting the dura, a pool was formed from skin flaps, and the spinal cord and nerve roots were immersed in warm (37°C) mineral oil to prevent them from drying. The electrical stimulation was applied at sciatic nerve and the neural signal was recorded at the spinal nerve. The impulses on two channels were amplified, monitored on an oscilloscope and an audio monitor, digitized, and analyzed using PC-based spike discrimination and frequency analysis software. All software was part of the Computerscope Enhanced Graphics Acquisition and Analysis (EGAA) system (R.C. Electronics, Goleta, CA). For later detailed analysis, the data were also simultaneously recorded on an analog tape recorder (MR-30, TEAC, Montebello, CA).

2.3 Results and Discussion

2.3.1 Characterization of the flexible device and CNTs

Figure 2.2(a) is the optical image of the obtained device. The electrodes can be flexed by tweezers over almost 180° without breaking. The good flexibility is owing to the low elastic modulus of parylene C, which is of 2~4 GPa, about two to three orders of magnitude lower than that of metal and silicon [67]. Micrometer-scale thickness is also important to provide the required flexibility. To evaluate the thickness, clean glass slide was used as control in the parylene growth processes. The thickness of the parylene on control sample was measured by Bruker Dektak XT surface profiler. The two times of evaporations produced about 10 um thick parylene. Electrodes were observed under microscope before and after bending. No obvious changes of CNT electrodes were found, indicating good adhesion between the CNTs and polymer substrate.

The overall surfaces of the CNT electrodes are revealed by white light interferometer

image in Figure 2.2(b). The device is featured with 16 electrodes. Each electrode consists of array of 12 carbon nanotube pillars. Each CNT pillar is sized of 20 x 20 um with distance of 50 um to each other. Thousands of nanotubes interact through Van der Waals to form free standing pillars projecting orthogonally from the surface. The height of the CNT pillar is measured to be about 2um. The cross-sectional SEM image of an as grown CNT pillar (Figure 2.2(c)) also proves a homogeneous height of 2um and an average nanotube diameter of 35 nm. Figure 2.2(d) is the SEM image of the CNT electrode on parylene. The undercut can be clearly seen, in consistent with the described fabrication process. Higher magnification SEM (Figure 2.2(e)) reveals that CNTs are freely standing instead of lying on the surface after the process, proving the advantage of our technology to integrate parylene substrate with 3D CNT structure. The intrinsic 3D nanostructure is believed to be more effective in neural stimulation/recording than CNT mesh that is often associated with the transferring techniques [68]. The height of CNTs seems to be shrunken compared with the as grown CNTs. This may be due to the diffusion of parylene which results in crouched CNT tips. Raman spectra (Figure 2.2(f)) have verified the materials distribution over the electrode. In specific, ordered graphite induces G band at $\sim 1580\text{ cm}^{-1}$, defective/amorphous carbon is indicated by the D band at $\sim 1350\text{ cm}^{-1}$. The I_G/I_D is about 0.9, indicating high degree of graphitization of the CNTs in our research [69]. Although no Raman spectra was provided in the low temperature growth techniques for flexible CNT devices, other researches have proven the poor properties resulted from lowering the CNT growth temperature [70].

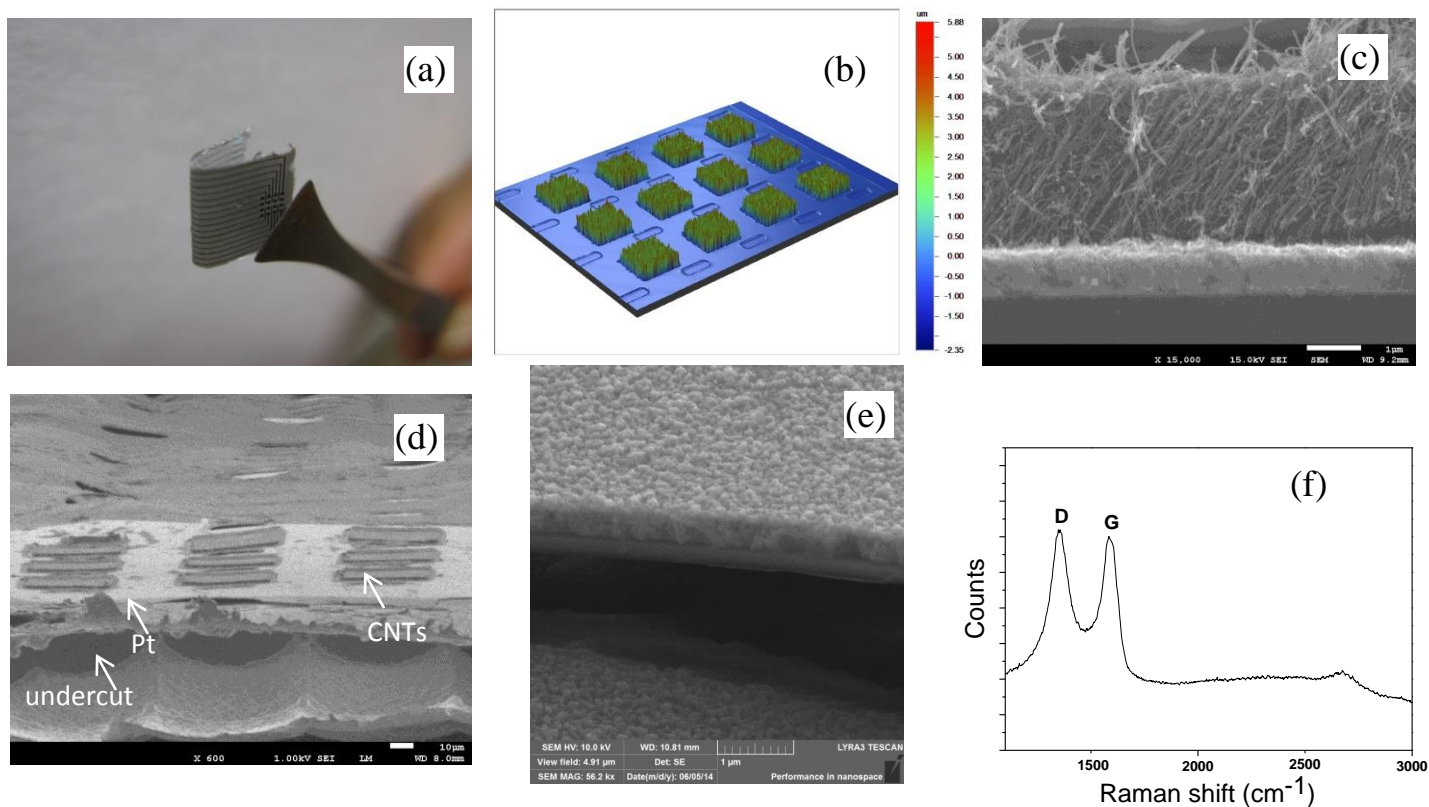


Figure 2.2 (a) optical image of the flexible devices, (b) white light image of the electrode area, (c) SEM image of the as grown CNTs, (d) SEM image of the flexible CNT electrode before neural stimulation and recording, (e) higher magnification SEM of (d), (f) Raman spectra of the CNT electrode.

2.3.2 Electrochemical characterization of CNTs electrode

The CNT electrodes were characterized electrochemically by cyclic voltammetry (CV) and electrochemical impedance spectroscopy (EIS), as depicted in the materials and methods section. Electrochemical performances of the electrodes were evaluated in terms of impedance (Z) and charge storage capacity (CSC). The calculation of CSC was done with a custom MATLAB (mathworks Inc., MA) script. Although the applications may vary, the primary requirements for neural electrodes are low Z for recording or large CSC for stimulation [71]. Low Z can minimize the noise. On the other hand, large CSC can potentially reduce the electrical damage to the electrodes and tissues, thus improve long

term stability.

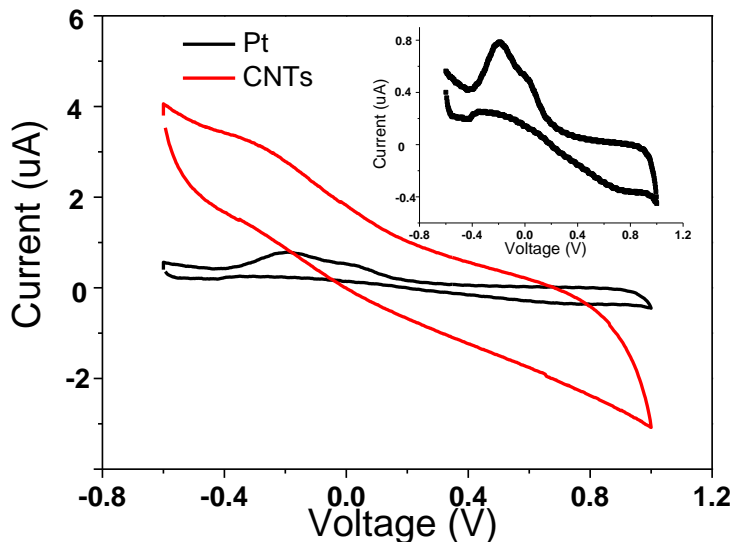


Figure 2.3 CV of the CNT electrode and Pt electrode, the inset is the CV for Pt electrode at different scale.

The Figure 2.3 is the typical voltammograms obtained with the CNT and Pt electrodes. Cyclic voltammetry is normally used to evaluate the redox characteristics and the charge storage capacity of the electrodes. For neural stimulation, it is critical to avoid faradic reactions that may cause degradation of electrodes and/or release toxic chemical species that may damage the surrounding tissue [72]. In figure 2.3, CNT electrode shows a strong capacitive response as evidenced by the large area under the CV curve and the lack of large faradic features. In contrast, the voltammogram for Pt, as shown in the inset of Figure 4, exhibits typical H adsorption and desorption between -0.6 and -0.2V and a broad Pt oxidation band between 0.25 and 0.9V. The large current step in the cathodic sweep between 0 and 0.2V is due to the reduction of dissolved O_2 [73]. The difference in the currents (Δi) between positive and negative potential cycles corresponds to the sum of the charging and discharging currents at the electrode-electrolyte interface [74]. Clearly, the

greater the Δi , the larger the enclosed area of the CV curve, the larger the amount of the mobile charges that were moved in and out of the interface during the cycle. The amount of charge passed during the CV cycle is also referred to as charge storage capacity (CSC). The visual comparison of the CV curves reveals that the CSC of the CNT electrodes is much larger than that of the Pt electrodes. For quantitative comparison, the integrated areas of CV of both electrodes were calculated. The CSC of CNT electrodes were about 8 times larger than bare Pt electrodes. This disparity is due to the roughness and 3D structure of the CNT films. Greater interfacial area provides more sites for ions to interact with. As the CSC is essentially a measure of the total amount of charge available for a stimulation pulse [42], greater CSC generally means higher efficiency for neural stimulation.

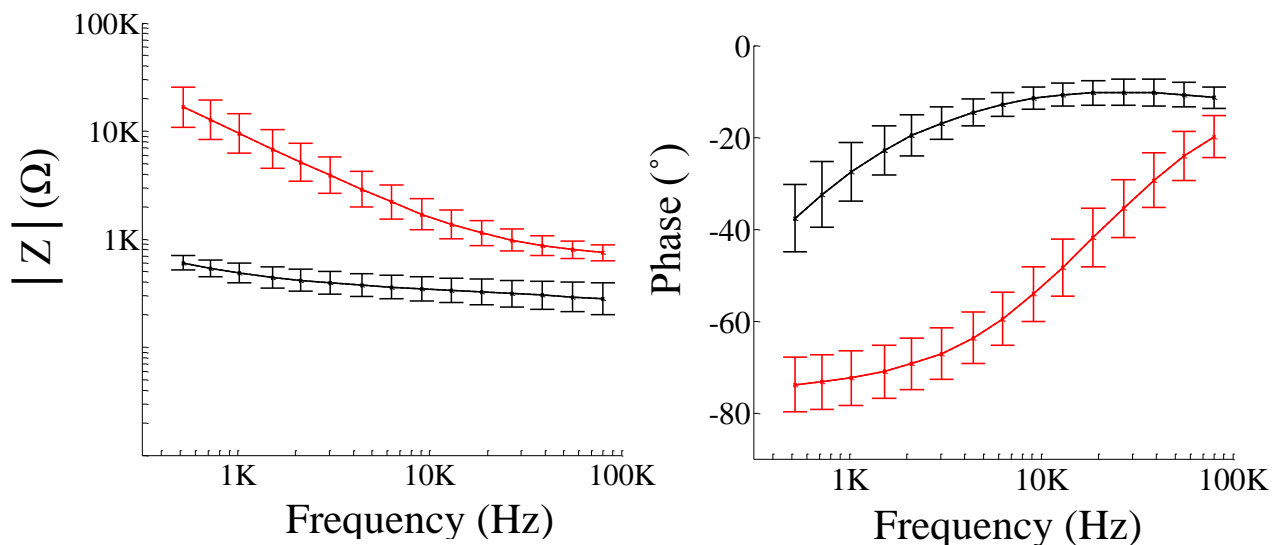


Figure 2.4 (a) magnitude of impedance spectra, (b) phase of impedance spectra (red is the Pt electrodes, black if the CNT electrodes)

The impedance spectrum of CNT coated electrodes in comparison to bare Pt electrodes is represented in Bode plots (Figure 2.4). The modulus of impedance of the bare Pt electrodes is significantly lowered after CNT deposition, particularly at frequencies below 10 KHz. The dramatic reduction of impedance of CNT electrodes is possibly due to increase of effective surface area and the high electrical conductivity of the CNT films. The efficiency of a recording electrode is usually measured in terms of its impedance magnitude at 1 kHz, which is the physiological relevant spiking frequency of neurons. It is reported that $Z = 1\sim 2$ MOhm is sufficiently low for successful neural recording [75]. In this research, impedance of CNT electrodes is about 480 Ohm at 1 KHz, about 10 times smaller than that of Pt electrodes. Decreasing the impedance of an interfacial electrode would enhance the ratio of signal to noise (SNR) of the neural spike by increasing the

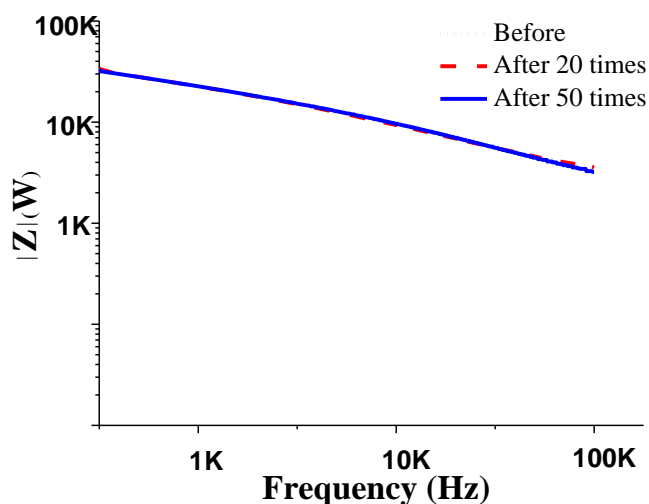


Figure 2.5 Impedance spectra of flexible devices before, after 20 times and 50 times bending

transmitted electric current and decreasing the noise. The accessible surface area of the CNT electrodes is not directly measurable, but is proportional to the interfacial capacitance. The interfacial capacitance can be calculated by fitting the impedance data to an equivalent

circuit model, where the interface is represented by a constant phase element in parallel with the faradic impedance and then in series with the solution spreading resistance [47]. The fitted capacitance is 1.1 mF/cm^{-2} for CNT and 0.1 mF/cm^{-2} for Pt. The ranges of the measured capacitance for the existing CNT MEAs are between 0.1 to 10 mF/cm^{-2} [54]. It is worth noting that for the direct grown CNT on polyimide electrodes, the value is 0.2 mF/cm^{-2} [56]. This difference may be due to the inferior CNT properties caused by low growth temperature. The long term stability of the flexible CNT electrodes was also tested by means of impedance measurements. Figure 2.5 presents the impedance spectrum of a flexible device before and after 20 and 50 times of being bent and flattens. The variation of the interface impedance was less than 1% after 50 times bending. It confirms the good adhesion of the CNT films to the substrate. The Pt tracts must also have remained intact without break during the bending.

2.3.3 Neural stimulation and recording by flexible CNTs electrode

To demonstrate the capability of the CNTs electrodes for neural recording and stimulation, neurophysiologic experiments were conducted with rats. The animal

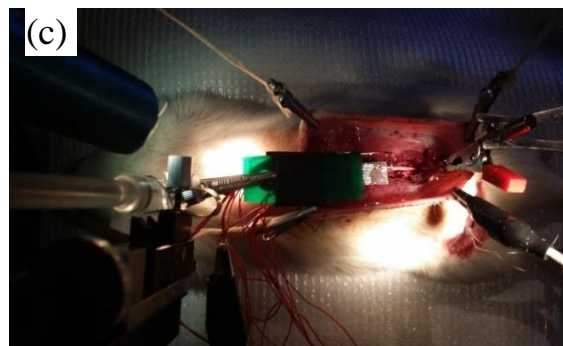
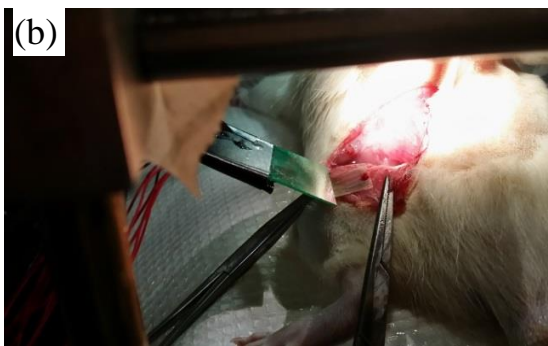
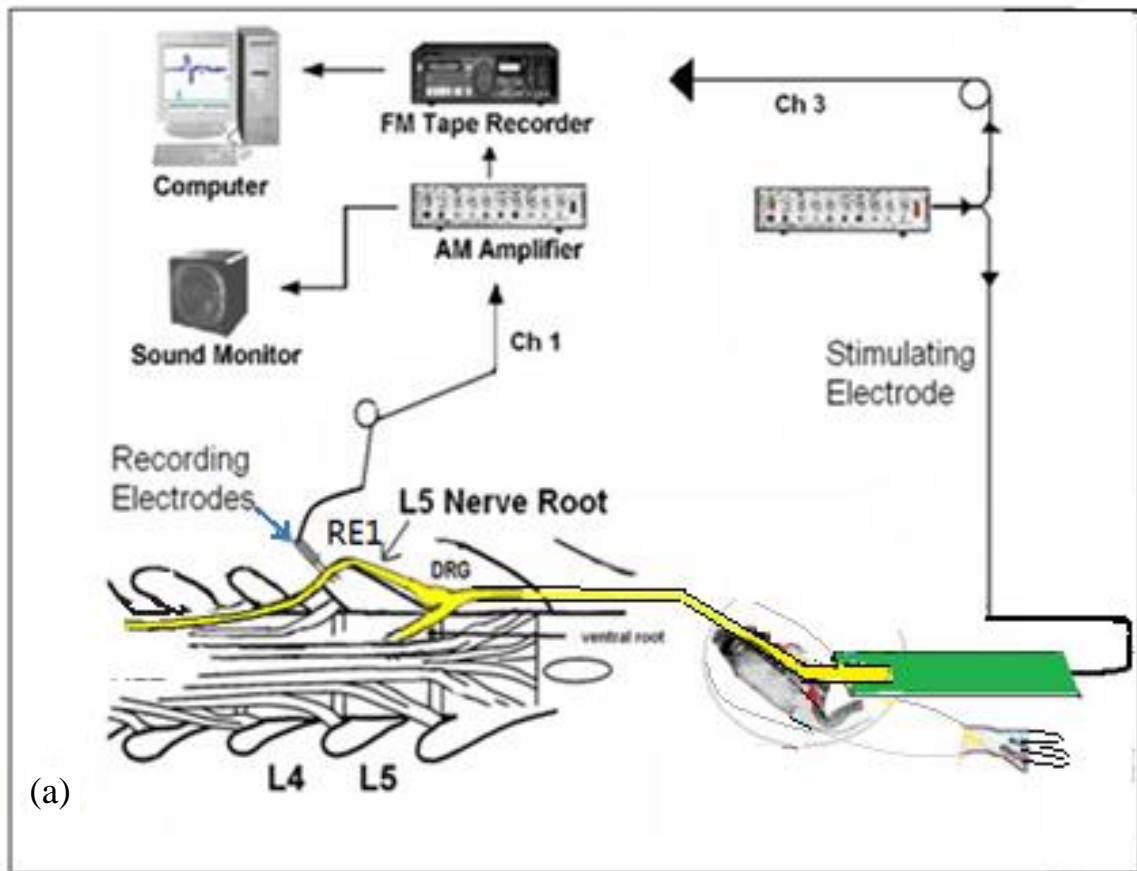


Figure 2.6 (a) schematic of experimental set-up for physiological testing (b) neural stimulation at sciatic nerve with flexible CNT electrode (c) neural recording at spinal cord with flexible CNT electrode

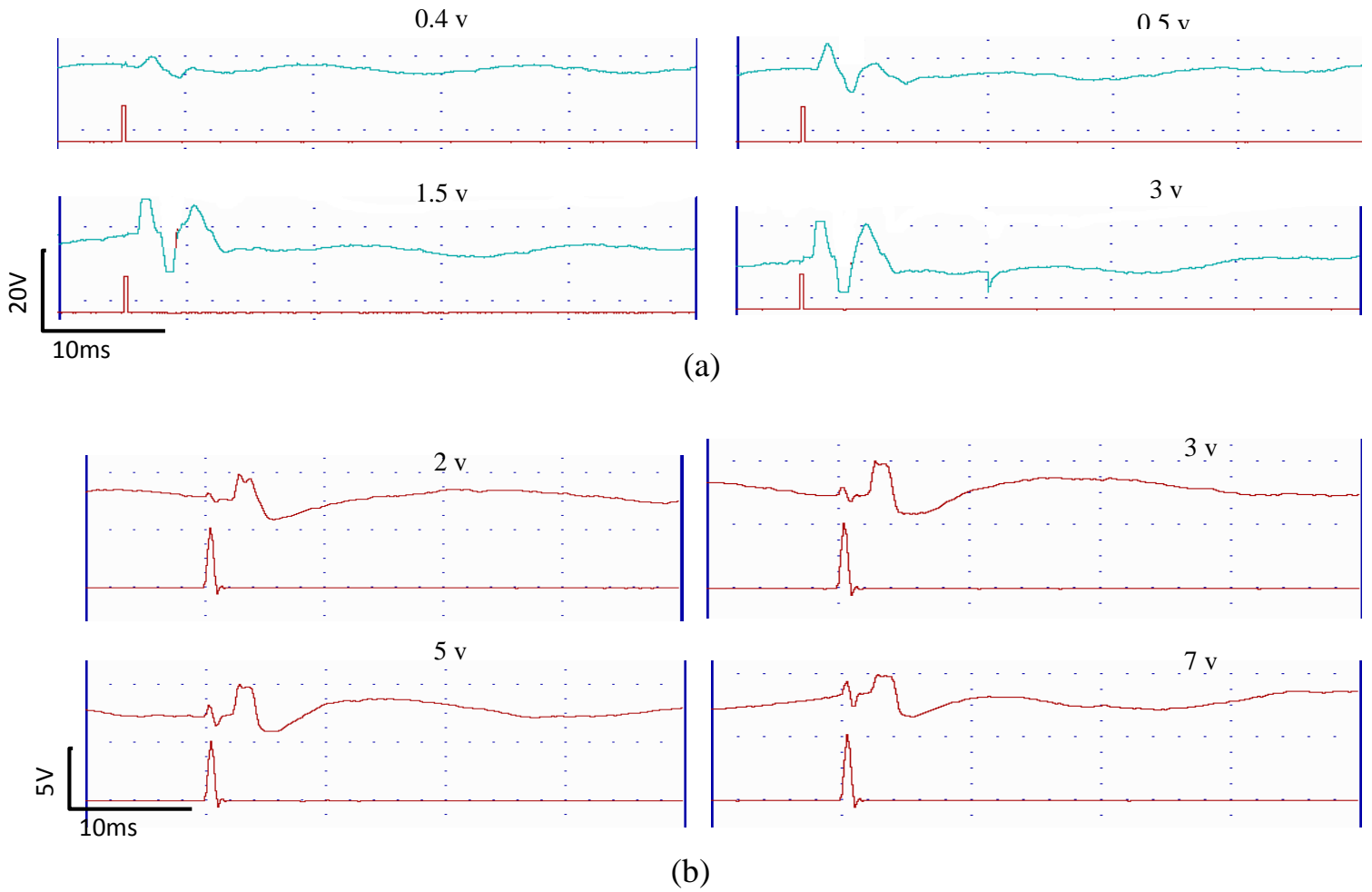
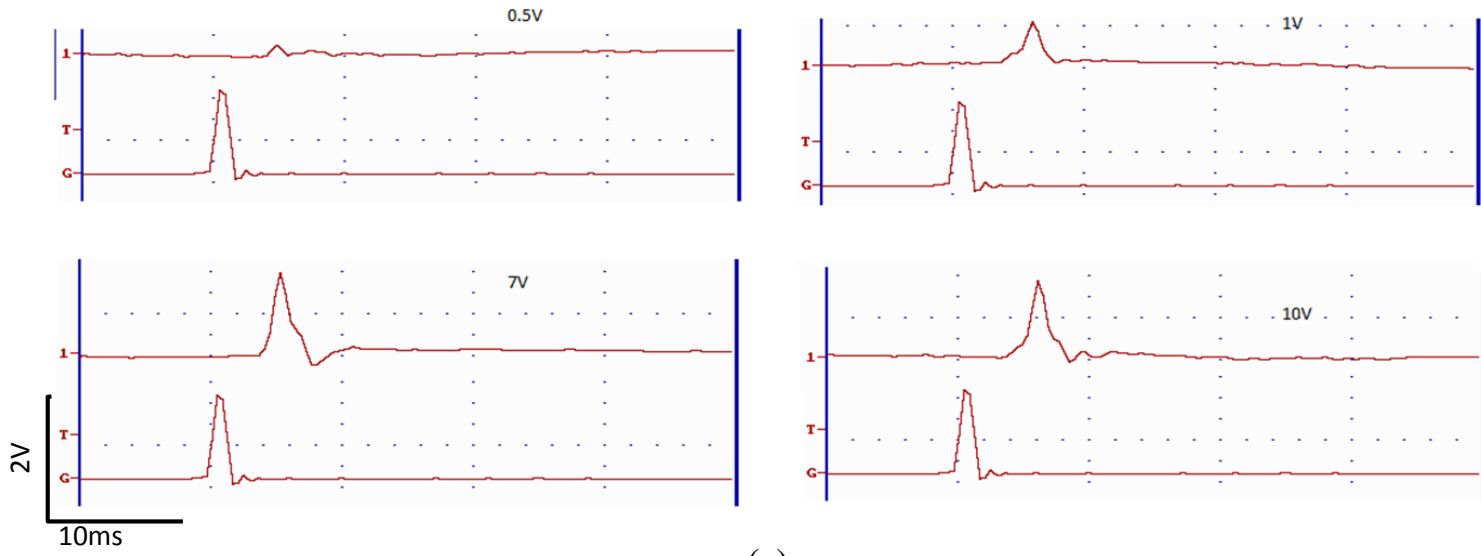
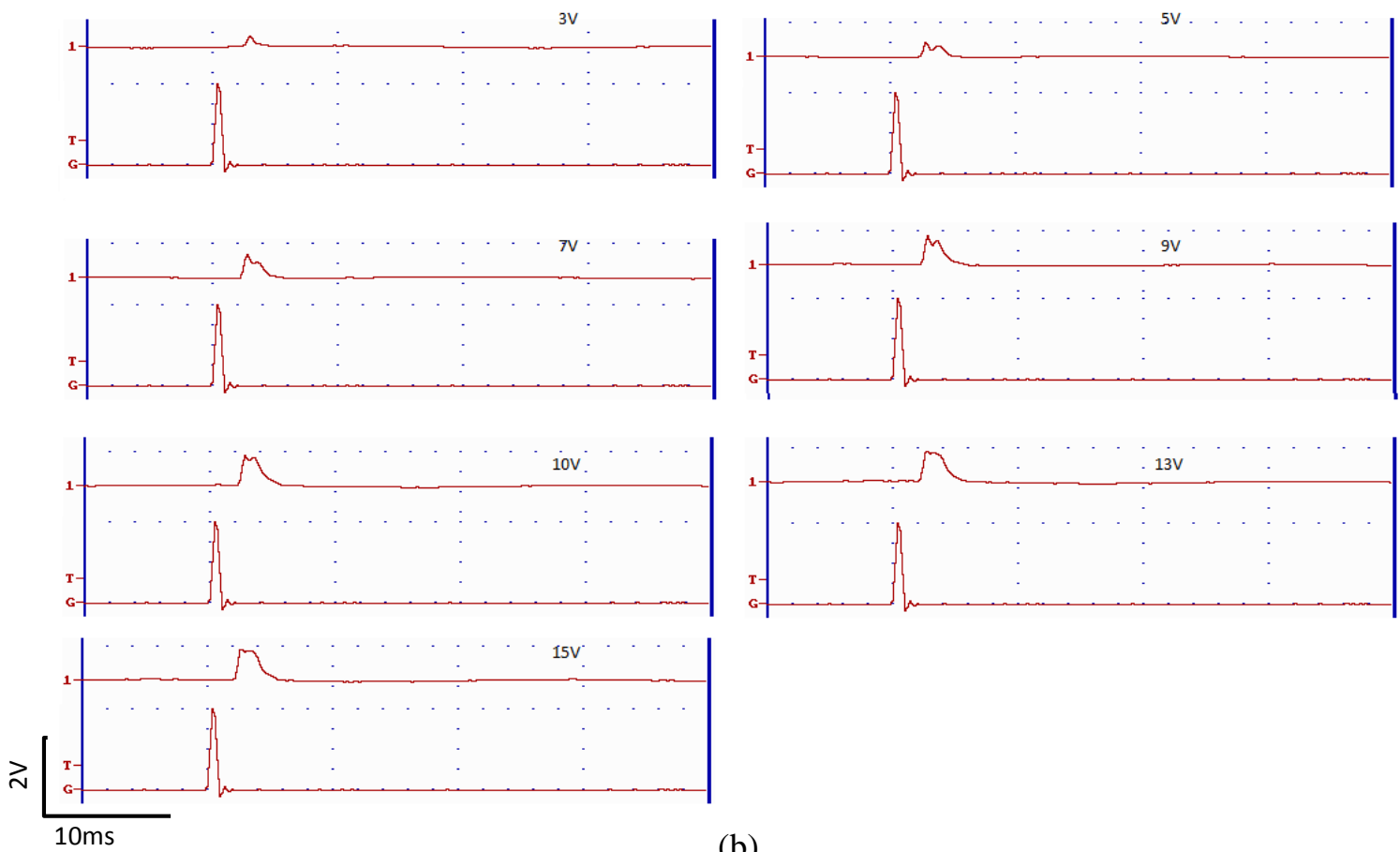


Figure 2.7 (a) neural recording with the flexible CNT electrodes (b) neural recording with the Pt electrodes



(a)



(b)

Figure 2.8 (a) neural stimulation with the flexible CNT electrodes (b) neural stimulation with the Pt electrodes

preparation procedure and the neural recording/stimulation have been described in the Materials and Methods section. Figure 2.6 shows the experimental setup. The proximal end of the L5 spinal nerve was separated from the spinal cord. The sciatic nerve was cut at the distal end before the sciatic nerve divides into the tibia and peroneal nerve. For neural recording, the L5 spinal nerve was draped over the flexible CNT MEA to record impulses. The stimulation was applied in the sciatic nerve stump by bipolar Pt electrodes. The data recorded on a tape cassette were digitized and analyzed using spike discrimination and frequency analysis software. Figure 2.7(a) shows the neural activity recorded by CNT electrodes. The quality of the recordings is typically evaluated in terms of signal amplitude and signal-to-noise ratio. The root-mean-square of the noise voltage is about 12. Dividing the peak-to-peak amplitude of action potentials by the root-mean-square of the noise generates the signal to noise ratio (SNR) [76]. The calculated SNR is 12.5. However, it should be noted that the amplitude of the signals in extracellular recordings depends on the distance between the neuron and the electrodes; the SNR depends on the examined tissue as well as the size and shape of the electrode. Thus they can only be used to confirm the acceptable performance of the MEAs but not a direct measure [54]. Compare with platinum electrodes (Figure 2.7(b)), we can see that CNT electrodes are able to detect action potential generated by lower stimulation voltage, indicating higher sensitivity. The flexible CNT MEAs were also employed as a neural stimulator to evoke CAPs in sciatic neurons with a pair of platinum hook used as recording electrodes. 0.1-10 V of stimulus pulse (1 Hz, 0.3 ms duration) was applied. As shown in Figure 2.8(a), the threshold voltage to initiate the spike was determined to be 0.4V, lower than that reported by other CNT MEA technologies. In comparison, the Pt electrodes (Figure 2.8(a)) exhibit higher threshold voltage for

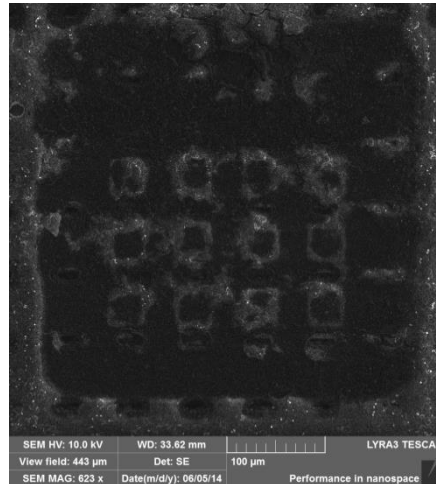


Figure 2.9 SEM image of flexible CNT electrodes after neural recording and stimulation (3V). The electrodes were precisely positioned using the micromanipulator to decrease the effect caused by position difference between testing of CNT electrodes and Pt electrodes. The results are in good agreement with the aforementioned electrochemical characteristics. The SEM image of flexible CNT devices was taken after neural recording and stimulation (Figure 2.9). The tissue coverage caused serious charging effect. But it still can be seen that the CNT bundles still existed, indicating good stability of the device.

2.4 Conclusions

Despite the great efforts, fabrication of reliable, efficient, and long term stable electrodes for neural stimulation/recording still remains challenges. One of the keys is to reduce the electrode size but still keep low impedance and high charge injection capacity. To meet the requirements, high surface area coatings are usually applied. CNT is one of the research focuses because of their extremely large surface area and superior electrical conductivity, as well as good chemical inertness. Furthermore, CNT is mechanically strong but also compliant to bending or twisting without break, which makes CNT very suitable for flexible electronic applications, especially for flexible MEAs in implantable

applications. The current technologies to integrate the CNTs with the flexible substrates usually suffer from low CNT yield and bad adhesion in transfer printing process or inferior properties in low temperature direct growth on polymers. In this paper, we demonstrated a new technology to fabricate flexible CNT based MEAs. The whole device is encapsulated by two layers of parylene. CNT growth is done before parylene evaporation thus eliminating the low temperature limitation as in the direct growth of CNTs on polymers. Consequently, it is realizable to control the properties, height, and density of the CNTs. Another advantage of our technology is that it maintains vertically standing CNTs (3D) rather than CNT meshes (2D). The 3D structure take the greatest advantage of the strength and the flexibility of CNTs, predicting higher efficiency in neural implant applications. Compared with polymer binding method, our technique integrates 3D CNT structure with flexible substrate in a more controllable way. The electrochemical performances of the fabricated devices were assessed by CV and EIS in PBS and compared against co-fabricated Pt microelectrodes. The impedance for CNT electrodes at 1 KHz was 10 times smaller than that of Pt electrodes. The voltammogram indicate capacitive current delivery for CNT electrodes and faradic for Pt electrodes. Also the CSC of the former is 8 times larger than that of the latter ones. The results revealed superiority of CNT as electrode for neural prosthetic applications compared with Pt. The interfacial capacitance (1.1 mF/cm^2) is comparable to the reported values measured with CNTs on either rigid or flexible substrates ($0.1\sim 10 \text{ mF/cm}^2$). The evident improvement compared with the directly grown CNT electrodes on polyimide ($0.1\sim 0.2 \text{ mF/cm}^2$) may be due to the higher growth temperature. Testing of flexible CNT electrode was also performed on rat spinal nerve and sciatic nerve. CNT electrodes demonstrate a SNR of 10 and a

stimulation threshold of 0.4V. This work represents an innovative approach toward realizing advanced flexible neural probes for high resolution neural recording and stimulation.

CHAPTER 3 CARBON NANOFIBER MICROELECTRODE ARRAYS FABRICATED BY PLASMA ASSISTED PYROLYSIS FOR FAST SCAN CYCLIC VOLTAMMETRY ANALYSIS

3.1 Background and motivation

3.1.1 Carbon based microelectrodes for electrochemical detection

Carbon materials have been widely employed in micro-sensor fabrication because they afford excellent biocompatibility and rich surface chemistry at low cost [77, 78]. Traditional manufacturing processes for carbon-based microelectrodes include encapsulation of carbon fibers with insulation materials [79-81], deposition of carbon materials directly on micro-pipets [82, 83], and formation of carbon from pyrolysis of polymer or photoresist coated on micro-pipets [84, 85]. The application of these single-unit configurations is limited in integrative environments where spatial resolution and multiple targets are of great significance.

Recently, micro-fabricated carbon electrodes with multiple sensing elements have become a promising alternative. Carbon films were sputtered [86] or vacuum-deposited to the substrates [87]. However, these microfabrication processes suffer from poor adhesion [88]. A more encouraging microfabrication process involving pyrolysis of a patterned photoresist has recently been developed to form carbonaceous microelectrode arrays (MEAs) [42, 77, 88-99]. Photoresist, as an initial material for microelectrode fabrication, is especially advantageous because it is finely patterned by lithography techniques with high spatial resolution and repeatability [100]. Plenty of work has been done on characterization of photoresist derived carbon films, and they have shown electrochemical properties comparable to glassy carbon [100-102]. The pyrolyzed photoresist microelectrodes have been applied to sensing various species, such as neurotransmitters

[42, 91, 93-95], O₂ [42], glucose [98, 99], H₂O₂ [96], DNA [103], oncoprotein [97], Hg [104], Ni [92], etc.

3.1.2 Fast scan cyclic voltammetry

For the in-vivo measurements of neurotransmitters, high sensitivity, chemical selectivity, and fast temporal resolution are desired. Various detection schemes have been used to analyze concentrations of biological species *in vivo* and *in vitro* [40]. Microdialysis is the most widely used for sampling the chemical environment of the brain. This technique provides high degree of sensitivity and selectivity. But it suffers from the slow temporal resolution. Constant potential amperometry offers the best temporal resolution. But it lacks of chemical selectivity. In comparison, background-subtracted fast-scan cyclic voltammetry (FSCV) has been shown good chemical selectivity while retaining subsecond temporal resolution. These characteristics make FSCV a very useful tool especially in studies of the brain, as it is able to easily identify oxidized compounds, such as catecholamines [41]. For example, it can be used to evaluate the drug mechanisms associated with the dopaminergic transmission, which may guide the therapeutic intervention in pathologies such as Parkinson disease, schizophrenia, and drug addiction [33]-[34].

FSCV measurements is usually conducted in a flow injection system [3]. A flow injection system consists of a six port injection valve and a variable resistance infusion pump. The pump is used to introduce the buffer and analytes to the electrodes. A potentiostat is used to apply waveform and record current. The CV plot, obtained when only buffer is introduced, is used as background. After dopamine injection, the obtained

CV plot will subtract the background and generate the FSCV plot with clear oxidation and reduction peaks. The FSCV working theory is demonstrated in Figure 3.1.

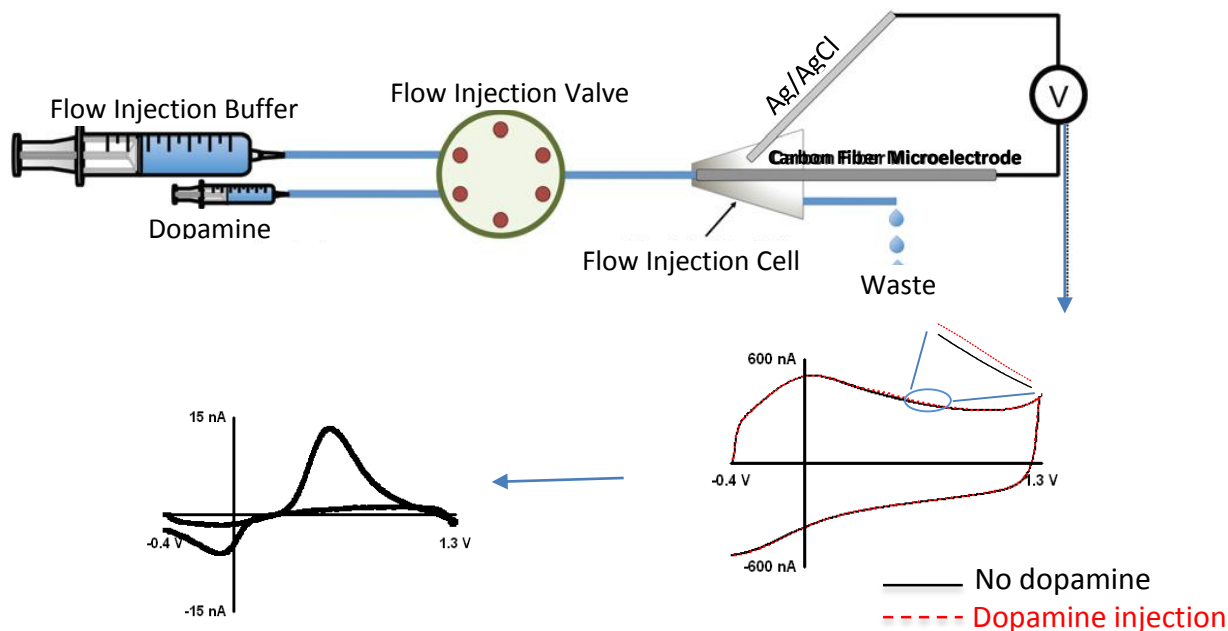


Figure 3.1 Schematic of FSCV working theory [3].

3.1.3 Challenges and motivations

FSCV with carbon fiber microelectrodes (CFMs) has been extensively applied for electrochemical analysis of neurotransmitters (i.e., dopamine, serotonin, histamine) and trace metal ions (i.e., Cu^{2+} , Pb^{2+}) [105-107]. Pioneering work on developing FSCV compatible pyrolyzed photoresist film arrays has been reported by Zachek and Wightman [42, 95]. They employed photoresist derived MEAs for dopamine detections using FSCV and applied an extended electrochemical waveform to over-oxidize the carbon surfaces for improved sensitivity [42, 95]. The surface modification by over-oxidation is believed to enhance the adsorption of dopamine and consequently increase the sensitivity [108].

It has been well accepted that increasing reactive surface area is an effective way to decrease limit of detection (LOD) and improve sensitivity of microelectrodes [89]. While

geometry surfaces are miniaturized, a number of approaches have been used to increase the physical reaction sites, including 3D architecture [89, 91, 98], coatings of nanomaterials [96, 99], flame etching [80], laser activation [109], and electrochemical treatments (e.g., overoxidation) [108, 110-112]. These methods either generate new surface area or refresh the surface by removing uninterested reactants. However, none of these methods retain both good controllability/repeatability and easy processibility.

In this paper, we propose a novel method to fabricate nanofiber structured MEAs from pyrolyzed photoresist. Dual oxygen plasma treatments were employed to achieve excellent electrochemical sensitivity. The plasma treatments are easy to control and readily integrated with microfabrication process. Moreover, it is believed that the plasma treatment causes compressive stress within the electrodes, which contributes to the improvement of the adhesion between the carbon films and the substrate, therefore boosting electrode stability. Dopamine, which is extensively characterized via FSCV, was chosen as the probe to display the electrochemical response of the MEAs fabricated in different conditions. The stability of the obtained MEAs have also been investigated for the first time for photoresist originated carbon electrodes. And the synergistic effects of using negative photoresist, two step pyrolysis, and the compressive stress caused by plasma on enhanced stability has been proposed and discussed. The carbon based MEAs developed in this work shows excellent unit sensitivity and stability. This advanced strategy represents a robust approach to fabricate MEAs with good control of surface area and conditioning, which will eventually be differently functionalized for simultaneous multi-target detections.

3.2 Experimental

3.2.1 Chemicals

Dopamine solutions were prepared by immediately dissolving dopamine HClO into Tris-buffer prior to each experiment. Tris-buffer ingredients (15 mM $\text{H}_2\text{NC}(\text{CH}_2\text{OH})_3 \text{HCl}$, 140 mM NaCl, 3.25 mM KCl, 1.2 mM CaCl_2 , 1.25 mM $\text{NaH}_2\text{PO}_4 \cdot \text{H}_2\text{O}$, 1.2 mM MgCl_2 and 2.0 mM Na_2SO_4 with the pH adjusted to 7.4) were purchased from EMD Chemicals Inc, USA. All aqueous solutions were made with deionized water.

3.2.2 Electrode fabrication

The process flow of the electrode fabrication is shown in Figure 3.2. After standard RCA cleaning, 1 μm low-stress silicon nitride was grown on a silicon substrate by low-pressure chemical vapor deposition (LPCVD). Ti/Pt (20 nm/200 nm) was deposited by e-beam evaporation and patterned by lift-off to serve as electrode pads and interconnection. 2 μm silicon oxide was deposited by plasma enhanced chemical vapor deposition (PECVD) and patterned to expose electrodes and contact pads. SU-8 photoresist was patterned onto the electrode area. Next, the sample was treated by primary O_2 plasma (8min, 300W, 30 sccm O_2 , 160 mTorr) in order to create filament-like nanostructures in SU-8. A two-step pyrolysis was performed to convert the SU-8 polymer to carbon. The samples were first heated in a nitrogen environment at 300 $^\circ\text{C}$ for 30min. Then the temperature was risen to 900 $^\circ\text{C}$ in 20 min. The nitrogen gas was turned off and a mixture of H_2 (2%)/Ar was introduced for 1h. The furnace was slowly cooled down to room temperature. The wafer was diced to release the devices. A secondary O_2 plasma step was applied to the obtained

electrodes (30 s, 100 W, 30 sccm O₂, 160 mTorr) in order to enhance sensitivity. In the following discussion, the samples with different treatments are labeled in Table 3.1.

Table 3.1 Parameters for dual oxygen plasma treatment in the device fabrication

	0s O ₂ plasma post-treat	10s O ₂ plasma post-treat	20s O ₂ plasma post-treat	30s O ₂ plasma post-treat
0W O ₂ plasma pretreat, before pyrolysis	CMEA 001	N/A	N/A	N/A
300W O ₂ plasma pretreat, before pyrolysis	CMEA 002	N/A	N/A	N/A
0W O ₂ plasma pretreat, after pyrolysis	CMEA 100	CMEA 101	CMEA 102	CMEA 103
300W O ₂ plasma pretreat, after pyrolysis	CMEA 200	CMEA 201	CMEA 202	CMEA 203

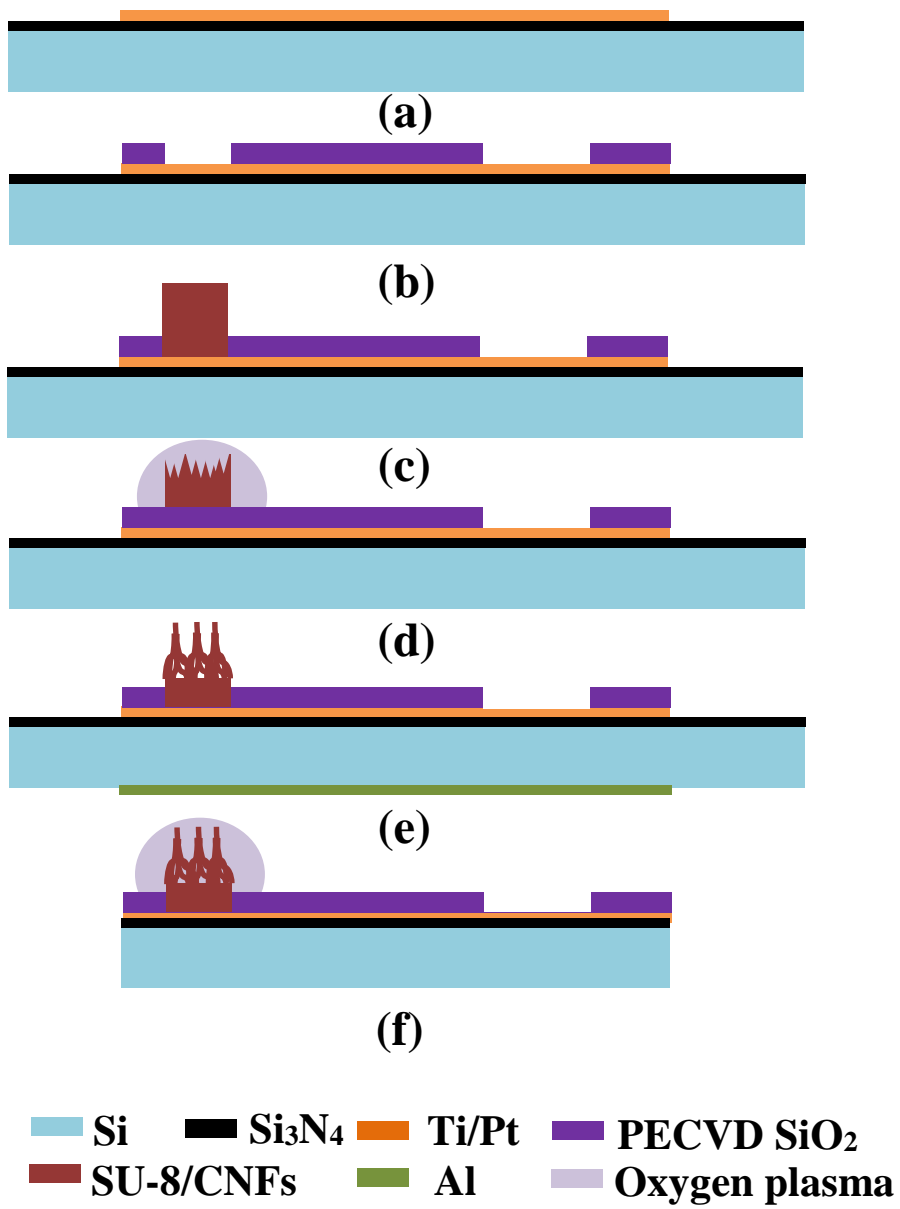


Figure 3.2 process flow for the fabrication and treatment of carbon nanofiber MEAs. A description of each step can be found in Section 3.2.2

3.2.3 Electrode characterizations

The morphologies of the produced PPF electrodes were observed by SEM. The images were taken using a TUSCAN GAIA dual beam focused ion beam system. The surface roughness of the PPF electrodes were assessed using a NanoScope AFM with silicon TESP probe tips (Nanosensors). The degree of graphitization was measured using the E-Z Raman spectroscopy system at 532 nm excitation. X-Ray photoelectron spectroscopy (XPS) measurements were performed on a Kratos Axis Ultra spectrometer that was equipped with a monochromatic Al X-ray source ($h\nu = 1486.6$ eV). The measurements were carried out at 150W power (15KV, 10mA) in an analysis chamber at a pressure of $< 5 \times 10^{-9}$ mbar.

3.2.4 Instrumentation and data acquisition

All electrochemical experiments were performed in a two-electrode setup using Dagan ChemClamp potentiostat (Dagan, Minneapolis, MN). Custom-built software, CV (Knowmad Technologies, AZ), written in LABVIEW 2012 (National Instruments, Austin, TX), was used for background subtraction, data analysis and signal processing. An Ag/AgCl reference electrode was fabricated by electroplating Cl^- ions onto a silver wire (A-M systems, WA) for 5 s. All color plots and cyclic voltammograms (CVs) were collected and averaged across 8 different electrodes. Pooled data is presented with error bars signifying the standard error of the mean (SEM). Student's t tests were performed on paired data sets; $p < 0.05$ was taken as significant and signified with a star.

3.2.5 Flow Injection Analysis

The MEAs was inserted into a flangeless short 1/8 nut (PEEK P-335, IDEX, Middleboro, MA) and fastened to a modified HPLC union (Elbow, PEEK 3432, IDEX, Middleboro, MA) placed in the output of the flow injection apparatus. The apparatus

consisted of a six-port HPLC loop injector affixed to a two-position actuator (Rheodyne model 7010 valve and 5701 actuator) and a syringe infusion pump (kd Scientific, model

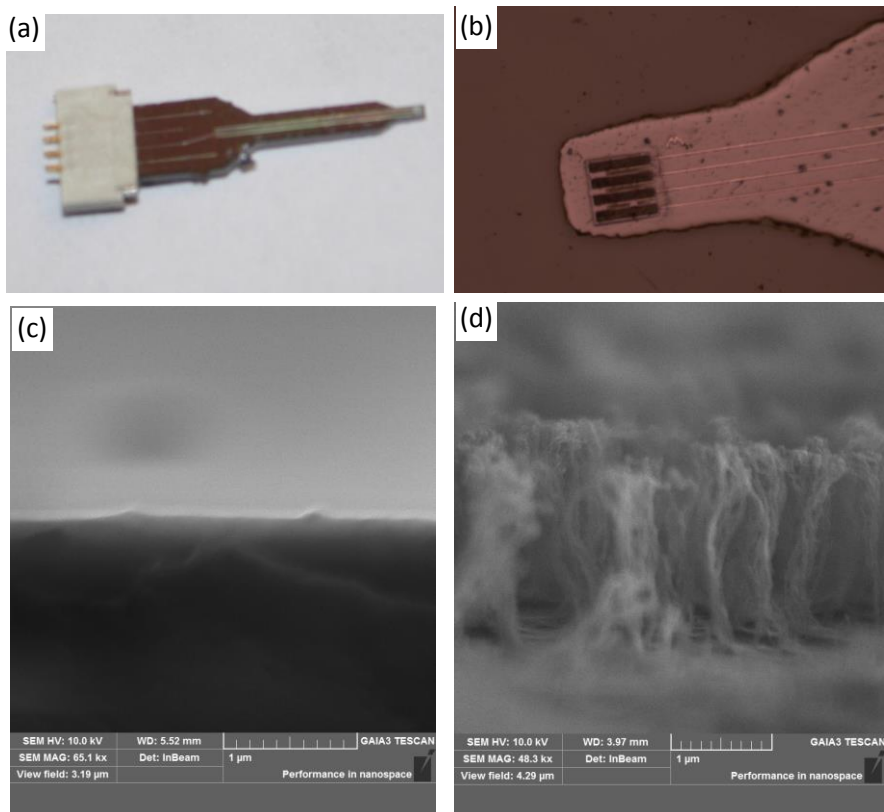


Figure 3.3 optical (a-b) images of carbon nanofiber MEAs, (c) and (d) SEM images showing the microstructure of the pyrolyzed photoresist without and with primary oxygen plasma treatment respectively

KDS-410, Holliston, MA). A rectangular pulse of analyte was introduced to the MEA surface at a flow rate of 2 mL min^{-1} . For calibration and surface variation experiments, standard dopamine solutions were injected in a random order instead of sequentially to avoid tenting effects.

3.3 Results and Discussion

3.3.1 Electrode design and fabrication

Spin coating with subsequent photoresist photolithographic patterning is a well-developed technique in the semiconductor industry. Pyrolysis of the photoresist material

in an oxygen-free atmosphere is known to form carbon structures via depletion of volatile materials. Therefore, we employed photoresist as a structural material to create carbon electrodes in array formation which are integratable into microdevices. The novelty in our work is incorporation of a two step pyrolysis procedure (two temperatures) and a dual O₂ plasma treatment (different power and duration) and into the fabrication procedure.

In our electrode design and fabrication, there are three aspects to address:

- a) *Electrode geometry and dimensions:* Our interests lie in biological and environmental analysis, thus electrode dimensions should be minimized, as a starting point, we chose an active geometric surface area ranging from 3000 to 5000 μm^2 which is comparable to the surface area of cylindrical CFMs used in previous studies [106, 107]. As shown in the optical images in Fig 3.3 (a,b), four electrodes were fashioned in parallel as an array to form the tip of a single device with a spacing of 30 μm , in order to keep our device under 30 μm to maintain negligible tissue damage [113] and to prevent cross-talk [42].
- b) *Control of surfaces and structures:* It is important to produce an active carbon surface with sufficient reaction sites over a fixed geometric area. Our O₂ plasma pretreatment creates a forest of highly reactive carbon nanofibers, with abundant edge planes, as evident in Fig. 3.3c. These carbon nanofibers are responsible for greatly augmenting surface area compared with flat carbon film electrodes. This phenomenon can be seen in the SEM images of the PPF electrodes with and without O₂ plasma in Fig 3.3(c) and (d) respectively where untreated PPF resembles a flat plane while the pretreated PPF consists of carbon nanofiber structures. The mechanisms of nanofiber formation are well described [114]; in brief, the SU-8

polymer chain is comprised of both aromatic and linear sections thus the etching rates of these two sections are different. This phenomenon, which results in a higher vertical than parallel growth rate, promotes the the formation of nano-filaments, which are predecessors for nanofibers. In addition, SU-8's high number of aliphatic chains means that the crystallization temperature for SU-8 is general higher than for positive photoresist which already tend to contain high numbers of ringed hexagons. This means that at the same pyrolysis temperature, more defect sites will be formed on SU-8 than on positive photoresist [101]; an auspicious surface effect for electrochemical applications [112].

- c) *Stability*: Here we define stability as adhesion of carbon structures to the substrate. SU-8 is known to provide better adhesion after pyrolysis compared with positive photoresists [78, 101]. A likely reason is that negative photoresists have low glass transition temperatures and low molecular weights, which means that the photoresist flows once melted during pyrolysis. The result of this effect is fewer pores and cracks that arise due to gas [78, 101]. Because pores and cracks are usually the cause of poor adhesion, negative photoresists tend to display better stability. However, we and others still experienced instability via peeling of carbon patterns from the insulated substrate when using a traditional one step pyrolysis [101, 114]. (data not shown) We addressed this problem by employing a two-step heating process, as previously described [114]. The two measure process involves employing a lower temperature (300 °C) as an initial step before utilizing 1000 °C. The additional lower temperature lead to better adhesion and allowed us to form devices stable in aqueous environments. This is likely because compared to a one-

step process, the two-step process will reach the pyrolysis temperature less dramatically. This more gradual meander towards 1000 °C more readily releases tensile stress near the interface between the photoresist and the substrate, that exists because of the thermal expansion coefficient. Additionally, for the same reason, less dramatic degassing reduces the odds of micro-crack formation. Both of these effects improve the adhesion of the film. Finally, we postulated that the primary O₂ plasma step itself contributed to improving adhesion, and tested this notion in section 3.3.3 (*vide infra*).

3.3.2 Characterization of PPF MEAs

Our electrodes were characterized by different methods in surface analysis and electrochemistry.

AFM

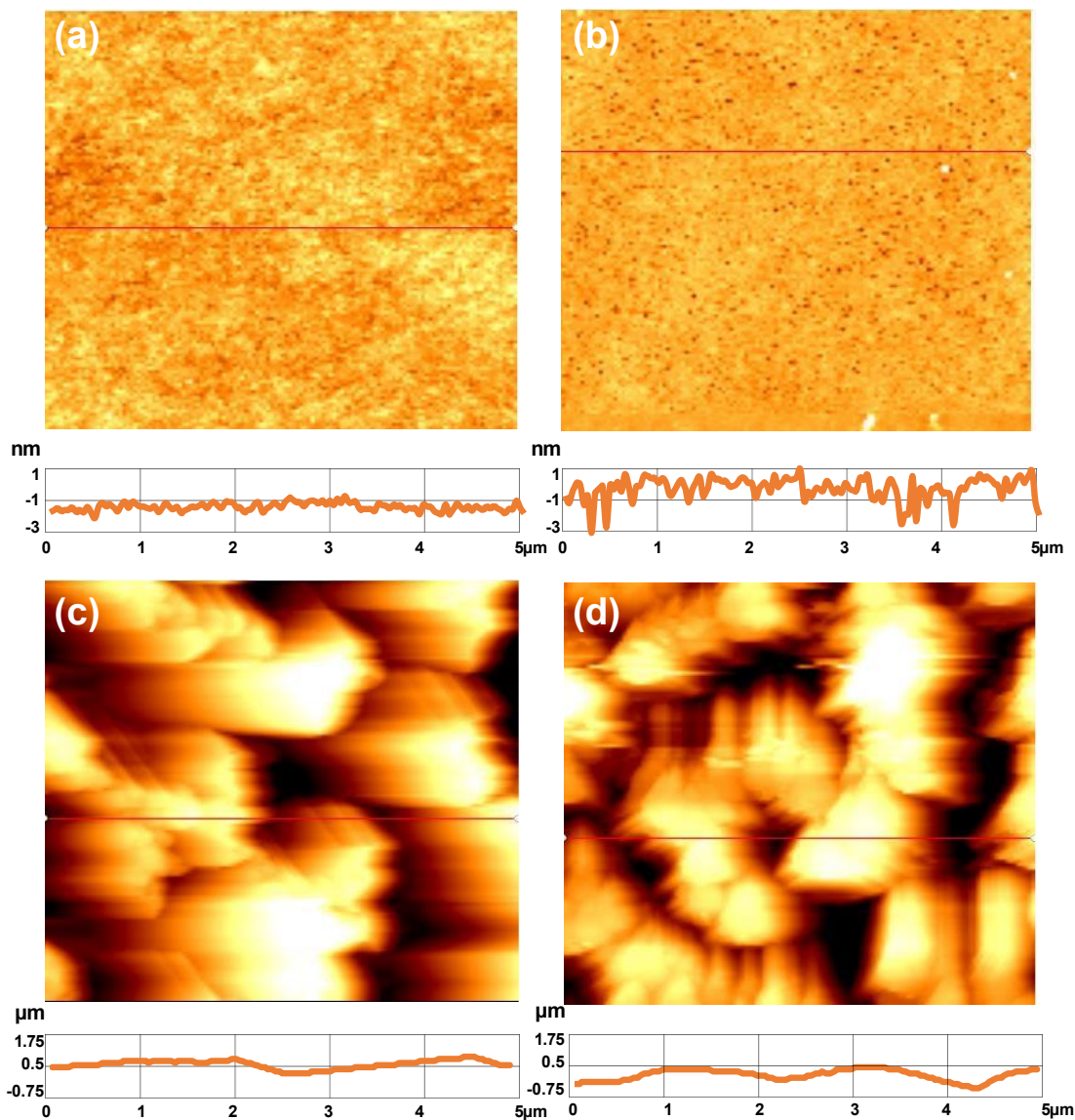


Figure 3.4 AFM images with associated line plots collected at electrodes CMEA 100 (a), CMEA 103 (b), CMEA 200 (c), and CMEA 203 (d). The primary oxygen plasma treatment does contribute to increase the surface roughness, while secondary oxygen plasma treatment does not.

To ensure that a dual O₂ plasma treatment (vs. a one step treatment) does not negatively influence carbon nanofiber electrode surface structure, we employed atomic force microscopy (AFM). The surface topography of the our MEAs was evaluated by tapping mode AFM. Images (5 x 5 μm) are presented in Figure 3.4. Cross-sectional plots accompany each image. The surface features on PPF MEAs after primary O₂ plasma are

greatly enhanced (c,d) compared to PPF MEAs with no plasma treatment (as see in the SEM image, *vide supra*). For both PPF MEAs with and without primary O₂ plasma, there are no significant structural changes after the secondary plasma, showing that a dual plasma process does not unfavorably impact the PPF surface.

Raman

To verify that the surface of the nanofibers formed after the dual O₂ plasma treatment is suitable for electrochemistry, we took advantage of the ability of Micro-Raman spectroscopy to indicate the presence of edge planes, regions with more reaction sites for electrochemical reactions, on our carbon nanofiber surfaces. Figure 3.5 shows Raman spectra of SU-8 before pyrolysis (CMEA 001/002), after pyrolysis and no O₂ plasma (CMEA 100), after pyrolysis and the secondary plasma (CMEA 103), after pyrolysis and the primary plasma (CMEA 200) and after pyrolysis and dual plasma (CMEA 203). Before pyrolysis, no characteristic peaks were observed, however after pyrolysis, two broad peaks centered around 1350 (D band) and 1590 (G band) cm⁻¹ were present. The band at around 1350 cm⁻¹ is consistent with disordered carbon, while the band at around 1590 cm⁻¹ can be assigned to crystallized graphitic structure [115]. The integrated intensity ratio of D/G is frequently used as an indicator of the fraction of disordered SP₂ C-C bonding present in the graphitic structure, therefore higher I_D/I_G is indicative of presence of more edge planes [116]. The ratios for the different samples are summarized in Table 3.2. The primary plasma treated samples presents a higher I_D/I_G ratio (~1.1) compared to the untreated samples (I_D/I_G ~0.9) showing presence of more edge planes. It also can be seen that the primary plasma treated sample has lower peak intensity than the untreated one, possibly due to the change of morphology and the formed nano structure [102]. Interestingly,

CMEA 100 and CMEA 103 had the same I_D/I_G ratio, indicating the secondary O_2 plasma did not introduce significant amount of defects to the structures.

Table 3.2 Comparison of I_D/I_G and O/C ratio of electrodes under different treatments

	CMEA 001	CMEA 002	CMEA 100	CMEA 103	CMEA 200	CMEA 203
Raman I_D/I_G	No peak	No peak	0.90	0.91	1.10	1.11
O/C ratio from XPS	1.01	10.02	0.13	1.06	0.13	3.5

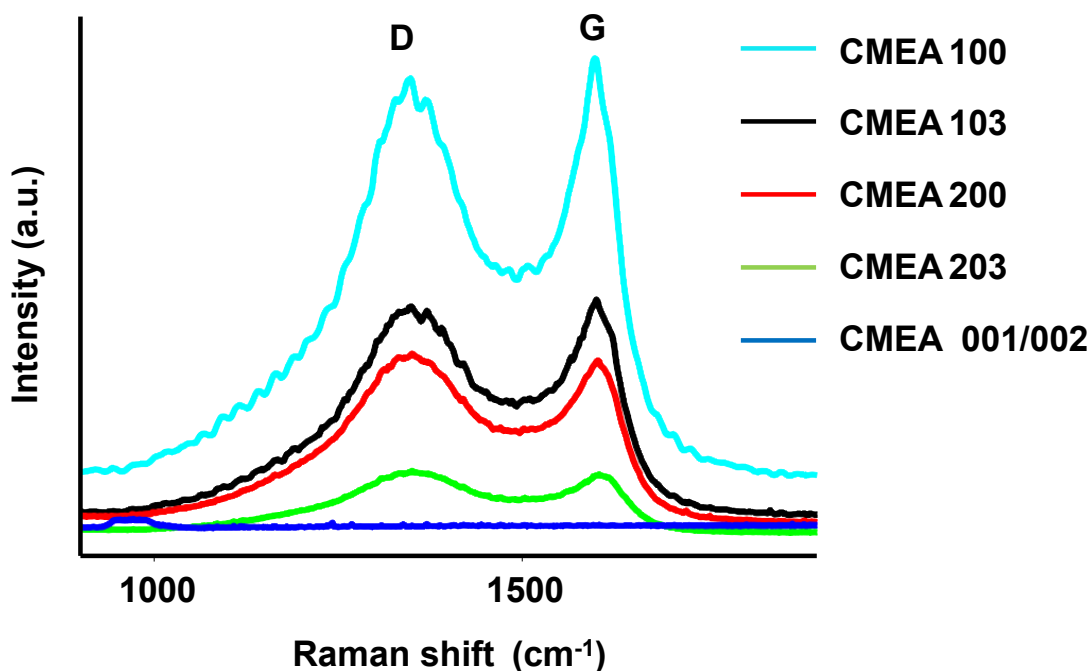


Figure 3.5 Raman spectra of photoresist derived carbon electrode with different treatments

On CFMs, the electrochemical signal is inherently regulated by analyte adsorption, which itself is controlled by the presence of oxygen moieties on the carbon surface. Thus to verify that our electrodes contain sufficient surface oxygen, we utilized x-ray photoelectron spectroscopy (XPS) to analyze surface groups. Samples were vacuum sealed immediately upon removal from pyrolysis furnaces or other process steps for later XPS spectra. Although this short-time exposure to air may result in some oxidation of the surface, it is thought that oxidation of pyrolyzed photoresist in air is slow enough to be negligible within the time frame of our experiment [117]. Despite this, as a cautionary measure, we kept the exposure time in air for all our samples consistent. The changes in the XPS spectra, therefore, are considered to be primarily caused by our different fabrication conditions and treatments. Atomic concentration ratio, O/C, (see Table 2) was determined from the C_{1s} and O_{1s} spectra (Fig. 3.6). Primary O_2 plasma introduced more O_2 to the surface as expected. After pyrolysis, the O_{1s} peak diminished drastically for both O_2 plasma treated and untreated samples. Previous studies on the pyrolysis of photoresist have indicated that oxygen and nitrogen are removed at $300\sim 500^\circ\text{C}$ [116]. In our case, the pyrolysis was carried out at 900°C , which explains the O_{1s} peak reduction. In fact, the reductive atmosphere used for pyrolysis is expected to generate a hydrogen terminated surface [78], which may interfere with electrochemical behavior of carbon surfaces. The increase in O/C after plasma treatment elicits the elimination of hydrogen and subsequent surface occupation of oxygen groups, consistent with prior work showing that plasma treatments can form surface carboxyl functional groups [118]. It is worth noting that the increase of O/C in primary plasma treated samples is greater than the one without primary plasma which may be attributable to more reactions sites for binding oxygen groups on the

nanostructured surface originating from the primary plasma treatment. These data imply that primary O₂ plasma is responsible for creating more reaction sites; while the secondary O₂ plasma accounts for bringing O₂ containing groups to the surface.

These surface analyses illustrate that two step pyrolysis and dual O₂ plasma treatment (CMEA 202) create a rich carbon surface for electrochemistry, we next explore the suitability of this surface for FSCV analysis.

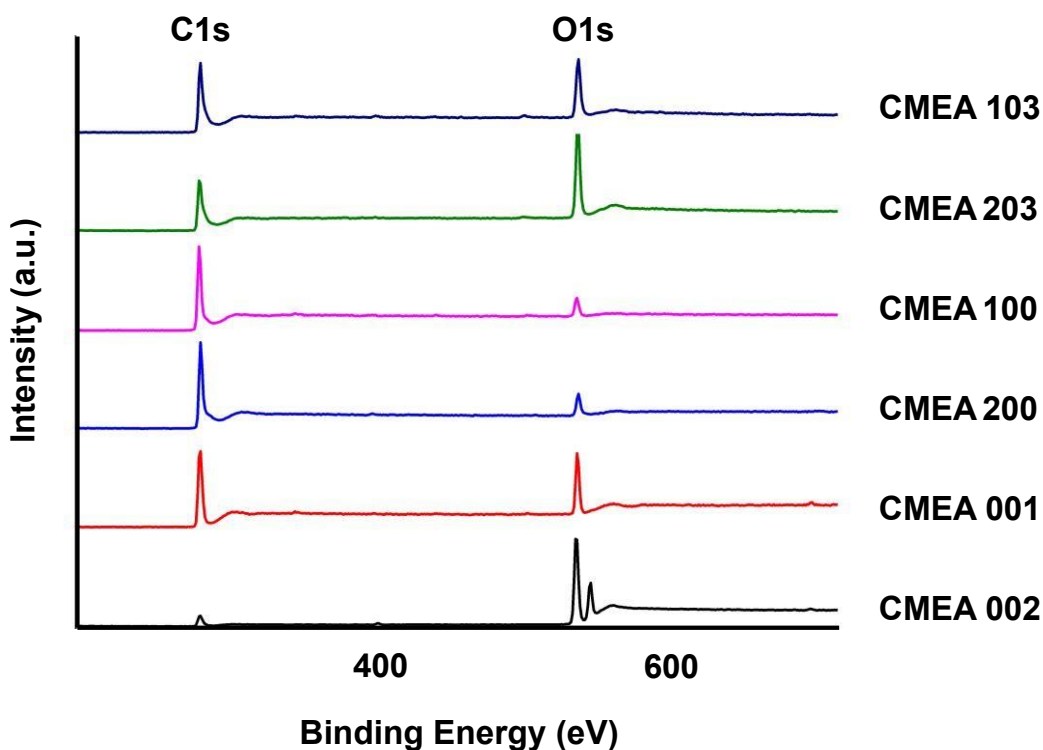


Figure 3.6 XPS comparison of photoresist derived carbon electrode with different treatments

3.3.3 FSCV Characterizations

3.3.3.1 Electrochemical effects of dual O₂ plasma treatments on MEAs

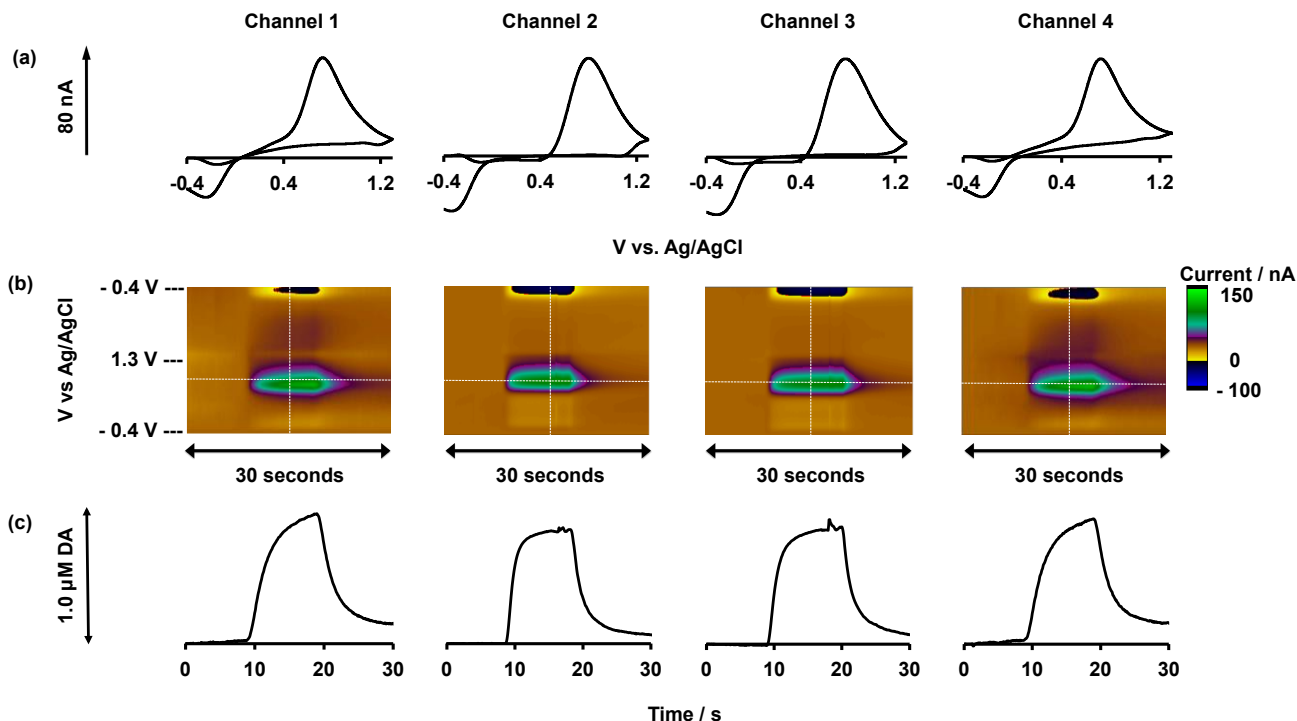


Figure 3.7 (a) a FIA response of electrode CMEA 202 to injection of 1 μM DA. (a) shows a CV taken at the vertical white dashed line from the color plot in (b). (c) shows a plot of response current vs time, which was determined by taking i vs t from the horizontal white dashed line in the color plot (b).

FSCV utilizes scan rates typically between 400 and 1000 Vs^{-1} and acquires one cyclic voltammogram in approximately 2 ms every 100 ms. The fast scan rate renders the method highly selective but also generates a large charging current. Background subtraction eliminates the charging current, resulting in cyclic voltammograms characteristic of redox active species that can be used as a “fingerprint” for analyte identification. Dopamine, as a biologically important and well-characterized molecule, was chosen as a standard analyte herein to compare with related studies. A typical FSCV characterization for the 4-electrode array is shown in Fig. 3.7. Cyclic voltammograms were collected for 30 s during a flow

injection analysis (FIA) of 1.0 μM dopamine onto the 2-step pyrolysis, dual O_2 plasma electrodes (CMEA 202). The traditional triangular waveform for dopamine detection was employed where the potential ramps from -0.4 V to $+1.3\text{ V}$ and back at a scan rate of 400 Vs^{-1} and application frequency of 10 Hz . The color plot illustrates this 30 s FIA event with an injection of dopamine between 5 and 15 s (interpretation of a color plot can be found in Hashemi *et al.* [119]). Fig. 3.7(a) is a cyclic voltammogram taken during the dopamine injection, indicated by the vertical white dashed line in the color plots Fig. 3.7(b), shows a redox couple at $0.75\text{ V} / -0.25\text{ V}$, which is in accord with values reported for conventional CFMs under the same experimental conditions. Figure 3.7 (c) displays the current vs. time profile at the maximum oxidation potential taken from the horizontal white dashed line in the color plot. Our optimized electrodes are highly sensitive, yielding $76.6 \pm 4.9\text{ nA}$ ($n = 12 \pm \text{SEM}$) for a $1.0\text{ }\mu\text{M}$ dopamine injection, (compared with prior studies showing 10 nA for conventional CFMs with surface areas $\sim 1000\text{ }\mu\text{m}^2$) [42].

The vast sensitivity improvements was attributed to the O_2 plasma treatments for three reasons:

- a) Our pre-treatment leads to formation of fine structures on the MEAs and increased physical surface areas within equivalent geometric surfaces. The result is increased FSCV response because mass-transport is less hindered thus analyte flux is increased.
- b) An additional advantage of O_2 plasma treatment is the creation of edge planes (indicated by the Raman spectra, *vide supra*). Prior studies on pyrolytic graphite have shown that edge planes are the primary reaction site [120, 121].

c) Previous studies on conventional CFMs have shown that the dopamine FSCV response is adsorption-controlled at physiological pH [81, 94], thus over oxidation (to induce oxygen moieties on the carbon surface) [42, 94] and a negative resting potential between scans [42, 94] are used to promote this adsorption. Our O₂ plasma treatment induces many oxygen containing functional groups to the reactive sites (XPS data, *vide supra*). As a result, dopamine adsorption, and hence sensitivity, on the electrode surface is greatly enhanced.

We next optimized the dual O₂ plasma treatment conditions to establish the optimal electrode performance. 12 electrodes (3 devices) were selected for a primary plasma treated (green) and untreated (purple) group. Figure 3.8 compares the average current responses at the maximum dopamine oxidation potential for both groups under secondary O₂ plasma for 0, 10, 20, and 30 s. In general, the green group showed more current response than the purple group. When the secondary plasma treatment time increased, the current response for both groups showed an overall increasing trend and reached plateau at 20 s. The plateaued response of the green group (~80 nA) was almost 3 times that of the purple group (~27 nA). At 30 s, both groups reached saturation state, likely due to a damaged surface via extended secondary plasma [122, 123]. Because there was no significant difference between the current responses at 20s and 30s for both groups ($p = 0.8015$), the duration of secondary O₂ plasma treatment was set at 20s.

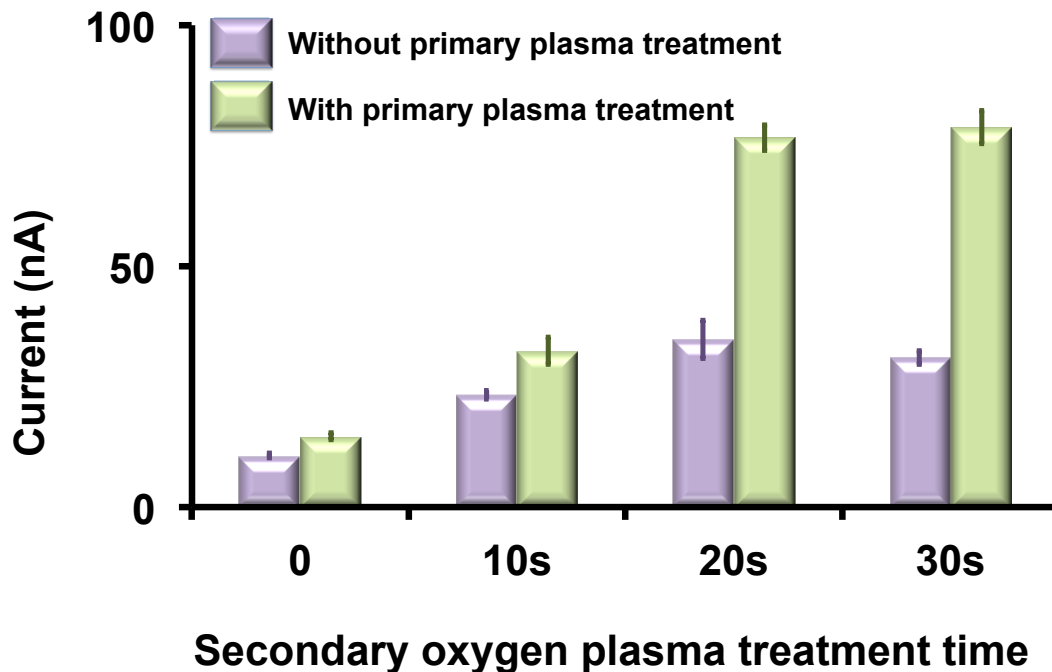


Figure 3.8 Effect of pre and post treatment on the sensitivity. The pre-treated samples show greater response current than non-pre-treated ones. 20s post-pyrolysis treatment saturates the surfaces with oxygen containing functional group

3.3.3.2 Calibration and limit of detection

A standard calibration of the optimized MEAs for dopamine is presented in Fig. 3.9 ($n = 12 \pm \text{SEM}$). The calibration was conducted within a concentration range from $0.10 \mu\text{M}$ to $10 \mu\text{M}$. The limit of detection (LOD) was $0.10 \mu\text{M}$, which is significantly lower than reported values for PPF electrodes [42]. A linear calibration range up to $5.0 \mu\text{M}$ is appropriate for biological analyses. The sensitivity (slope) in this range is $80 \text{ nA}/\mu\text{M}$ as shown in the inset.

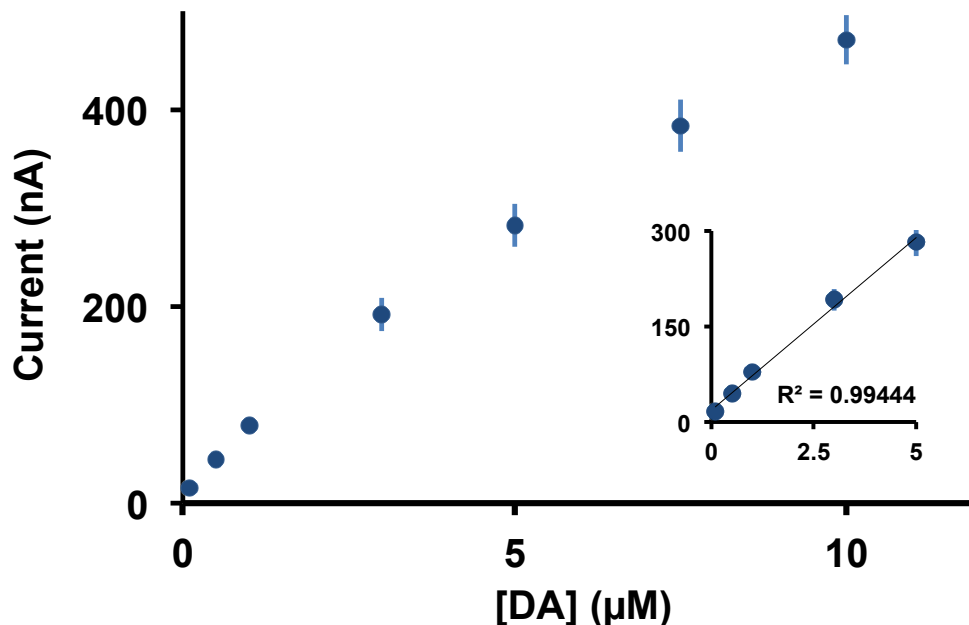


Figure 3.9 detection limit (sensitivity) of the optimized electrodes. The plot shows voltammetric peak current as a function of dopamine concentration. The error bars are the standard deviation ($n=12$). Inset: linear range of dopamine on MEAs. All measurements were done at 400 v/s, 10Hz in TRIS buffer, pH 7.4.

3.3.3.3 Stability

As previously discussed, the primary reason for conventional PPF electrodes stability failure is peeling of the carbon film off the substrate and we addressed this by employing negative photoresist instead of positive photoresist. Successive injection tests were performed for both primary O_2 plasma treated and untreated groups. We injected 1 μM dopamine onto a device 50 times, and we recorded the peak oxidation peak currents at different channels each time. The normalized currents (observed current / average current) are plotted versus injection number in Figure 3.10. Both groups showed consistent responses with 50 successive injections, yet the untreated PPF electrodes displayed a greater standard deviation, likely because the primary O_2 plasma can cause certain compressive stress that further enhances the adhesion of the generated carbon films.

The minimal standard deviation of pretreated MEAs also implies good reproducibility. Highly reproducible batch microfabrication processes are advantageous in decreasing electrode surface area deviations, thus improving the capability of reproducible electrochemical detection. In contrast, the traditional manually cut carbon fiber microelectrodes are less precisely controlled, and are not suitable for accurate multi-site and multi-analyte detection, even though they can be bundled up to create a compact unit.

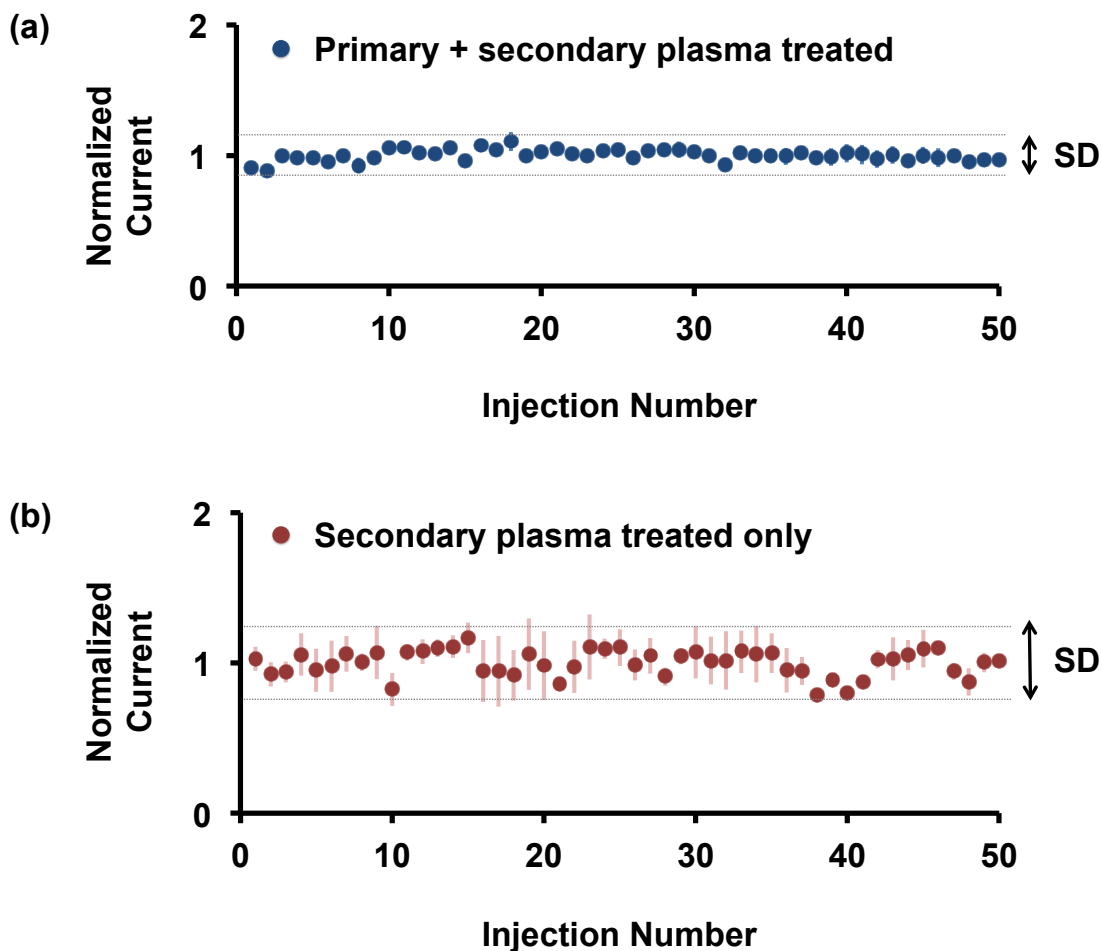


Figure 3.10 Effect of oxygen plasma pre-treatment on device stability. Figure (a) and (b) show the peak oxidation current of successive DA injection onto pre-treated and un-pretreated MEAs respectively with FIA (positive potential limit +1.3V, negative potential limit -0.4V, scan rate 400 V/s). Horizontal lines indicate SD limits.

3.4 Conclusions

PPF MEAs are an important tool for providing multiple measurement platforms with versatile spatial geometry. In this paper, we described the development of a new type of PPF MEAs that give highly reproducible, sensitive and stable responses when coupled to FSCV. These desirable characteristics are due to nanofiber formation via a novel strategy, application of a two step pyrolysis process and dual O₂ plasma. We utilized a host of analytical methods to show that our strategy greatly improve film adhesion and surface reactivity. These devices represent an important first step towards dynamic, simultaneous and selective multi-analyte FSCV detection.

CHAPTER 4 FLEXIBLE CNT BASED CUFF ELECTRODE FOR PERIPHERAL STIMULATION

4.1 Background and motivation

4.1.1 Functional electrical stimulations and applications in peripheral nervous system

Central nervous system and peripheral nervous systems

The human nervous system is mainly consisted of the central nervous system (CNS) and the peripheral nervous systems (PNS). The CNS includes the brain and the spinal cord, while the peripheral system is composed by the spinal, cranial and autonomic nerves and their branches. The CNS processes the information and store data through brain and flows information through the spinal cord as channels. The PNS, composed by the spinal, cranial and autonomic nerves and their branches, takes the information from the environment or transmit orders to muscles or organs. More specifically, the peripheral nervous system relays information from the brain and spinal cord to the extremities, and vice versa. Damage or trauma can compromise the nervous functions partially or completely. Interfacing to nervous system is of interest to restore the lost function or to discern the information they carry so that appropriate prosthetic interventions can be implemented. Peripheral nerve tissue provides an ideal neural interfacing site for prosthetic limb control. An amputated peripheral nerve contains all of the motor and sensory pathways associates with the lost limb, and these pathways retain significant function after injury. The candidate interfacing sites in the CNS is encased within the cranium and vertebral column, which makes it more difficult to access noninvasively [124]. In contrast, direct peripheral nerve is easy to access to avoid the reactive gliosis and electrode failure in cortical interface due to tethering forces and mechanical damage, thus minimizing surgical risk and

complications [125]. Also, it has been reported that the peripheral neural tissue is viable for interfacing even years after injury or amputation [125].

There are a wide variety of neuron types which form separate nerve pathways for different functions [126]. The sensory system transfer physical energy from the environment into neural signals. The motor system produces movement by translating neural signals into contractile. When a limb is amputated or injured, all of the associated motor and sensory pathways in the peripheral nerve still retain most functions. Thus it is possible to restore the lost or impaired peripheral nerve functions. Moreover, successful peripheral nerve interfacing can also restore some functions (e.g. voluntary movement) due to stroke or injury in spinal cord. The voluntary movement is generated in the brain neurons which send signals to spinal cord and finally to motor neurons. In the cases of spinal cord injury, the peripheral nerves largely remain intact and can be interfaced to initiate peripheral muscle contraction efficiently.

Peripheral nerve stimulation

The peripheral nerve stimulation has many applications, including the treatment of pain, restoration of motor functions, and treatment of epilepsy by electrical stimulation of the vagus nerve [126]. This chapter will focus on the restoration of limb motor functions on patients who have damaged neural pathways. For better understanding of motor function restoration, a brief introduction of motor system is given as following. Large motor neurons lie their cell bodies in the spinal and or brain, and spread axons out of spinal cord through a ventral root. Each axon traverses small branch of peripheral nerves until it enters the muscle it controls. At this point, a synapse takes place to functionally connect a motor neuron and a target muscle fiber. Through this connection, an action potential (AP)

transmitted to motor neuron will produce a “twitch” type myofibril contraction as an output. This contraction is all or none type, independent of the stimulus intensity. For neuromuscular electrical stimulation (NES), electric currents onto the target nerve. The ions flow from the anode to the cathode passing through the nerve and generates an AP. The AP reaches the motor neuron and cause the corresponding movement. A few examples of NES are illustrated in the following paragraph.

Drop foot is a common gait abnormality caused by a neurological disorder in stroke patients who are unable to achieve dorsiflexion of the foot. It has been successfully compensated in some patients with stimulation of the peroneal nerve with FES to initiate ankle dorsiflexion. This application also has been demonstrated to improve patients’ rehabilitation. FES is also used for patients who have good stance ability but problems with gait. In this case, electrical stimulation assists the swing phase so that the patients gain the ability to walk for short periods. Another application of FES in lower limbs is to assist the standing process. Regarding upper limbs, grasping impairment is one of the severe consequences of stroke or spinal cord injury. The patients usually unable to produce voluntary wrist or finger extension or grasping. To restore grasping, electrodes are placed along the forearm to stimulate radial, median or ulnar nerves. Stimulation of radial nerve provoke wrist and finger extension, while the stimulation of median and ulnar nerves is responsible for wrist and finger flexion.

4.1.2 Cuff electrodes for peripheral nerve stimulation

Electrodes are main components of neural interface. Two main approaches in the design of peripheral nerve interface are extrafascicular electrodes and intrafascicular electrodes[127, 128]. Extrafascicular electrodes are placed in contact with the nerve

epineurium, yet with no invasion. Examples include cuff, wire, hook electrodes. The second approach is invasive, used to penetrate nerve and locally stimulate the fascicles. The intrafascicular electrodes provides higher level of selectivity but potentially cause nerve damage. Therefore, non-invasive neural interfaces are preferred for clinical applications. For many physiological acute studies, a length of nerve needs to be dissected and suspended onto hook-shaped wire electrodes and elevated into a pool of nonconductive fluid (usually paraffin or mineral oil). By doing so, the electrical signals are confined within the nerve trunk and isolated from the surrounding tissues. The preparation becomes difficult particularly for short or deeply located nerves or when testing multiple sites in different parts of the body. It is especially unsuitable for repeated stimulation over a long period of time. For this reason, nerve cuff electrodes have increasingly aroused attention. Cuff electrodes have conductive electrodes embedded in an insulating sheath (cuff), in immediate contact with peripheral nerve epineurium. The insulating sheath makes it possible to eliminate use of oil pool, therefore simplify the preparation. The testing repeatability has also been improved due to the fixed position on nerve.

In old days, the fabrication of cuff electrode involve handmade parts and assembly of discrete components [129]. For example, stich wires into the side walls of commercially available silicone rubber tubing. The devices fabricated by these traditional methods have a bulky size and a limited number of channels, limiting their clinical applications. Today, the MEMS technologies offer great capability in device minimization and multi electrode sites integration. Electrode arrays on a flexible polymeric substrate have been fabricated by MEMS technologies. Electrode materials such as Pt, roughened Pt, IrOx, Ir, gold, and

polymer substrates such as polyimide, parylene, PDMS have been employed for the fabrication.

4.1.3 Motivations

Besides of general mechanical and biocompatible issues, there are a number of additional considerations in design of cuff electrodes for effective electrical stimulation:

- (1) The electrode material must have sufficient surface area to acquire large enough charge capacity. In this way, the stimulus magnitude required for nerve activation is minimized. Also minimized is the possibility of electrically-induced tissue destruction.
- (2) Selectivity must be improved to stimulate different sub-populations of axons.
- (3) Chronic applications require good adhesion between electrode contact and polymer substrate.

For the first design consideration, coatings of Pt black or roughened Pt has been employed to increase the surface area. CNTs have recently aroused tremendous interests in neural electrode because of their extraordinary good electrical and mechanical properties, especially their intrinsically large surface area. In regard of the second design principle, multi electrode arrays have been integrated into the flexible substrate to improve selectivity. Recently, a polyimide split-ring shaped cuff electrode was designed with four triangular bendable platinum electrode protruding the ring. The protruding electrode can make tight contact with the nerve without really penetrating the epineurium. This design takes the form of penetrating electrodes to increase the selectivity while using the soft polymer substrate to reduce the invasiveness and minimize the nerve damage. Regarding to the third

design concern, few works have been done to increase the adhesion between the normally used metallic thin film electrode and polymer substrate in cuff electrodes.

In this chapter, we illustrate a novel design of CNT based cuff electrode (the schematic of the design is shown in Figure 4.1 (a)). CNTs were used as electrode to achieve large charge capacity. And the CNTs were integrated vertically into polymer substrate, analogue to penetrating electrodes to increase the contact and selectivity. On the other hand, CNTs are much less stiff than Si based penetrating electrodes. Therefore nerve damage is limited. Furthermore, the CNTs and flexible parylene substrate were integrated through a novel sandwich manner to enhance the adhesion, making the device potentially suitable for

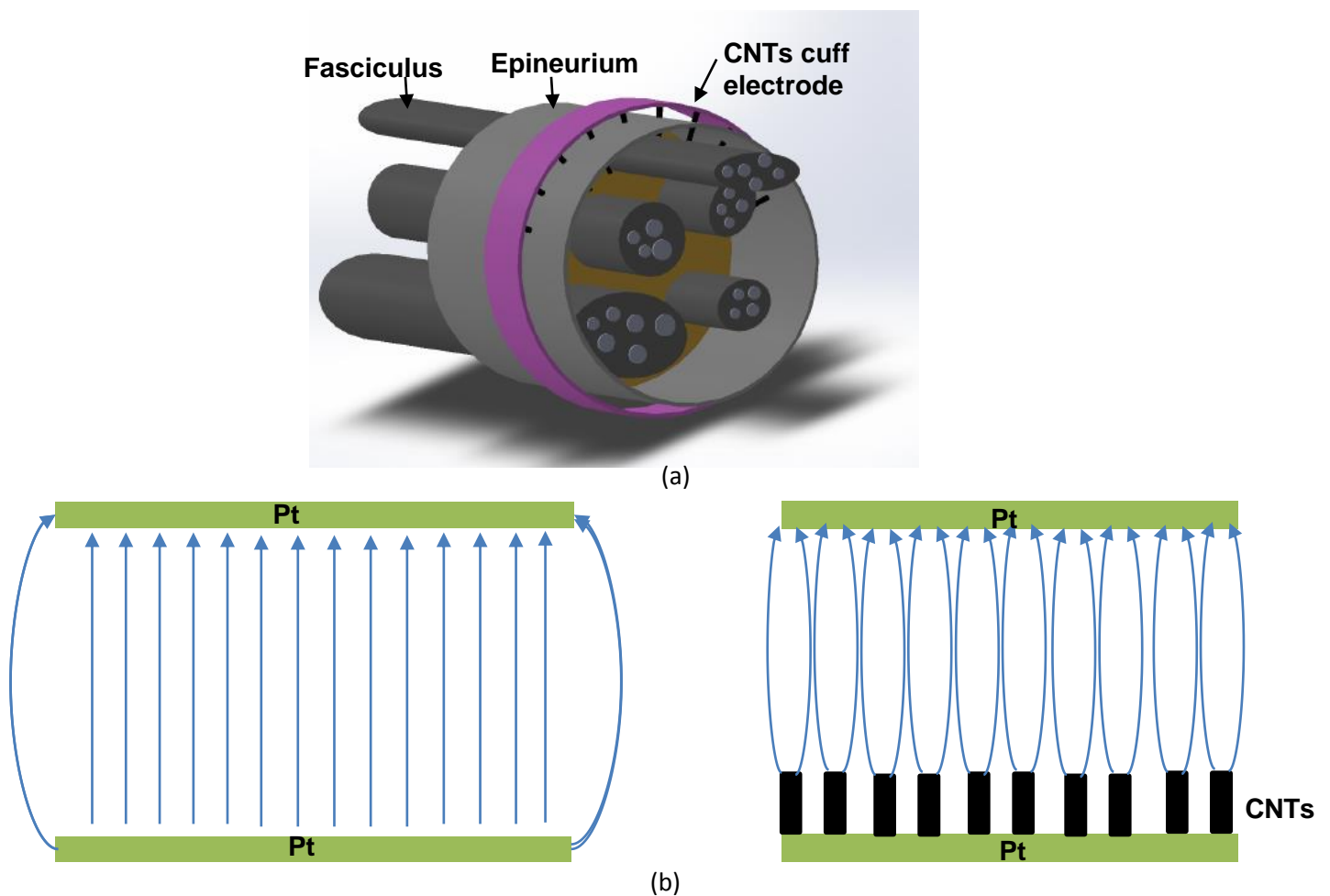


Figure 4.1 Schematic of the flexible CNTs cuff electrode (a); improved uniformity of electric field generated by CNT electrodes (b).

chronic application. Another advantage of using CNTs electrode is the improved uniformity of the electric field. For flat electrode, the electrode field distortion usually happens at the edge. But for CNTs electrode, the distribution of this edge effect is more uniform, which will reduce the deviation caused by the distorted electric field, as demonstrated in Figure 4.1 (b).

4.2 Experimental

4.2.1 Fabrication of flexible CNT based cuff electrode

The fabrication process has been described in experimental section in Chapter 2. Briefly, low stress silicon-rich nitride was grown on a silicon substrate using a low pressure chemical vapor deposition (LPCVD) as insulation. Ti/Pt (20nm/200nm) was evaporated and then patterned by lift-off to serve as electrodes, contact pads, and interconnects. Arrays of holes were defined on Pt to serve as etching windows for the final release step. In a second lift-off step, TiN (100nm) was selectively patterned on the electrode areas, followed by RF sputtering of a 2nm thick Fe layer. The wafers were then loaded to the thermal CVD chamber for the CNT growth. The growth took place in a gas atmosphere of C_2H_4/NH_3 at 80 torr for 120 min to achieve higher CNTs. To protect the synthesized CNT arrays from the following process steps, a layer of photoresist was spun to coat the CNTs. Afterwards, a 3µm thick parylene C layer was deposited by CVD. Then oxygen plasma etching was applied to open the etching holes. XeF₂ isotropic gas phase silicon etchant is applied to undercut the bulk silicon in the handle wafer for device release. This technology is simple and CMOS compatible. No transfer printing process is involved. Subsequently, a second parylene layer (10µm) was deposited to encapsulate the device and seal the etching window as well. Finally, electrodes and contact pads were opened by oxygen plasma before the

release of the flexible device from the substrate.

4.2.2 Characterization of flexible CNT based cuff electrode

The morphologies of the synthesized CNTs were analyzed by Scanning Electron Microscopy (SEM). The images were obtained using a JSM-6510LV SEM at 15KV accelerating voltage.

4.2.3 Electrophysiological experiments

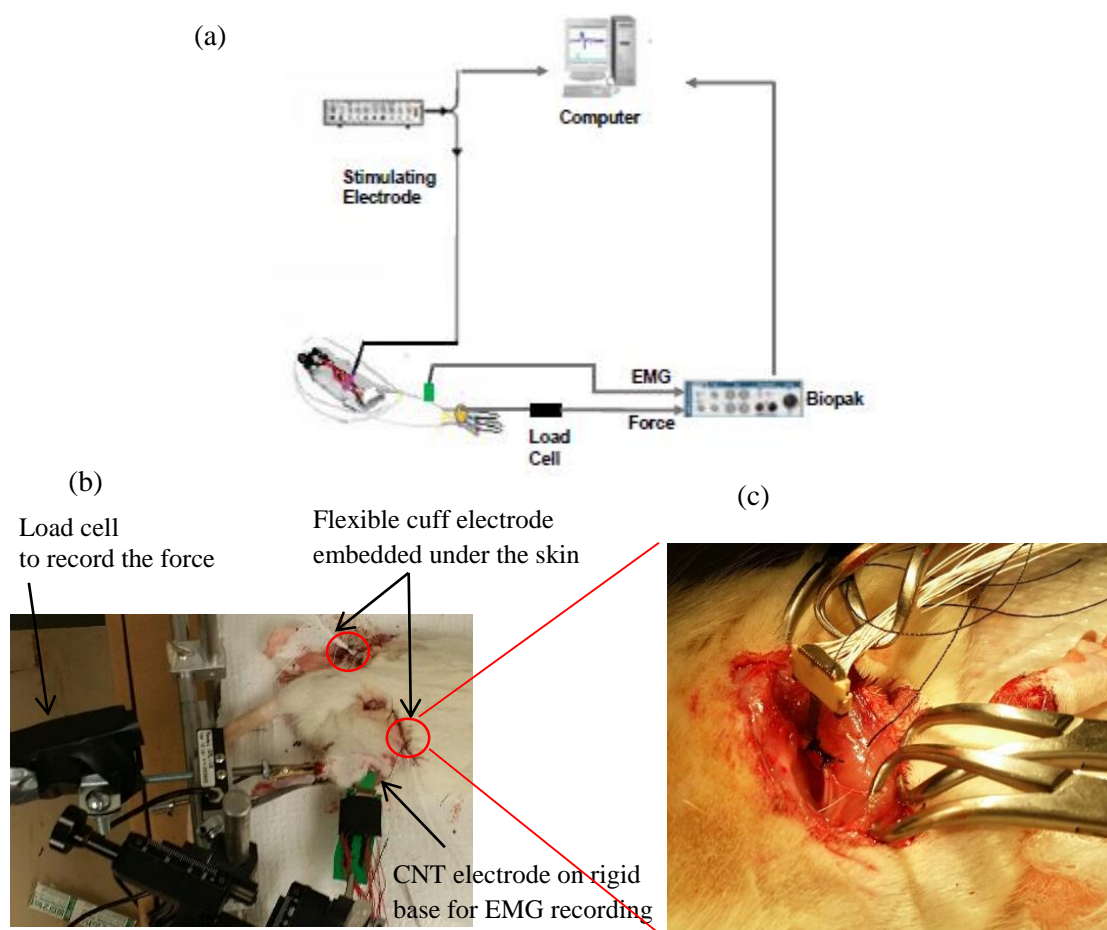


Figure 4.2 experiment setup for sciatic nerve stimulation

Five male adult Sprague Dawley rats (weighted 400 grams) were used in this initial study. The rats were anesthetized with an intraperitoneal injection of Xylazine and Ketamine. All procedures were approved by the Wayne State University Animal

Investigation Committee. The right sciatic nerve were exposed. The flexible CNT cuff electrode were wrapped around the sciatic nerve. The cathode and anode of the stimulator were connected alternatively to each of the contact pairs of the CNTs electrode. Stimulation was performed by application of a single monophasic pulse. CNTs based electrodes on rigid substrates were placed in the gastrocnemius muscle through a 2-3 mm incision. EMG signals were recorded using BioPak system. A clip on the base of the tail was used as ground. The muscle contraction force was measured using a load cell connected to the right leg. The experimental setup in shown in Figure 4.2.

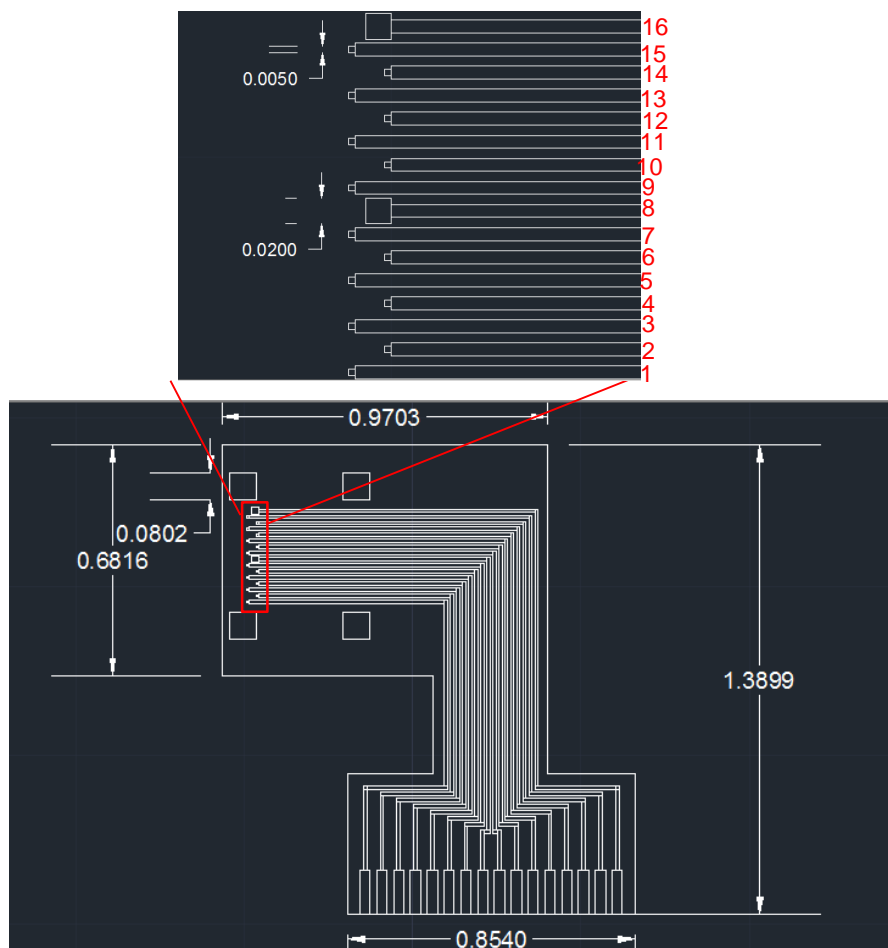


Figure 4.3 Cuff electrode design plots: (a) the size of the whole device, (b) the size of electrodes (the unit is cm).

4.3 Results and discussion

4.3.1 Characterization of device

Fig. 4.3(a) shows the design layout with dimensions of the parylene planar device. Fig. 4.3 (b) shows the design layout with dimensions of the CNT electrodes and array spacing. The CNT electrode is in size of 2500 um^2 . Two Pt electrodes with area of 40000 um^2 are also in the array (labeled as 8 and 16 in Figure 4.3). The device consists of three parts: microelectrode sites, parylene wrapped leads, and contact pads. The device is designed to wrap around the sciatic nerve of rat (0.8~1 mm of diameter). The electrode size and spacing were chosen to evenly locate around the nerve when the flexible device is rolled around the rat sciatic nerve. Thread is inserted into the holes at the edge of flexible device to tie the device onto the nerve in order to further improve the contact. The photograph of the flexible parylene cuff electrode is shown in Figure 4.4(a). Figure 4.2 (c) exhibits the close-up view of one parylene cuff electrode implanted around the sciatic nerve. The external connector is commercial FPC. Through this connector, a flexible nerve cuff electrode can be freely connected with external instruments. And in the acute rat experiment, the contact pads are inserted into the connector and fixed, with only the other parts can be stretched. The electrode sites is composed of vertically grown CNTs. Figure 4.4 (b) depicts the CNTs grown on Si substrate before coating of parylene. The CNTs are well aligned with height of about 60 um .

Direct mechanical interaction between cuff and nerve is an obvious means by which neural damage might be inflicted. The main consideration for safe design of nerve cuff electrodes is mechanical flexibility. In this work, parylene was chosen as the substrate

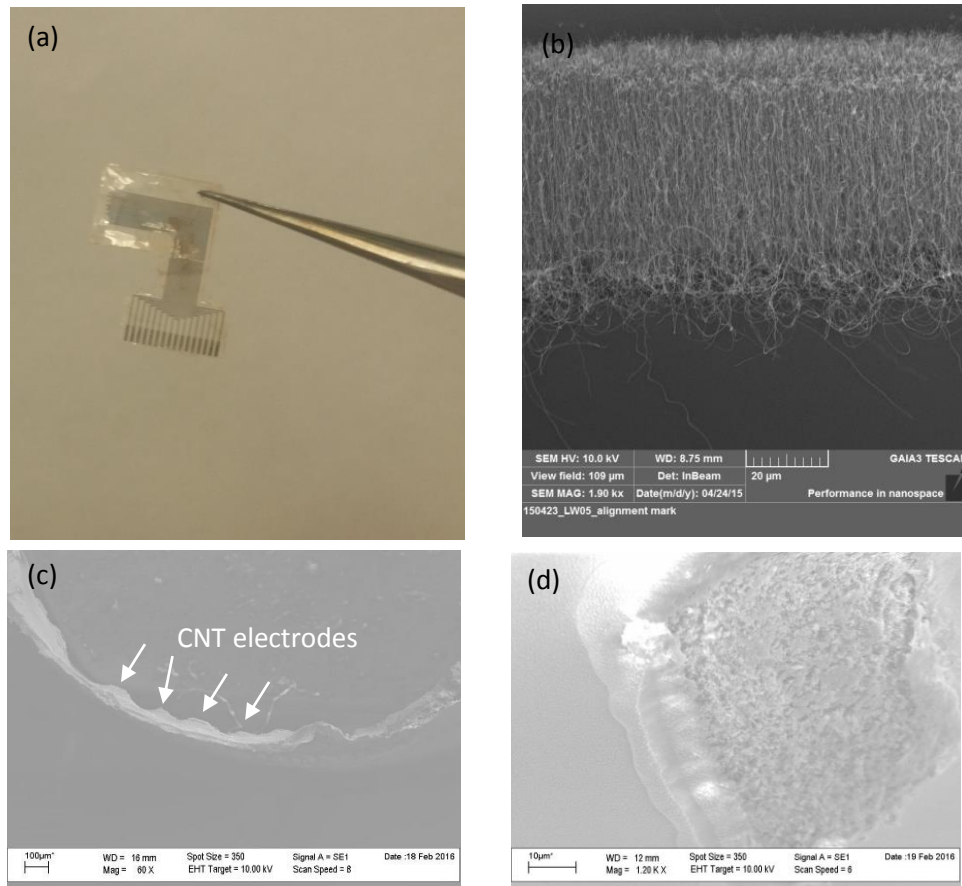


Figure 4.4 (a) photos of the fabricated device, (b) the CNTs on Si before the coating of parylene, (c) CNT electrode arrays on flexible parylene substrate, (d) Single CNT electrode on parylene substrate.

material for the development of highly flexible and re-formed nerve cuff electrodes. Parylene has been applied in a variety of biomedical devices due to its superior mechanical strength and biocompatibility. Successful implantation of the fabricated parylene electrode also demonstrates a high level of conformability. Apart from these general considerations, there are a number of additional factors in design of cuff electrodes for safe and effective electrical stimulation, as stated above. Our design has coped with these issues correspondingly:

(1) For safe and effective electrical stimulation, the stimulus magnitude should remain below the charge-carrying capacity of the electrode to avoid an irreversible reaction

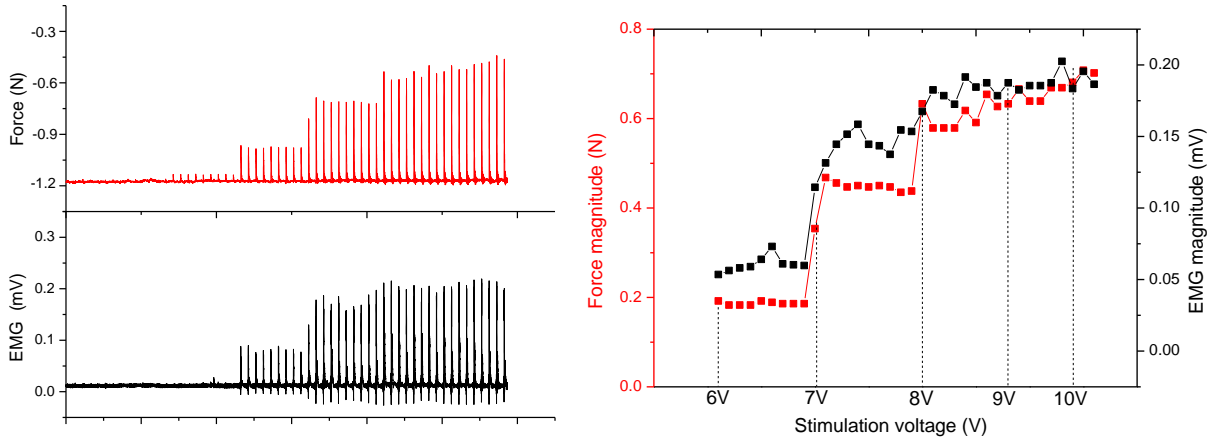
including water hydrolysis, electrode dissolution, and evolution of gases (6). Lots of electrode modification techniques (such as coatings of large surface area materials like IrOx, black Pt, PEDOT, or roughening the electrode surface: roughened Pt) have been performed to enlarge surface activation area to increase the electrode charge capacity and to minimize the required stimulus magnitude for nerve activation (1). In our work, CNTs has been adopted as electrode due to its intrinsically large surface area.

(2) Selective stimulation is challenged by the three dimensional structures of peripheral nerves, in which individual fibers connected to and coded for unique motor and sensory information. Nerve fiber more close to a stimulation electrode will be evoked and give out more selective or specific signal. Penetrating electrodes afford direct contact with axons, thus pertaining higher selectivity. However, invasiveness of penetrating electrodes also induce nerve damage. Cuff electrodes has no invasiveness, but with the compromised selectivity due to electrodes positioned outside the epineurium. As a result, innovative designs have been developed to increase the selectivity of non-invasive electrodes. Recently, a split ring shaped polyimide based electrode has been designed. The device consisted of four bendable triangular sharp contact probes around the polyimide frame. The probes, taking the form of penetrating electrode, are confined by the polyimide ring to provide a good contact with the nerve. Nonetheless, these probes are based with polyimide, which is much less invasive than silicon based penetrating electrodes. Our work further expanded this design by using vertically grown CNTs as electrodes. CNTs have high strength and high stiffness. It has been reported that the strength and stiffness of CNTs can be significantly improved by using longer and denser CNT arrays. The vertical CNT arrays protruding out of the parylene substrate plane to fill the gap that normally exists between

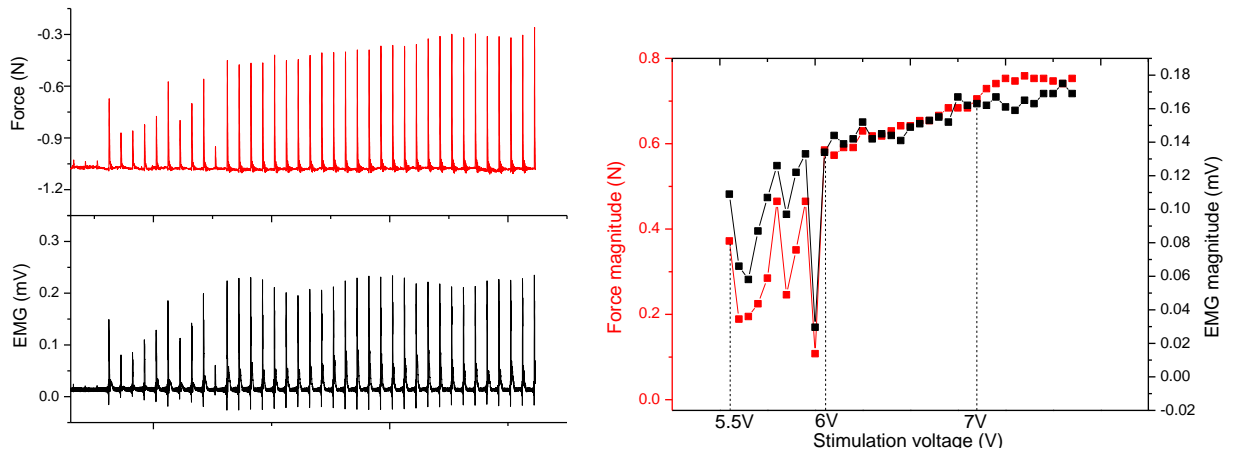
the cuff electrode and nerve. The strong stiffness afford the CNT arrays with resistance to bending and make it possible for CNTs to penetrate through the epineurium and access to individual axon. More importantly, the small radius of the CNT is more advantageous than normally used penetrating electrode: small radius will cause less damage, meanwhile avoid stimulus of adjacent axons.

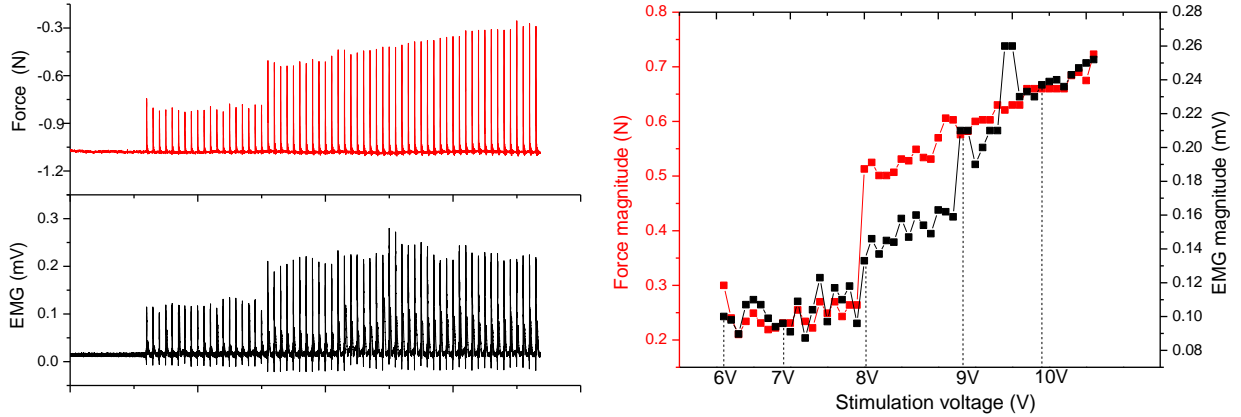
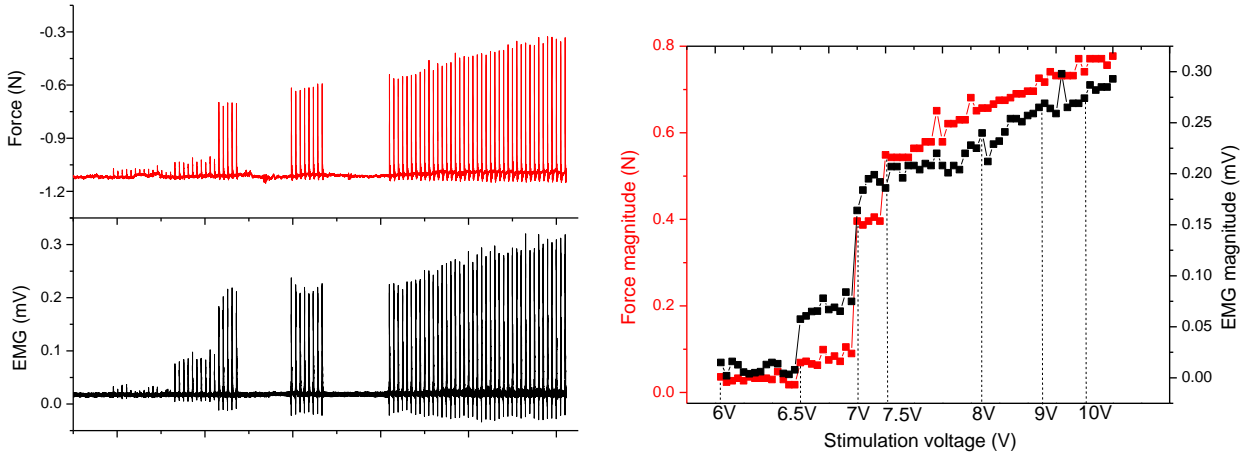
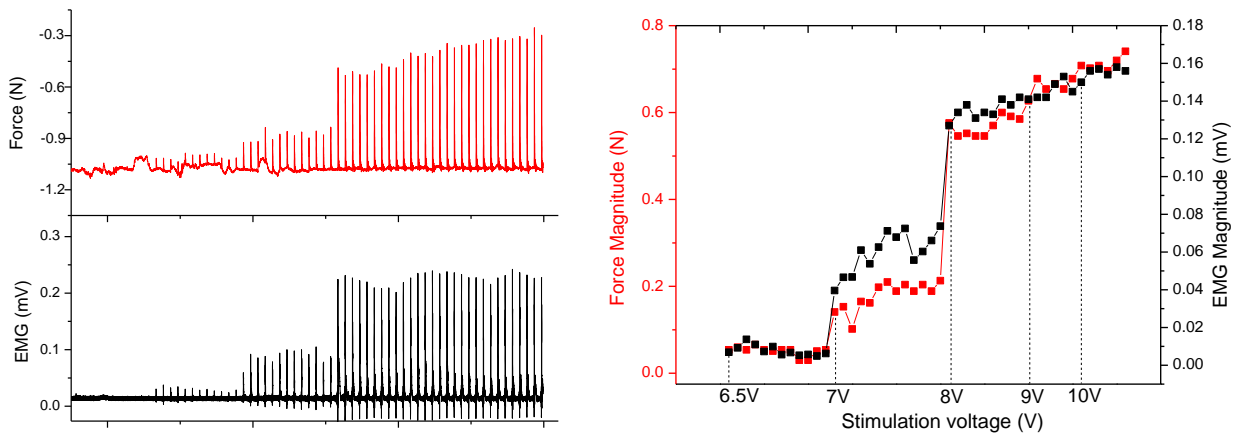
(3) For chronic applications, nerve electrodes have to be stable inside the physiologic environment. Poor adhesion between electrode contact and polymer substrate is normally one of the most common reason for instability. Compared to the usually used sputtering of metal thin films onto the polymer substrate, our work provides a more reliable way to fabricate flexible cuff electrode. The two layer of parylene sandwiched not only the conductive CNT electrode and metal trace, but also the SiN as a buffering layer. Therefore the adhesion of the electrode to the flexible substrate has been greatly enhanced.

(a) 8 (Pt) and 16 (Pt) (distance between electrodes: 0.143cm):

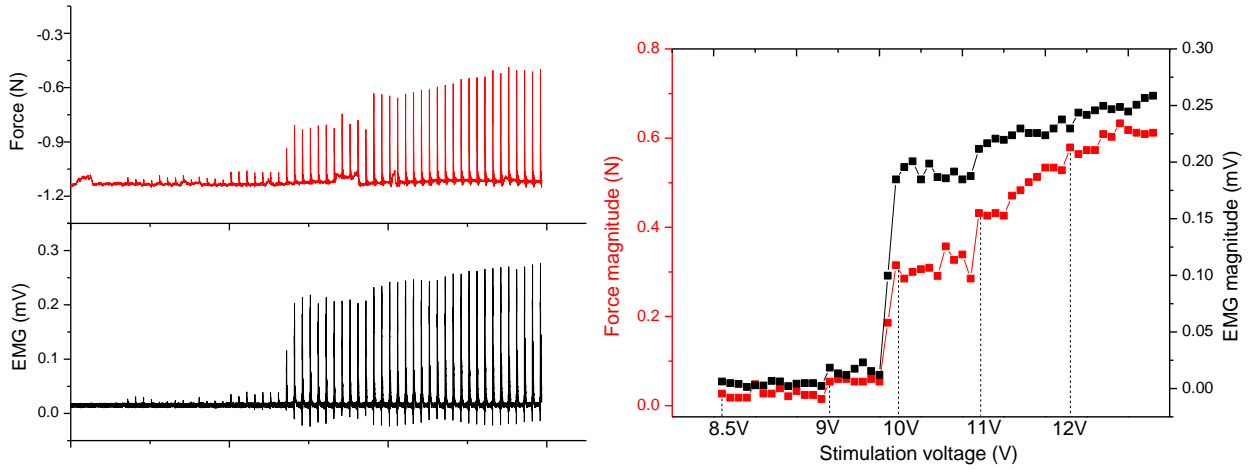


(b) 6(CNT) and 13 (CNT) (distance between electrodes: 0.130cm):



(c) 8(Pt) and 15 (CNT) (distance between electrodes: 0.130cm)::**(d) 8 (Pt) and 2 (CNT) (distance between electrodes: 0.106cm, the discontinuity is pause of stimulation because of change of tape):****(e) 8 (Pt) and 13 (CNT) (distance between electrodes: 0.0946cm):**

(f) 8 (Pt) and 10 (CNT) (distance between electrodes: 0.0363cm):



(g) 8 (Pt) and 7 (CNT) (distance between electrodes: 0.0263cm):

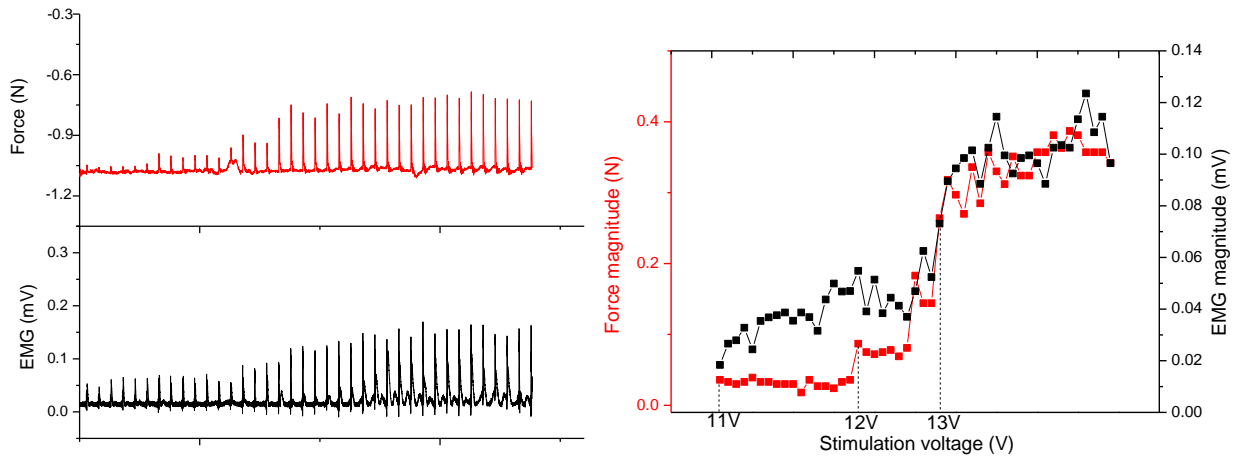


Figure 4.5 the measured force magnitude and the corresponded EMG magnitude for each pair of electrodes.

4.3.2 Comparison of the CNTs and Pt based flexible cuff electrode for neural stimulation

Functional electrical stimulation has many applications. In this thesis, we will focus on restoration of motor functions. The applied stimulus is aimed to achieve contraction in a muscle to perform the desired movement. The amplitude of the pulse must be adequate to successfully stimulate the muscle fibers. The fibers that are nearest to the electrode and have the largest diameters will be excited first. As the amplitude increases, those away from the electrode or with smaller diameters will be recruited. The contraction force generated by the stimulus needs to be properly regulated to reduce the possibilities for muscle damage or fail of function (for example, too much force for grasping will break the

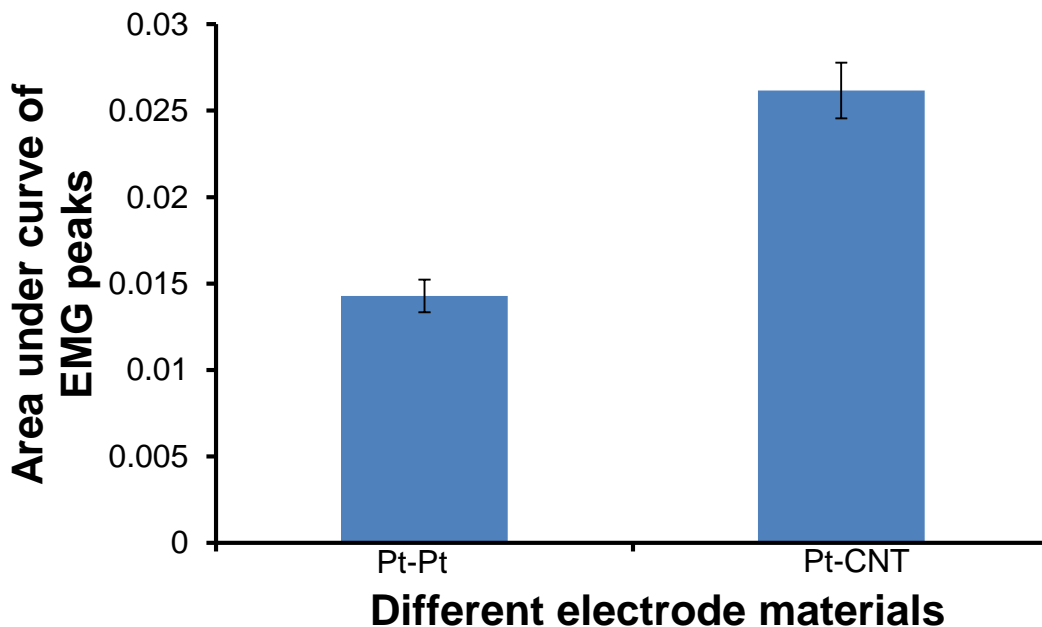


Figure 4.6 the calculated area under curve of EMG peaks at the stimulation voltage 10 V for Pt/Pt (8/16) electrode pair and CNT/Pt (8/15) electrode pair. The error bars are the standard deviation (n = 6).

target item). Thus it is very important to quantify the contraction force when applying different amplitude of stimulus. In this work, a load cell was used to measure the force of

twitching. Figure 4.5 shows the measured EMG response and contraction force generated by the sciatic nerve stimulation. The larger the electrical potential generated by muscle cells, the bigger the force of the twitching. This work provides a reliable way to make guidelines for safe functional electrical stimulation for motor function restoration and rehabilitation.

As discussed in Chapter 2, CNTs is a more effective neural stimulator compared to Pt mainly because of enlarged surface area. In this chapter, we also compared CNTs and Pt in cuff electrode for peripheral nerve stimulation. Figure 4.6 shows the EMG signals collected from 10V stimulation by CNTs/Pt and Pt/Pt electrode couples. At the same level of stimulation magnitude, the area under area of the peak is larger for the signals initiated by CNTs compared to Pt. It indicates that more axons are excited by CNTs electrodes.

4.3.3 Effect of electrode positions

Theoretically, the excitatory field within a cuff can be accurately controlled. Hence, it is possible to precisely manipulate the current flow and regulate the particular neural elements to be activated or blocked. The electric field depends on the distance between the cathode and anode pair. In this work, all 16 electrode sites on a cuff device is labeled as shown in Figure 4.3. Couples of electrodes with different spacing were chosen as anode and cathode for stimulation. The threshold voltage for the muscle fibers to be excited were recorded in Figure 4.8 to compare the effect of the electrode position around the nerve epineurium. The electrode couples that positioned further apart will start twitching at lower voltage. It is because that short circuit is formed easily by putting electrodes closely. As a result, the current will mostly flow through the epineurium. In contrast, current is forced to flow through axons when electrodes are placed far away. Figure 4.7 are the area under

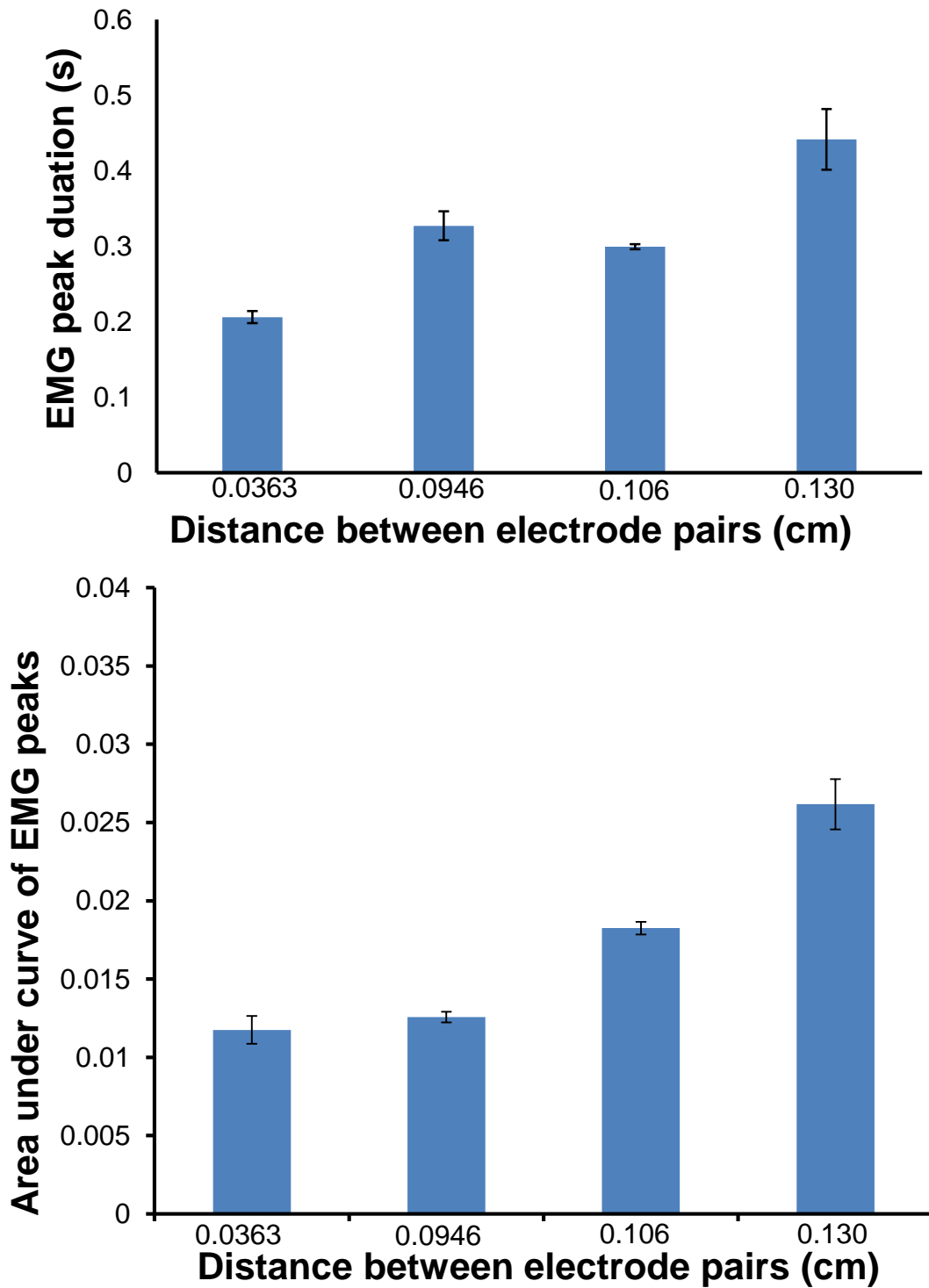


Figure 4.7 Duration (a) and AUC (b) of EMG peaks generated by 10V stimulation via electrode pairs positioned with different distances. The error bars are the standard deviation (n = 6).

curve (AUC) and duration of EMG peaks by 10V stimulation via electrodes at different

distances. When electrodes are placed further away, the electrical route is longer, the number of neurons to be recruited is bigger. Consequently, the duration and AUC of the EMG peak is bigger for the more separated electrodes. The completed mapping of stimulation in future work will be of great significance to guide selective stimulation.

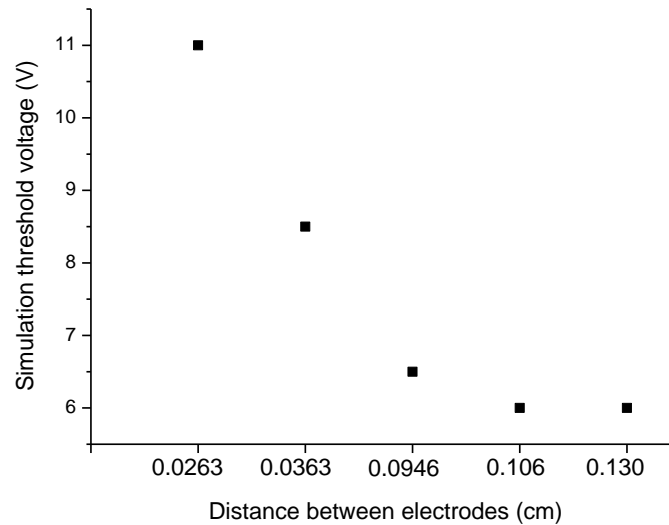


Figure 4.8 Threshold voltage of 10V stimulation via electrode paris positioned at different distances

4.3.4 Effect of stimulation frequency

Neural stimulation is affected not only by stimulation pulse amplitude, but also by frequency. Stimulation frequency determines the output force and the type of contractions. This is possibly due to a process known as “sum of contractions” which takes place in the myofibrils. If the muscle fibers are already in a contracted state and not relaxed before another excitatory stimulus is received, an increased force is generated. At low firing frequency, muscle fibers are contracted with small tension and have enough time to relax before next stimulus takes place. At higher firing rate, muscle contracts with higher force magnitude and less distinction of individual twitches. As the frequency keeps increasing and finally exceed the frequency of tetany, force saturation is achieved. Tetany is the state at which the stimulated muscle will no longer have tremor. As a result, muscle fatigue is

inflicted. Figure 4.9 shows how the muscle respond to different stimulation pulse frequencies (1 Hz, 10 Hz, 100 Hz). At 100 Hz, the muscle fibers reaches the tetany state and the contraction force shows no fluctuation. Our device affords a good platform to investigate the fatigue effect of muscles and facilitate many applications. For example, diagnose the fatigue frequency caused by vibration in driving vehicles in order to support the design of vehicles for comfort driving.

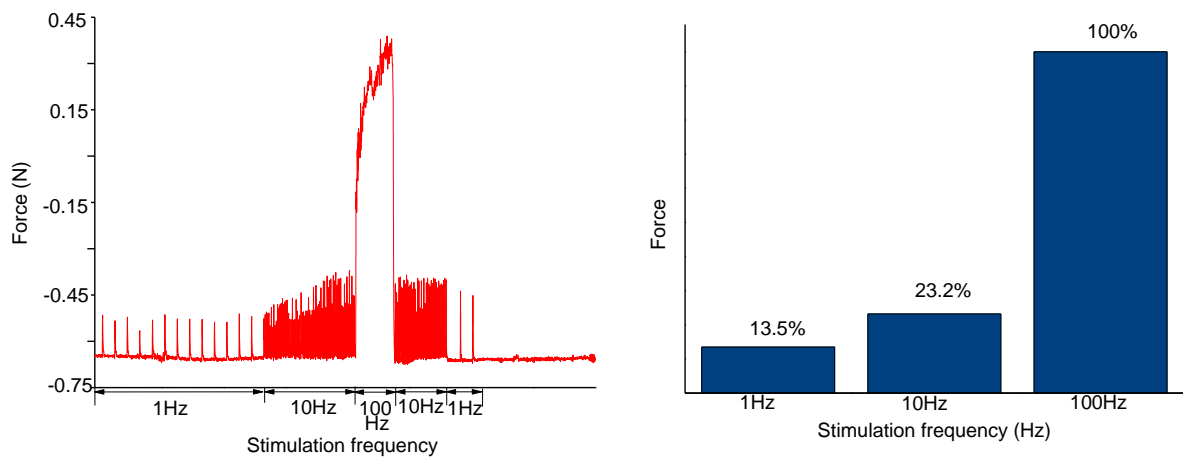


Figure 4.9 (a) EMG magnitude at different stimulation frequency. (b) The percentage of force generated at 1Hz and 10Hz related to the normalized force at 100Hz.

4.3.5 Summary of rat experiments and root cause analysis

Table 4.1 summaries the failed rat experiments that have been done using the fabricated parylene cuff electrode. The success rate is low (2 out of 5) and the failure reasons include: complicate operation procedure leads to dry nerve or device failure; unregulated tightening force blocked the neural transmission. In the future, we need to design simple operation procedure and packaged device to facilitate the mounting of cuff electrode and reduce the damage.

Table 4.1 Analysis of experimental failure

Experiment #	Failure reason	Future resolution
1	Tried to test two limbs. Started testing after operation on two limbs. Nerve died after long time waiting.	Do testing on limbs one by one.
2	Tied the cuff electrode too tight around nerve. The nerve lost function.	Regulation of the suture tightening force.
3	Everything is normal, but no signal.	Electrodes broke during the operation. Need to simplify the operation procedure and make sturdier electrode.

4.4 Conclusions

This chapter has demonstrated a prototype of flexible cuff electrode based on CNTs. The combination of parylene and vertical CNTs is advantageous in safe and effective peripheral nerve stimulation. The preliminary animal test show that CNT is more effective as electrode material than Pt. The electrode couple spaced farther away generates stimulation at lower threshold voltage and with larger amplitude. The work in this chapter provides a promising alternation for the currently used metal on polymer cuff electrodes for clinical applications.

CHAPTER 5 CONCLUSIONS AND FUTURE WORKS

5.1 Conclusions

In this thesis, we developed MEMS devices for neural stimulation/recording and neural chemicals detection, using carbon nanotube/nanofiber bundles as electrodes. Compared to traditionally used planar metal films or carbon films, the carbon nanotube/nanofiber bundles are more advantageous in above applications because: (1) Carbon is more stable and has wider water safe window than metals; (2) The intrinsic 3D nature of carbon nanotube/nanofiber bundles provides more surface area to restore charges and offer more sites for electrochemical reactions to happen. (3) The high strength but low stiffness of CNTs inflicts less tissue damage, critical for effective and long-term neural stimulation/recording. Moreover, the novel fabrication technique demonstrated in the thesis enables the integration of 3D carbon nanotubes with flexible parylene substrate for many non-invasive potential applications.

In Chapter two, we developed a novel fabrication technique to combine CNTs grown at high temperature and heat-sensitive parylene substrate. This method applied two XeF₂ etching steps to wrap the CNTs electrodes with insulating parylene layers. In comparison to normally used fabrication approaches for flexible CNT electrodes, our method can preserve the 3D structures of CNT bundles, consequently more surface area, lower impedance and larger charge capacity. The animal experiment results show that our electrodes can initiate neural signal at voltage as low as 0.3 V, and record signals with high SNR of 12, superior than Pt electrodes and most of other CNT electrodes. It also demonstrates good adhesion of CNTs to the parylene substrate, which is of great significance for chronic applications. This flexible CNT based neural interface is ideal for

effective neural stimulation/recording and has wide applications in pain treatment, prosthetic and therapeutic devices.

In Chapter three, we developed a novel carbon nanofiber structured micro-electrode arrays, derived from photoresist, for FSCV detection of neural transmitters. This design is aimed to address three problems associated with traditional single carbon fiber microelectrode in glass tube: (1) multi-sensing unit make it possible for detection of multi-analysis at different locations in the target; (2) MEMS fabrication techniques improves the repeatability of electrode production and the performances; (3) Carbon nanofiber 3D structure afford more reaction sites for neural chemicals, thus higher detection sensitivity (80nA compared to 10nA for detection of 1uM Dopamine). In particular, our work adopted two-step pyrolysis and dual oxygen-plasma treatment for the electrode fabrication and processing and achieved better performance than other photoresist derived film electrode in dopamine detection using FSCV (fill in numbers). The likely reasons are: (1) We used negative photoresist as precursor material instead of positive photoresist. The flow of negative photoresist during pyrolysis results in better adhesion. In addition, we applied the two-step pyrolysis of the negative photoresist to further improve the adhesion due to the low heating rate; (2) We employed dual oxygen plasma treatment to create nanofiber structure and increase the attachment of oxygen containing functional groups to the fiber surface, facilitating the reaction of dopamine and consequently enhancing the detection sensitivity.

In Chapter four, we extended the work of Chapter two and designed a CNT based flexible cuff electrode for peripheral nerve stimulation. The fabricated cuff electrode can successfully wrap around the rat sciatic nerve and function as stimulator. We also connect

a load cell to record the force associated with the muscle twitching due to the neural stimulation. The results show that CNT electrodes can initiate stronger neural signals than Pt electrodes, indicating that the 3D structure is accessible to more neurons than planar Pt. We also did experiments to illustrate the effect of stimulating frequency and electrodes spacing on the neural stimulation and muscle response. The higher stimulating frequency led to stronger muscle twitching. The tetany frequency is 100Hz. The electrode couples that positioned further apart will generate twitching at lower voltage. These works exhibit the potentiality of this cuff electrode for study of muscle fatigue and mapping of stimulation and use in rehabilitation and peripheral prostheses. But we also noticed the low success rate in the rat experiments and summarized the possible reasons as well as the corresponding solutions. Optimal device geometry and experimental procedures need to be designed for the future work.

5.2 Future works

This thesis has clearly shown that carbon nanotube bundles outperform Pt as neural electrode in effective neural stimulation/recording. However, there are still a number of problems need to be addressed before real clinical applications.

(1) Optimization of synthesis and surface modification of nanotubes/nanofibers pillars

For neural stimulating and neural transmitter detection, the accessible surface area needs to be maximized. The diameter, height and density of the nanotubes/nanofibers in a pillar can be optimized to maximize the active surface area. For CNTs, It can be achieved by better control of the catalyst layer thickness and the synthesis process. For carbon nanofibers derived from photoresist, it can be achieved by better control of photoresist

thickness, the pyrolysis process, and treatment conditions. Surface modification by attached functional groups is another measure to increase the active surface area.

(2) Multi analyte detection

The carbon nanofiber structured electrodes have been proved to be an efficient dopamine detector. Our next step is detection of multiple analytes. Recently, a covalent functionalization strategy to modify surface with specific molecules in controlled densities for FSCV applications has been reported. It was an effective method to integrate selective components to the electrode surfaces without comprising the fast response time of FSCV. In the future work, different channels of an MEA will be modified with certain selective molecules, for the purpose of simultaneous detections of different targets.

(3) Optimized design of flexible cuff CNT electrode

The prototype of flexible cuff CNT electrode has been fabricated and preliminary testing has been demonstrated. And the reason of low success rate has been analyzed. The design of the cuff electrode and operation procedure need to be optimized to achieve improved stimulation efficiency. It is also necessary for the device packaging for future clinical applications.

BIBLIORGRAPHY

- [1] G. Loeb, R. Peck, and J. Martyniuk, "Toward the ultimate metal microelectrode," *Journal of neuroscience methods*, vol. 63, pp. 175-183, 1995.
- [2] K. T. Kawagoe, J. B. Zimmerman, and R. M. Wightman, "Principles of voltammetry and microelectrode surface states," *Journal of neuroscience methods*, vol. 48, pp. 225-240, 1993.
- [3] S. Samaranayake, A. Abdalla, R. Robke, K. M. Wood, A. Zeqja, and P. Hashemi, "In vivo histamine voltammetry in the mouse preammillary nucleus," *Analyst*, vol. 140, pp. 3759-3765, 2015.
- [4] S. d. Bendahhou, T. R. Cummins, R. Tawil, S. G. Waxman, and L. J. Ptáček, "Activation and inactivation of the voltage-gated sodium channel: role of segment S5 revealed by a novel hyperkalaemic periodic paralysis mutation," *The Journal of neuroscience*, vol. 19, pp. 4762-4771, 1999.
- [5] D. R. Kipke, W. Shain, G. Buzsáki, E. Fetz, J. M. Henderson, J. F. Hetke, *et al.*, "Advanced neurotechnologies for chronic neural interfaces: new horizons and clinical opportunities," *The Journal of Neuroscience*, vol. 28, pp. 11830-11838, 2008.
- [6] S. E. Hochstetler, M. Puopolo, S. Gustincich, E. Raviola, and R. M. Wightman, "Real-time amperometric measurements of zeptomole quantities of dopamine released from neurons," *Analytical chemistry*, vol. 72, pp. 489-496, 2000.
- [7] S. F. Dressman, J. L. Peters, and A. C. Michael, "Carbon fiber microelectrodes with multiple sensing elements for in vivo voltammetry," *Journal of neuroscience methods*, vol. 119, pp. 75-81, 2002.

- [8] L. R. Hochberg, M. D. Serruya, G. M. Friehs, J. A. Mukand, M. Saleh, A. H. Caplan, *et al.*, "Neuronal ensemble control of prosthetic devices by a human with tetraplegia," *Nature*, vol. 442, pp. 164-171, 2006.
- [9] C.-W. Chang and J.-C. Chiou, "A wireless and batteryless microsystem with implantable grid electrode/3-dimensional probe array for ECoG and extracellular neural recording in rats," *Sensors*, vol. 13, pp. 4624-4639, 2013.
- [10] J. L. Vitek, R. A. Bakay, T. Hashimoto, Y. Kaneoke, K. Mewes, J. Y. Zhang, *et al.*, "Microelectrode-guided pallidotomy: technical approach and its application in medically intractable Parkinson's disease," *Journal of neurosurgery*, vol. 88, pp. 1027-1043, 1998.
- [11] S. Cash, I. Ulbert, O. Devinsky, E. Bromfield, J. Madsen, A. Cole, *et al.*, "Laminar microelectrode recordings of human interictal discharges in neocortical epilepsy reveal complex high-frequency oscillation patterns," in *Epilepsia*, 2005, pp. 93-94.
- [12] D. C. Shields, M. L. Cheng, A. W. Flaherty, J. T. Gale, and E. N. Eskandar, "Microelectrode-guided deep brain stimulation for Tourette syndrome: within-subject comparison of different stimulation sites," *Stereotactic and functional neurosurgery*, vol. 86, pp. 87-91, 2007.
- [13] K. W. Horch and G. S. Dhillon, *Neuroprosthetics: theory and practice*: World Scientific, 2004.
- [14] V. D. Chase, *Shattered Nerves: How Science is Solving Modern Medicine's Most Perplexing Problem*: JHU Press, 2006.
- [15] M. De Vittorio, L. Martiradonna, and J. Assad, *Nanotechnology and Neuroscience: Nano-electronic, Photonic and Mechanical Neuronal Interfacing*: Springer, 2014.

- [16] S. L. Foote, R. Freedman, and A. P. Oliver, "Effects of putative neurotransmitters on neuronal activity in monkey auditory cortex," *Brain research*, vol. 86, pp. 229-242, 1975.
- [17] W. S. Agnew, A. C. Moore, S. R. Levinson, and M. A. Raftery, "Identification of a large molecular weight peptide associated with a tetrodotoxin binding protein from the electroplax of *Electrophorus electricus*," *Biochemical and biophysical research communications*, vol. 92, pp. 860-866, 1980.
- [18] A. L. Hodgkin and A. F. Huxley, "A quantitative description of membrane current and its application to conduction and excitation in nerve," *The Journal of physiology*, vol. 117, p. 500, 1952.
- [19] M. A. Nicolelis, D. Dimitrov, J. M. Carmena, R. Crist, G. Lehew, J. D. Kralik, *et al.*, "Chronic, multisite, multielectrode recordings in macaque monkeys," *Proceedings of the National Academy of Sciences*, vol. 100, pp. 11041-11046, 2003.
- [20] E. W. Keefer, B. R. Botterman, M. I. Romero, A. F. Rossi, and G. W. Gross, "Carbon nanotube coating improves neuronal recordings," *Nature nanotechnology*, vol. 3, pp. 434-439, 2008.
- [21] H.-B. Zhou, G. Li, X.-N. Sun, Z.-H. Zhu, Q.-H. Jin, J.-L. Zhao, *et al.*, "Integration of Au nanorods with flexible thin-film microelectrode arrays for improved neural interfaces," *Microelectromechanical Systems, Journal of*, vol. 18, pp. 88-96, 2009.
- [22] H. Yoon, D. C. Deshpande, V. Ramachandran, and V. K. Varadan, "Aligned nanowire growth using lithography-assisted bonding of a polycarbonate template for neural probe electrodes," *Nanotechnology*, vol. 19, p. 025304, 2008.

- [23] V. Lovat, D. Pantarotto, L. Lagostena, B. Cacciari, M. Grandolfo, M. Righi, *et al.*, "Carbon nanotube substrates boost neuronal electrical signaling," *Nano letters*, vol. 5, pp. 1107-1110, 2005.
- [24] F. Patolsky, B. P. Timko, G. Yu, Y. Fang, A. B. Greytak, G. Zheng, *et al.*, "Detection, stimulation, and inhibition of neuronal signals with high-density nanowire transistor arrays," *Science*, vol. 313, pp. 1100-1104, 2006.
- [25] T. Dvir, B. P. Timko, M. D. Brigham, S. R. Naik, S. S. Karajanagi, O. Levy, *et al.*, "Nanowired three-dimensional cardiac patches," *Nature nanotechnology*, vol. 6, pp. 720-725, 2011.
- [26] L. H. Hess, M. Jansen, V. Maybeck, M. V. Hauf, M. Seifert, M. Stutzmann, *et al.*, "Graphene transistor arrays for recording action potentials from electrogenic cells," *Advanced Materials*, vol. 23, pp. 5045-5049, 2011.
- [27] C. Chen, C. Lin, J. Chen, W. Hsu, Y. Chang, S. Yeh, *et al.*, "A graphene-based microelectrode for recording neural signals," in *Solid-State Sensors, Actuators and Microsystems Conference (TRANSDUCERS), 2011 16th International*, 2011, pp. 1883-1886.
- [28] M. R. Abidian, K. A. Ludwig, T. C. Marzullo, D. C. Martin, and D. R. Kipke, "Interfacing Conducting Polymer Nanotubes with the Central Nervous System: Chronic Neural Recording using Poly (3, 4-ethylenedioxythiophene) Nanotubes," *Advanced Materials*, vol. 21, pp. 3764-3770, 2009.
- [29] K. N. Layton and M. R. Abidian, "Conducting polymer nanofiber-based biosensor for detection of neurochemicals," in *Neural Engineering (NER), 2011 5th International IEEE/EMBS Conference on*, 2011, pp. 298-301.

- [30] E. R. Kandel, J. H. Schwartz, and T. M. Jessell, *Principles of neural science* vol. 4: McGraw-Hill New York, 2000.
- [31] K. J. Ressler and C. B. Nemeroff, "Role of serotonergic and noradrenergic systems in the pathophysiology of depression and anxiety disorders," *Depression and anxiety*, vol. 12, pp. 2-19, 2000.
- [32] M. Jouvet, "Biogenic amines and the states of sleep," *Science*, 1969.
- [33] C. C. Meltzer, G. Smith, S. T. DeKosky, B. G. Pollock, C. A. Mathis, R. Y. Moore, *et al.*, "Serotonin in aging, late-life depression, and Alzheimer's disease: the emerging role of functional imaging," *Neuropsychopharmacology*, vol. 18, pp. 407-430, 1998.
- [34] S. J. Kish, K. Shannak, and O. Hornykiewicz, "Uneven pattern of dopamine loss in the striatum of patients with idiopathic Parkinson's disease," *New England Journal of Medicine*, vol. 318, pp. 876-880, 1988.
- [35] I. Creese, D. R. Burt, and S. H. Snyder, "Dopamine receptor binding predicts clinical and pharmacological potencies of antischizophrenic drugs," *Science*, vol. 192, pp. 481-483, 1976.
- [36] W. Schultz, "The reward signal of midbrain dopamine neurons," *Physiology*, vol. 14, pp. 249-255, 1999.
- [37] K. B. Fink and M. Göthert, "5-HT receptor regulation of neurotransmitter release," *Pharmacological reviews*, vol. 59, pp. 360-417, 2007.
- [38] M. Wang, G. T. Roman, M. L. Perry, and R. T. Kennedy, "Microfluidic chip for high efficiency electrophoretic analysis of segmented flow from a microdialysis

- probe and in vivo chemical monitoring," *Analytical chemistry*, vol. 81, pp. 9072-9078, 2009.
- [39] S. S. Park, M. Hong, C.-K. Song, G.-J. Jhon, Y. Lee, and M. Suh, "Real-time in vivo simultaneous measurements of nitric oxide and oxygen using an amperometric dual microsensor," *Analytical chemistry*, vol. 82, pp. 7618-7624, 2010.
- [40] R. M. Wightman, "Probing cellular chemistry in biological systems with microelectrodes," *Science*, vol. 311, pp. 1570-1574, 2006.
- [41] M. Armstrong-James, J. Millar, and Z. Kruk, "Quantification of noradrenaline iontophoresis," 1980.
- [42] M. K. Zachek, P. Takmakov, B. Moody, R. M. Wightman, and G. S. McCarty, "Simultaneous decoupled detection of dopamine and oxygen using pyrolyzed carbon microarrays and fast-scan cyclic voltammetry," *Analytical chemistry*, vol. 81, pp. 6258-6265, 2009.
- [43] P. E. Phillips, P. J. Hancock, and J. A. Stamford, "Time window of autoreceptor-mediated inhibition of limbic and striatal dopamine release," *Synapse*, vol. 44, pp. 15-22, 2002.
- [44] T. Gabay, M. Ben-David, I. Kalifa, R. Sorkin, R. A. Ze'ev, E. Ben-Jacob, *et al.*, "Electro-chemical and biological properties of carbon nanotube based multi-electrode arrays," *Nanotechnology*, vol. 18, p. 035201, 2007.
- [45] G. Gabriel, R. Gómez, M. Bongard, N. Benito, E. Fernández, and R. Villa, "Easily made single-walled carbon nanotube surface microelectrodes for neuronal applications," *Biosensors and Bioelectronics*, vol. 24, pp. 1942-1948, 2009.

- [46] K. Fuchsberger, A. L. Goff, L. Gambazzi, F. M. Toma, A. Goldoni, M. Giugliano, *et al.*, "Multiwalled Carbon-Nanotube-Functionalized Microelectrode Arrays Fabricated by Microcontact Printing: Platform for Studying Chemical and Electrical Neuronal Signaling," *Small*, vol. 7, pp. 524-530, 2011.
- [47] K. Wang, H. A. Fishman, H. Dai, and J. S. Harris, "Neural stimulation with a carbon nanotube microelectrode array," *Nano letters*, vol. 6, pp. 2043-2048, 2006.
- [48] Z. Yu, T. E. McKnight, M. N. Ericson, A. V. Melechko, M. L. Simpson, and B. Morrison, "Vertically aligned carbon nanofiber arrays record electrophysiological signals from hippocampal slices," *Nano letters*, vol. 7, pp. 2188-2195, 2007.
- [49] M. Shein, A. Greenbaum, T. Gabay, R. Sorkin, M. David-Pur, E. Ben-Jacob, *et al.*, "Engineered neuronal circuits shaped and interfaced with carbon nanotube microelectrode arrays," *Biomedical microdevices*, vol. 11, pp. 495-501, 2009.
- [50] M. S. Idelson, E. Ben-Jacob, and Y. Hanein, "Innate synchronous oscillations in freely-organized small neuronal circuits," *PLoS One*, vol. 5, p. e14443, 2010.
- [51] A. Shoval, C. Adams, M. David-Pur, M. Shein, Y. Hanein, and E. Sernagor, "Carbon nanotube electrodes for effective interfacing with retinal tissue," *Frontiers in neuroengineering*, vol. 2, 2009.
- [52] D. Edward Jr, T. B. Nguyen-Vu, P. U. Arumugam, H. Chen, A. M. Cassell, R. J. Andrews, *et al.*, "High efficient electrical stimulation of hippocampal slices with vertically aligned carbon nanofiber microbrush array," *Biomedical microdevices*, vol. 11, pp. 801-808, 2009.

- [53] H.-C. Su, C.-M. Lin, S.-J. Yen, Y.-C. Chen, C.-H. Chen, S.-R. Yeh, *et al.*, "A cone-shaped 3D carbon nanotube probe for neural recording," *Biosensors and Bioelectronics*, vol. 26, pp. 220-227, 2010.
- [54] Y. Hanein, "Carbon nanotube integration into MEMS devices," *physica status solidi (b)*, vol. 247, pp. 2635-2640, 2010.
- [55] C.-M. Lin, Y.-T. Lee, S.-R. Yeh, and W. Fang, "Flexible carbon nanotubes electrode for neural recording," *Biosensors and Bioelectronics*, vol. 24, pp. 2791-2797, 2009.
- [56] H. L. Hsu, I. J. Teng, Y. C. Chen, W. L. Hsu, Y. T. Lee, S. J. Yen, *et al.*, "Flexible UV-Ozone-Modified Carbon Nanotube Electrodes for Neuronal Recording," *Advanced Materials*, vol. 22, pp. 2177-2181, 2010.
- [57] Y.-C. Chen, H.-L. Hsu, Y.-T. Lee, H.-C. Su, S.-J. Yen, C.-H. Chen, *et al.*, "An active, flexible carbon nanotube microelectrode array for recording electrocorticograms," *Journal of neural engineering*, vol. 8, p. 034001, 2011.
- [58] H. S. Mayberg, A. M. Lozano, V. Voon, H. E. McNeely, D. Seminowicz, C. Hamani, *et al.*, "Deep brain stimulation for treatment-resistant depression," *Neuron*, vol. 45, pp. 651-660, 2005.
- [59] T. Nguyen-Vu, H. Chen, A. M. Cassell, R. Andrews, M. Meyyappan, and J. Li, "Vertically aligned carbon nanofiber arrays: an advance toward electrical–neural interfaces," *Small*, vol. 2, pp. 89-94, 2006.
- [60] T. B. Nguyen-Vu, H. Chen, A. M. Cassell, R. J. Andrews, M. Meyyappan, and J. Li, "Vertically aligned carbon nanofiber architecture as a multifunctional 3-D

- neural electrical interface," *Biomedical Engineering, IEEE Transactions on*, vol. 54, pp. 1121-1128, 2007.
- [61] A. Parent, "Giovanni Aldini: from animal electricity to human brain stimulation," *The Canadian Journal of Neurological Sciences*, vol. 31, pp. 576-584, 2004.
- [62] V. S. Polikov, P. A. Tresco, and W. M. Reichert, "Response of brain tissue to chronically implanted neural electrodes," *Journal of neuroscience methods*, vol. 148, pp. 1-18, 2005.
- [63] P. J. Rousche and R. A. Normann, "Chronic recording capability of the Utah Intracortical Electrode Array in cat sensory cortex," *Journal of neuroscience methods*, vol. 82, pp. 1-15, 1998.
- [64] F. Sauter-Starace, O. Bibari, F. Berger, P. Caillat, and A. Benabid, "ECoG recordings of a non-human primate using carbon nanotubes electrodes on a flexible polyimide implant," in *Neural Engineering, 2009. NER'09. 4th International IEEE/EMBS Conference on*, 2009, pp. 112-115.
- [65] J. R. Wolpaw, N. Birbaumer, D. J. McFarland, G. Pfurtscheller, and T. M. Vaughan, "Brain-computer interfaces for communication and control," *Clinical neurophysiology*, vol. 113, pp. 767-791, 2002.
- [66] J. R. Wolpaw and D. J. McFarland, "Control of a two-dimensional movement signal by a noninvasive brain-computer interface in humans," *Proceedings of the National Academy of Sciences of the United States of America*, vol. 101, pp. 17849-17854, 2004.
- [67] J. J. Pancrazio, "Neural interfaces at the nanoscale," 2008.

- [68] C. Thomsen and S. Reich, "Raman scattering in carbon nanotubes," in *Light Scattering in Solid IX*, ed: Springer, 2007, pp. 115-234.
- [69] M. Shao, D. Wang, G. Yu, B. Hu, W. Yu, and Y. Qian, "The synthesis of carbon nanotubes at low temperature via carbon suboxide disproportionation," *Carbon*, vol. 42, pp. 183-185, 2004.
- [70] S. F. Cogan, "Neural stimulation and recording electrodes," *Annu. Rev. Biomed. Eng.*, vol. 10, pp. 275-309, 2008.
- [71] D. R. Merrill, M. Bikson, and J. G. Jefferys, "Electrical stimulation of excitable tissue: design of efficacious and safe protocols," *Journal of neuroscience methods*, vol. 141, pp. 171-198, 2005.
- [72] L. Robblee, J. McHardy, W. Agnew, and L. Bullara, "Electrical stimulation with Pt electrodes. VII. Dissolution of Pt electrodes during electrical stimulation of the cat cerebral cortex," *Journal of neuroscience methods*, vol. 9, pp. 301-308, 1983.
- [73] C.-H. Chen, H.-C. Su, S.-C. Chuang, S.-J. Yen, Y.-C. Chen, Y.-T. Lee, *et al.*, "Hydrophilic modification of neural microelectrode arrays based on multi-walled carbon nanotubes," *Nanotechnology*, vol. 21, p. 485501, 2010.
- [74] J. Berg-Johnsen and I. Langmoen, "Isoflurane hyperpolarizes neurones in rat and human cerebral cortex," *Acta physiologica scandinavica*, vol. 130, pp. 679-685, 1987.
- [75] T. H. Yoon, E. J. Hwang, D. Y. Shin, S. I. Park, S. J. Oh, S. C. Jung, *et al.*, "A micromachined silicon depth probe for multichannel neural recording," *Biomedical Engineering, IEEE Transactions on*, vol. 47, pp. 1082-1087, 2000.

- [76] B. Zhang, K. L. Adams, S. J. Lubner, D. J. Eves, M. L. Heien, and A. G. Ewing, "Spatially and temporally resolved single-cell exocytosis utilizing individually addressable carbon microelectrode arrays," *Analytical chemistry*, vol. 80, pp. 1394-1400, 2008.
- [77] C. Wang, G. Jia, L. H. Taherabadi, and M. J. Madou, "A novel method for the fabrication of high-aspect ratio C-MEMS structures," *Microelectromechanical Systems, Journal of*, vol. 14, pp. 348-358, 2005.
- [78] S. Ranganathan and R. L. McCreery, "Electroanalytical performance of carbon films with near-atomic flatness," *Analytical chemistry*, vol. 73, pp. 893-900, 2001.
- [79] R. Wightman, C. Amatorh, R. Engstrom, P. Hale, E. Kristensen, W. Kuhr, *et al.*, "Real-time characterization of dopamine overflow and uptake in the rat striatum," *Neuroscience*, vol. 25, pp. 513-523, 1988.
- [80] A. M. Strand and B. J. Venton, "Flame etching enhances the sensitivity of carbon-fiber microelectrodes," *Analytical chemistry*, vol. 80, pp. 3708-3715, 2008.
- [81] A. G. Zestos, M. D. Nguyen, B. L. Poe, C. B. Jacobs, and B. J. Venton, "Epoxy insulated carbon fiber and carbon nanotube fiber microelectrodes," *Sensors and Actuators B: Chemical*, vol. 182, pp. 652-658, 2013.
- [82] M. G. Schrlau, N. J. Dun, and H. H. Bau, "Cell electrophysiology with carbon nanopipettes," *ACS nano*, vol. 3, pp. 563-568, 2009.
- [83] R. Singhal, S. Bhattacharyya, Z. Orynbayeva, E. Vitol, G. Friedman, and Y. Gogotsi, "Small diameter carbon nanopipettes," *Nanotechnology*, vol. 21, p. 015304, 2010.

- [84] K. C. Morton, C. A. Morris, M. A. Derylo, R. Thakar, and L. A. Baker, "Carbon electrode fabrication from pyrolyzed parylene C," *Analytical chemistry*, vol. 83, pp. 5447-5452, 2011.
- [85] A. Hermans and R. M. Wightman, "Conical tungsten tips as substrates for the preparation of ultramicroelectrodes," *Langmuir*, vol. 22, pp. 10348-10353, 2006.
- [86] O. Niwa, J. Jia, Y. Sato, D. Kato, R. Kurita, K. Maruyama, *et al.*, "Electrochemical performance of angstrom level flat sputtered carbon film consisting of sp² and sp³ mixed bonds," *Journal of the American Chemical Society*, vol. 128, pp. 7144-7145, 2006.
- [87] J. E. Koehne, M. Marsh, A. Boakye, B. Douglas, I. Y. Kim, S.-Y. Chang, *et al.*, "Carbon nanofiber electrode array for electrochemical detection of dopamine using fast scan cyclic voltammetry," *Analyst*, vol. 136, pp. 1802-1805, 2011.
- [88] O. Niwa and H. Tabei, "Voltammetric measurements of reversible and quasi-reversible redox species using carbon film based interdigitated array microelectrodes," *Analytical Chemistry*, vol. 66, pp. 285-289, 1994.
- [89] Y. Song, R. Agrawal, Y. Hao, C. Chen, and C. Wang, "C-MEMS based microsupercapacitors and microsensors," *ECS Transactions*, vol. 61, pp. 55-64, 2014.
- [90] R. KostECKI, X. Song, and K. Kinoshita, "Fabrication of interdigitated carbon structures by laser pyrolysis of photoresist," *Electrochemical and solid-state letters*, vol. 5, pp. E29-E31, 2002.
- [91] J. J. VanDersarl, A. Mercanzini, and P. Renaud, "Integration of 2D and 3D Thin Film Glassy Carbon Electrode Arrays for Electrochemical Dopamine Sensing in

- Flexible Neuroelectronic Implants," *Advanced Functional Materials*, vol. 25, pp. 78-84, 2015.
- [92] L. M. Moretto, A. Mardegan, M. Cettolin, and P. Scopece, "Pyrolyzed Photoresist Carbon Electrodes for Trace Electroanalysis of Nickel (II)," *Chemosensors*, vol. 3, pp. 157-168, 2015.
- [93] A. K. Dengler and G. S. McCarty, "Microfabricated microelectrode sensor for measuring background and slowly changing dopamine concentrations," *Journal of Electroanalytical Chemistry*, vol. 693, pp. 28-33, 2013.
- [94] M. K. Zachek, A. Hermans, R. M. Wightman, and G. S. McCarty, "Electrochemical dopamine detection: comparing gold and carbon fiber microelectrodes using background subtracted fast scan cyclic voltammetry," *Journal of Electroanalytical Chemistry*, vol. 614, pp. 113-120, 2008.
- [95] M. K. Zachek, J. Park, P. Takmakov, R. M. Wightman, and G. S. McCarty, "Microfabricated FSCV-compatible microelectrode array for real-time monitoring of heterogeneous dopamine release," *Analyst*, vol. 135, pp. 1556-1563, 2010.
- [96] V. Penmatsa, T. Kim, M. Beidaghi, H. Kawarada, L. Gu, Z. Wang, *et al.*, "Three-dimensional graphene nanosheet encrusted carbon micropillar arrays for electrochemical sensing," *Nanoscale*, vol. 4, pp. 3673-3678, 2012.
- [97] V. Penmatsa, A. R. Ruslinda, M. Beidaghi, H. Kawarada, and C. Wang, "Platelet-derived growth factor oncoprotein detection using three-dimensional carbon microarrays," *Biosensors and bioelectronics*, vol. 39, pp. 118-123, 2013.

- [98] H. Xu, K. Malladi, C. Wang, L. Kulinsky, M. Song, and M. Madou, "Carbon post-microarrays for glucose sensors," *Biosensors and Bioelectronics*, vol. 23, pp. 1637-1644, 2008.
- [99] S. Xi, T. Shi, D. Liu, L. Xu, H. Long, W. Lai, *et al.*, "Integration of carbon nanotubes to three-dimensional C-MEMS for glucose sensors," *Sensors and Actuators A: Physical*, vol. 198, pp. 15-20, 2013.
- [100] J. Kim, X. Song, K. Kinoshita, M. Madou, and R. White, "Electrochemical studies of carbon films from pyrolyzed photoresist," *Journal of the Electrochemical Society*, vol. 145, pp. 2314-2319, 1998.
- [101] A. Singh, J. Jayaram, M. Madou, and S. Akbar, "Pyrolysis of negative photoresists to fabricate carbon structures for microelectromechanical systems and electrochemical applications," *Journal of the electrochemical society*, vol. 149, pp. E78-E83, 2002.
- [102] R. Kostecky, B. Schnyder, D. Alliata, X. Song, K. Kinoshita, and R. Kötz, "Surface studies of carbon films from pyrolyzed photoresist," *Thin Solid Films*, vol. 396, pp. 36-43, 2001.
- [103] S. Donner, H.-W. Li, E. S. Yeung, and M. D. Porter, "Fabrication of optically transparent carbon electrodes by the pyrolysis of photoresist films: approach to single-molecule spectroelectrochemistry," *Analytical chemistry*, vol. 78, pp. 2816-2822, 2006.
- [104] D. Sánchez-Molas, J. Cases-Utrera, P. Godignon, and F. J. del Campo, "Mercury detection at microfabricated pyrolyzed photoresist film (PPF) disk electrodes," *Sensors and Actuators B: Chemical*, vol. 186, pp. 293-299, 2013.

- [105] P. Hashemi, E. C. Dankoski, R. Lama, K. M. Wood, P. Takmakov, and R. M. Wightman, "Brain dopamine and serotonin differ in regulation and its consequences," *Proceedings of the National Academy of Sciences*, vol. 109, pp. 11510-11515, 2012.
- [106] P. Pathirathna, Y. Yang, K. Forzley, S. P. McElmurry, and P. Hashemi, "Fast-scan deposition-stripping voltammetry at carbon-fiber microelectrodes: real-time, subsecond, mercury free measurements of copper," *Analytical chemistry*, vol. 84, pp. 6298-6302, 2012.
- [107] Y. Yang, P. Pathirathna, T. Siriwardhane, S. P. McElmurry, and P. Hashemi, "Real-time subsecond voltammetric analysis of Pb in aqueous environmental samples," *Analytical chemistry*, vol. 85, pp. 7535-7541, 2013.
- [108] P. Takmakov, M. K. Zachek, R. B. Keithley, P. L. Walsh, C. Donley, G. S. McCarty, *et al.*, "Carbon microelectrodes with a renewable surface," *Analytical chemistry*, vol. 82, pp. 2020-2028, 2010.
- [109] M. Poon and R. L. McCreery, "In situ laser activation of glassy carbon electrodes," *Analytical Chemistry*, vol. 58, pp. 2745-2750, 1986.
- [110] M. L. Heien, P. E. Phillips, G. D. Stuber, A. T. Seipel, and R. M. Wightman, "Overoxidation of carbon-fiber microelectrodes enhances dopamine adsorption and increases sensitivity," *Analyst*, vol. 128, pp. 1413-1419, 2003.
- [111] F. Gonon, C. Fombarlet, M. Buda, and J. F. Pujol, "Electrochemical treatment of pyrolytic carbon fiber electrodes," *Analytical Chemistry*, vol. 53, pp. 1386-1389, 1981.

- [112] J. G. Roberts, B. P. Moody, G. S. McCarty, and L. A. Sombers, "Specific oxygen-containing functional groups on the carbon surface underlie an enhanced sensitivity to dopamine at electrochemically pretreated carbon fiber microelectrodes," *Langmuir*, vol. 26, pp. 9116-9122, 2010.
- [113] A. S. Khan and A. C. Michael, "Invasive consequences of using micro-electrodes and microdialysis probes in the brain," *TrAC Trends in Analytical Chemistry*, vol. 22, pp. 503-508, 2003.
- [114] M. F. De Volder, R. Vansweevelt, P. Wagner, D. Reynaerts, C. Van Hoof, and A. J. Hart, "Hierarchical carbon nanowire microarchitectures made by plasma-assisted pyrolysis of photoresist," *Acs Nano*, vol. 5, pp. 6593-6600, 2011.
- [115] R. L. McCreery, "Advanced carbon electrode materials for molecular electrochemistry," *Chem. Rev.*, vol. 108, pp. 2646-2687, 2008.
- [116] G. M. Jenkins and K. Kawamura, *Polymeric carbons--carbon fibre, glass and char*: Cambridge University Press, 1976.
- [117] S. Ranganathan, R. McCreery, S. M. Majji, and M. Madou, "Photoresist-Derived Carbon for Microelectromechanical Systems and Electrochemical Applications," *Journal of the Electrochemical Society*, vol. 147, pp. 277-282, 2000.
- [118] M. Hirabayashi, B. Mehta, N. W. Vahidi, A. Khosla, and S. Kassegne, "Functionalization and characterization of pyrolyzed polymer based carbon microstructures for bionanoelectronics platforms," *Journal of Micromechanics and Microengineering*, vol. 23, p. 115001, 2013.

- [119] P. Hashemi, E. C. Dankoski, J. Petrovic, R. B. Keithley, and R. Wightman, "Voltammetric detection of 5-hydroxytryptamine release in the rat brain," *Analytical chemistry*, vol. 81, pp. 9462-9471, 2009.
- [120] R. T. Kachoosangi and R. G. Compton, "A simple electroanalytical methodology for the simultaneous determination of dopamine, serotonin and ascorbic acid using an unmodified edge plane pyrolytic graphite electrode," *Analytical and bioanalytical chemistry*, vol. 387, pp. 2793-2800, 2007.
- [121] J. G. Roberts, K. L. Hamilton, and L. A. Sombers, "Comparison of electrode materials for the detection of rapid hydrogen peroxide fluctuations using background-subtracted fast scan cyclic voltammetry," *Analyst*, vol. 136, pp. 3550-3556, 2011.
- [122] C. Chen, B. Liang, A. Ogino, X. Wang, and M. Nagatsu, "Oxygen functionalization of multiwall carbon nanotubes by microwave-excited surface-wave plasma treatment," *The Journal of Physical Chemistry C*, vol. 113, pp. 7659-7665, 2009.
- [123] A. Felten, C. Bittencourt, J.-J. Pireaux, G. Van Lier, and J.-C. Charlier, "Radio-frequency plasma functionalization of carbon nanotubes surface O₂, NH₃, and CF₄ treatments," *Journal of Applied Physics*, vol. 98, p. 074308, 2005.
- [124] I. P. Clements, V. J. Mukhatyar, A. Srinivasan, J. T. Bentley, D. S. Andreasen, and R. V. Bellamkonda, "Regenerative scaffold electrodes for peripheral nerve interfacing," *Neural Systems and Rehabilitation Engineering, IEEE Transactions on*, vol. 21, pp. 554-566, 2013.

- [125] R. K. Gore, Y. Choi, R. Bellamkonda, and A. English, "Functional recordings from awake, behaving rodents through a microchannel based regenerative neural interface," *Journal of neural engineering*, vol. 12, p. 016017, 2015.
- [126] W. M. Tsang, A. L. Stone, Z. N. Aldworth, J. G. Hildebrand, T. L. Daniel, A. I. Akinwande, *et al.*, "Flexible split-ring electrode for insect flight biasing using multisite neural stimulation," *Biomedical Engineering, IEEE Transactions On*, vol. 57, pp. 1757-1764, 2010.
- [127] N. Xue, T. Sun, W. M. Tsang, I. Delgado-Martinez, S.-H. Lee, S. Sheshadri, *et al.*, "Polymeric C-shaped cuff electrode for recording of peripheral nerve signal," *Sensors and Actuators B: Chemical*, vol. 210, pp. 640-648, 2015.
- [128] S. J. Park, Y. J. Lee, D. N. Heo, I. K. Kwon, K.-S. Yun, J. Y. Kang, *et al.*, "Functional nerve cuff electrode with controllable anti-inflammatory drug loading and release by biodegradable nanofibers and hydrogel deposition," *Sensors and Actuators B: Chemical*, vol. 215, pp. 133-141, 2015.
- [129] G. Loeb and R. Peck, "Cuff electrodes for chronic stimulation and recording of peripheral nerve activity," *Journal of neuroscience methods*, vol. 64, pp. 95-103, 1996.

ABSTRACT**DEVELOPMENT OF CARBON BASED NEURAL INTERFACE FOR
NEURAL STIMULATION/RECORDING AND
NEUROTRANSMITTER DETECTION**

by

WENWEN YI**May 2016****Advisor:** Dr. Mark Ming-Cheng Cheng**Major:** Electrical Engineering**Degree:** Doctor of Philosophy

Electrical stimulation and recording of neural cells have been widely used in basic neuroscience studies, neural prostheses, and clinical therapies. Stable neural interfaces that effectively communicate with the nervous system via electrodes are of great significance. Recently, flexible neural interfaces that combine carbon nanotubes (CNTs) and soft polymer substrates have generated tremendous interests. CNT based microelectrode arrays (MEAs) have shown enhanced electrochemical properties compared to commonly used electrode materials such as tungsten, platinum or titanium nitride. On the other hand, the soft polymer substrate can overcome the mechanical mismatch between the traditional rigid electrodes (or silicon shank) and the soft tissues for chronic use. However, most fabrication techniques suffer from low CNT yield, bad adhesion, and limited controllability. In addition, the electrodes were covered by randomly distributed CNTs in most cases. In this study, a novel fabrication method combining XeF_2 etching and parylene deposition was presented to integrate the high quality vertical CNTs grown at high temperature with the

heat sensitive parylene substrate in a highly controllable manner. Lower stimulation threshold voltage and higher signal to noise ratio have been demonstrated using vertical CNTs bundles compared to a Pt electrode and other randomly distributed CNT films. Adhesion has also been greatly improved. The work has also been extended to develop cuff shaped electrode for peripheral nerve stimulation.

Fast scan cyclic voltammetry is an electrochemical detection technique suitable for in-vivo neurotransmitter detection because of the miniaturization, fast time response, good sensitivity and selectivity. Traditional single carbon fiber microelectrode has been limited to single detection for in-vivo application. Alternatively, pyrolyzed photoresist film (PPF) is a good candidate for this application as they are readily compatible with the microfabrication process for precise fabrication of microelectrode arrays. By the oxygen plasma treatment of photoresist prior to pyrolysis, we obtained carbon fiber arrays. Good sensitivity in dopamine detection by this carbon fiber arrays and improved adhesion have been demonstrated.

AUTOBIOGRAPHICAL STATEMENT

WENWEN YI

Education

2011 ~ 2016 Doctor of Philosophy, Wayne State University, Detroit, MI, USA

2006 ~ 2009 Master Degree in Engineering, University of Saskatchewan, Canada

1999 ~ 2003 Bachelor Degree in Engineering, Hunan University, Changsha, China

Selected Publications

1. **W. Yi**, Y. Yang, P. Hashemi, M. Cheng, “Dual Plasma Treatment of 3D Nanofiber Structured Photoresist Film for Enhanced Sensitivity and Stability in Dopamine Detection,” Submitted to *Lab on a Chip*.
2. **W. Yi**, C. Chen, Z. Feng, C. Zhou, N. Kumar, Y. Xu, J. Cavanaugh, and M. Cheng, “A Flexible and Implantable Microelectrode Arrays Using High-temperature Grown Vertical Carbon Nanotubes and a Biocompatible Polymer Substrate,” *Nanotechnology*, 26 (2015) 125301.
3. **W. Yi**, Z. Feng, C. Zhou, J. Cavanaugh, C. Chen, and M. Cheng, “An Ultrathin Flexible Carbon Nanotube Microelectrode Array for Neural Recording and Stimulation,” Abstract in *the 2014 Biomedical Engineering Society Annual Meeting*, San Antonio, Texas, USA, October 22-25, 2014.
4. X. Tan, P. Zeng, **W. Yi**, and M. Cheng, Graphene Based Digital Microfluidics. *IEEE 26th International Conference on Micro Electro Mechanical Systems (MEMS)*, pp 1095-1098, 2013.